MODELING, CONTROL AND RELIABILITY ANALYSIS OF PV EMULATOR

A Thesis submitted

in partial fulfillment of the requirements

for the Award of the Degree of

Doctor of Philosophy

in

Electrical Engineering

by

Simmi Sharma

2k15/Ph.D./EE/03

Under the Guidance of

Dr. Dheeraj Joshi

Professor

Department of Electrical Engineering

Delhi Technological University, Delhi

Delhi Technological University,
Shahbad Daulatpur,
Main Bawana Road
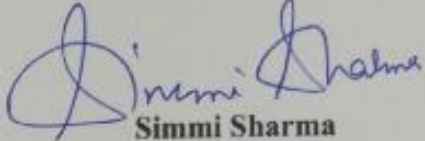**Delhi-110042**
October 2023

Dedicated to

my treasured brother "Sachin Sharma"

UNDERTAKING

I declare that the work presented in this thesis titled **"MODELING, CONTROL AND RELIABILITY ANALYSIS OF PV EMULATOR"**, submitted to the **Department of Electrical Engineering, Delhi Technological University, Delhi,** for the award of the **Doctor of Philosophy** degree is my original work. I have not plagiarized or submitted the same work for the award of any other degree. In case this undertaking is found incorrect, I accept that my degree may be unconditionally withdrawn.

Date: 6th Oct. 23

Simmi Sharma

Place: Delhi

DELHI TECHNOLOGICAL UNIVERSITY

(Govt. of National Capital Territory of Delhi)

Bawana Road, DELHI – 110042

CERTIFICATE

Date: 6ᵗʰ Oct. 23

This is to certify that the work embodied in the thesis titled **"MODELING, CONTROL AND RELIABILITY ANALYSIS OF PV EMULATOR"**, submitted by **Simmi Sharma** Roll No. **2k15/Ph.D./EE/03** as a research scholar in the Department of Electrical Engineering, Delhi Technological University is an authentic work carried out by her under our guidance.

The matter embodied in this thesis has not been submitted earlier for the award of any degree or diploma to the best of our knowledge and belief.

Supervisor

Dr. Dheeraj Joshi
Professor
Department of Electrical Engineering
Delhi Technological University
Delhi

DRC Chairman

ACKNOWLEDGEMENTS

Simmi Sharma
2k15/Ph.D./EE/03
Research Scholar
Department of Electrical Engineering
Delhi Technological University
email: simnit08@gmail.com

MODELING, CONTROL AND RELIABILITY ANALYSIS OF PV EMULATOR

A Thesis submitted

in partial fulfillment of the requirements

for the Award of the Degree of

Doctor of Philosophy

in

Electrical Engineering

by

Simmi Sharma

2k15/Ph.D./EE/03

Under the Guidance of

Dr. Dheeraj Joshi

Professor

Department of Electrical Engineering

Delhi Technological University, Delhi

Delhi Technological University,
Shahbad Daulatpur,
Main Bawana Road
Delhi-110042
October 2023

Dedicated to

my treasured brother "Sachin Sharma"

UNDERTAKING

I declare that the work presented in this thesis titled **"MODELING, CONTROL AND RELIABILITY ANALYSIS OF PV EMULATOR"**, submitted to the **Department of Electrical Engineering, Delhi Technological University, Delhi,** for the award of the **Doctor of Philosophy** degree is my original work. I have not plagiarized or submitted the same work for the award of any other degree. In case this undertaking is found incorrect, I accept that my degree may be unconditionally withdrawn.

Date: **Simmi Sharma**

Place: Delhi

DELHI TECHNOLOGICAL UNIVERSITY

(Govt. of National Capital Territory of Delhi)

Bawana Road, DELHI – 110042

CERTIFICATE

Date:

This is to certify that the work embodied in the thesis titled **"MODELING, CONTROL AND RELIABILITY ANALYSIS OF PV EMULATOR"**, submitted by **Simmi Sharma** Roll No. **2k15/Ph.D./EE/03** as a research scholar in the Department of Electrical Engineering, Delhi Technological University is an authentic work carried out by her under our guidance.

The matter embodied in this thesis has not been submitted earlier for the award of any degree or diploma to the best of our knowledge and belief.

Supervisor

Dr. Dheeraj Joshi
Professor
Department of Electrical Engineering
Delhi Technological University
Delhi

DRC Chairman

ACKNOWLEDGEMENTS

ABSTRACT

The depletion of non-renewable energy sources, combined with fatal environmental concerns such as global warming, pollution and rising fuel prices have prompted researchers to investigate alternatives to traditional power sources. Renewable energy sources such as solar and wind have grown in popularity over the last few decades. Solar energy has attracted widespread attention because of its immense potential, inexhaustible supply and environmentally friendly nature. Solar PV system research is heavily influenced by manufacturing costs, area, intermittent solar irradiation and peak power retrieval for trying multiple configurations. It is critical to model, design, control and finally emulate photovoltaic panels for optimal utilization. PV technology is also catching up to the incentives offered by governments all over the world. Power electronics is used to link up these renewable energy systems in an equitable way. A PV Emulator (PVE) is able to simulate many different types of solar panels in a wide range of temperature and weather conditions as a sterile environment to test photovoltaic equipment is difficult. When compared to a real PV panel, PVE simulate it more aptly and provides a more controlled environment for testing. It will also provide better control and thus allowing more accurate testing of PV equipment. The main advantage is that a new solar panel can be simulated by modifying the PV panel within the emulator, thereby rescuing the inconvenience of buying a brand-new PV panel and connecting it for testing.

This thesis identified the scope of research in the following directions:

- The mathematical model approach for the simulation of a solar panel under different conditions.

- Emulators used a single reference diode model or a look-up-table method to simulate a PV Panel. Reference models using more than one diode models effectively change the performance of PVE.

- The control strategies improvised by AI, hybrid and Non-linear controllers provide better performance indices.

- The performance analysis of PVE based on its reliability and availability.

Following are the major contributions of this Ph.D. work:

- Mathematical modeling of PVE with ideal and non-ideal components.

- Implementation of two diode and three diode reference model in feedback loop.

- Comparing the results obtained by lookup table and diode models for better analysis.
- Implementation of different controllers on a PVE for better understanding of system ranging from conventional to hybrid, AI based and non-linear robust controllers.
- Reliability and availability-based performance analysis of designed PVE.

TABLE OF CONTENTS

Notations

S.No.	Symbol	Meaning	Unit
1	I_{sc}	Short circuit current	A
2	V_{oc}	Open Circuit Voltage	V
3	Δi_L	ripple current	A
4	Δv	ripple voltage	V
5	P_p	Peak Power	W
6	f_{sw}	Switching frequency	Hz
7	V_{in}	DC input voltage to Power converter	V
8	I	Current through the inductor of DC-DC converter	A
9	I	Instantaneous current through the inductor of DC-DC converter	A
10	R	Coil resistance of DC-DC converter	Ω
11	L	Coil inductance of DC-DC converter	H
12	C	Capacitance of DC-DC converter	F
13	R	Load resistance of DC-DC converter	Ω
14	Vo	DC-DC converter output voltage	V
15	'd'	Duty cycle	
16	D	Duty ratio of DC-DC converter	
17	P	Power of DC-DC converter	W
18	I_{ph}	Photo current	A
19	k_i	Short circuit current of cell at 25 degree C and 1000 w/m2	A
20	T	Operating temperature	K
21	T_n	Normal temperature	K
22	G	Solar Irradiance	W/m^2
23	Q	electron charge	C
24	N	ideality factor of diode	eV
25	K	Boltzman's constant	eV/K
26	Ego	band gap energy of the semiconductor	eV
27	N_s	no. of cells connected in series	number
28	R_s	Series resistance	Ω
29	R_{sh}	Shunt resistance	Ω
30	V_t	diode thermal voltage	V
31	I_{01} and I_{02}	Reverse Saturation Currents of two diode model	A
32	a_1 and a_2	ideality factors of two diode model	eV
33	V_{T1} and V_{T2}	thermal voltages of two diode model	V

S.No.	Symbol	Meaning	Unit
34	t_r	Rise time	Sec
35	t_s	Settling time	Sec
36	POS	Percentage overshoot	%
37	ISE	Integral Square Error	
38	IAE	Integral Absolute Error	
39	ITAE	Integral Time Absolute Error	
40	λ_b	Base Failure rate	FIT
41	Π_T	Temperature factor	
42	Π_E	Environment Factor	
43	Π_C	Contact structure Factor	
44	λ_p	Part failure rate	Failure/10^6 hours
45	Π_Q	Quality Factor	
46	Π_S	Electrical stress Factor	
47	Π_v	Voltage stress Factor	
48	Π_{SR}	Series Resistance Factor	
49	Π_{C1}	Capacitor Factor	
50	T_{HS}	Thermal Hotspot	degree C

List of Acronyms

S. No.	Acronym	Full form
1	PV	Photo Voltaic
2	PVE	Photo Voltaic Emulator
3	DNES	Department of Non-Conventional Energy Sources
4	MNES	Ministry of Non-Conventional Energy Sources
5	MNRE	Ministry of New and Renewable Energy
6	PWM	Pulse Width Modulation
7	P	Proportional
8	I	Integral
9	D	Derivative
10	FOPID	Fractional Order PID
11	PSO	Particle Swarm Optimization
12	AI	Artificial Intelligence
13	ANN	Artificial Neural Network
14	FL	Fuzzy Logic
15	GA	Genetic Algorithm
16	MOSFET	Metal-oxide semiconductor field-effect transistor
17	MF	Membership Function
18	MPPT	Maximum Power Point Tracking
19	OF	Objective Function
20	STM	State Transition Matrix

List of Figures

List of Tables

CHAPTER 1
INTRODUCTION

1.1 INTRODUCTION

Solar energy is a plenteous renewable energy source that was discovered on Earth in the 7th century B.C. During special ceremonies, early humans harnessed sun energy by using magnifying glass materials and mirrors to light fire and torches. With current minimal solar cost, it's readily apparent that the term "Solar" held an entirely different connotation two decades ago. On April 22, 1970, the first Earth Day was observed, but researchers were already looking into solar energy to raise awareness and lay the groundwork for nature stewardship. It all started in France in 1839, when Edmond Becquerel noticed and identified the photovoltaic effect. Non-renewable sources like coal and diesel account for $1/3^{rd}$ of global greenhouse gas emissions. The carbon footprint (CFP) of electricity generation is created in a variety of ways. The total amount of CO_2 and other GHG emitted across the life cycle of the processes is indicated by the CFP. Solar technology is encouraged over the world since it has a lower CFP than fossil fuel technology. The world is undergoing an energy crisis, as non-renewable energy sources are unable to fulfil rising demand. The price of natural gas is rising, which is undermining country's economy. There have also been instances of dry gasoline pumps in the United Kingdom. China's industrial output dropped, preventing the country's economy from recovering from the coronavirus outbreak. China and India are Asian countries that are battling and facing a crisis of a major energy crisis. Another aspect contributing to the scenario is "Greenflation", which is driven by government restrictions on traditional energy sources. To reach global emission objectives, governments are supporting renewable energy. China has pledged to a 65 percent reduction in emissions by 2030, while Europe has set a 55 percent reduction goal. Wind energy is used by the UK government to achieve one-third of its electricity needs. Investors interest in traditional energy supplies is dwindling as a result of the circumstance. Between April and August of 2021, there was a surge in power demand. Following the damaging succeeding wave of Covid-19, this was the economy's regaining phase. The economic restoration was more rapid than the government had expected. The energy sector was also affected by a sharp increase in gas prices and nuclear power plant shutdowns.

Many countries are attempting to increase their capability for solar power generation. Climate change and pollution are held responsible the switching. Solar as a renewable form of energy has gained prominence as the best alternative source due to global warming and changing

economy. This technology is frequently referred to as carbon-neutral or low-carbon. It has a low carbon credit (CC) because of its less contribution of CO_2 emissions in the surrounding. The term "CC trading" refers to an administrative approach that uses economic incentives to achieve pollution reductions. It's a system of tradable permits. International conventions, such as the "Kyoto Protocol", impose restrictions on how much greenhouse gas a country can emit. Countries have also imposed limitations on commercial emissions. The percentage of CC garnered is correlated with the quantity of generated solar power, which is impacted by weather, cell efficiency and other operating parameters. Solar energy is often harnessed through the use of photovoltaic (PV) panels. However, the amount of silicon essential for solar panel preparation and the amount of carbon dioxide produced during its extraction from quartzite sand must be monitored. If sustainability is to be accomplished, fossil fuel consumption should only serve as an auxiliary rather than a primary energy source. The solution will be to rely on renewable energy sources to reduce the harmful effects of GHG. CO_2 emissions occur during the extraction, construction and maintenance processes; hence it is not a carbon-free source of electricity. The pandemic and Russia's invasion of Ukraine have caused the crisis to reach record levels and steadily rising energy prices in some advanced economies left policymakers scrambling to find cheaper and more reliable energy.

1.2 THE IMPORTANCE OF SOLAR ENERGY ON A GLOBAL SCALE

Improved energy security and access to energy in varying environmental conditions are two benefits of renewable energy installation. A country's economic development can be facilitated by a cost-effective, dependable and long-term energy supply. As a contrary, many historical structures have solar panels installed to lower their energy consumption after restoration. Hereunder are a few of them [1]:

- **The Vatican City**: In 2008, the Vatican City chose solar electricity to safeguard the environment and generate solar energy. The goal was to supply electricity to every family in the city.
- **Dubai (UAE)**: The world-famous Burj Khalifa has solar panels on its roof that heat approximately 1.4 lac litres of water every seven hours to control water consumption and save resources.
- **White House**: In 1979, solar panels were installed on the White House's roof. However, the panels were removed in 1986 as part of a roof refurbishment.
- **The Eiffel Tower**: In 2015, the tower was refurbished as part of the "Paris Climate Plan". Panels to save energy and water were installed as part of this project.

- **Dezhou (China)**: It is known as Solar Valley and is the world's first solar metropolis. This was created specifically as a symbol of renewable energy.
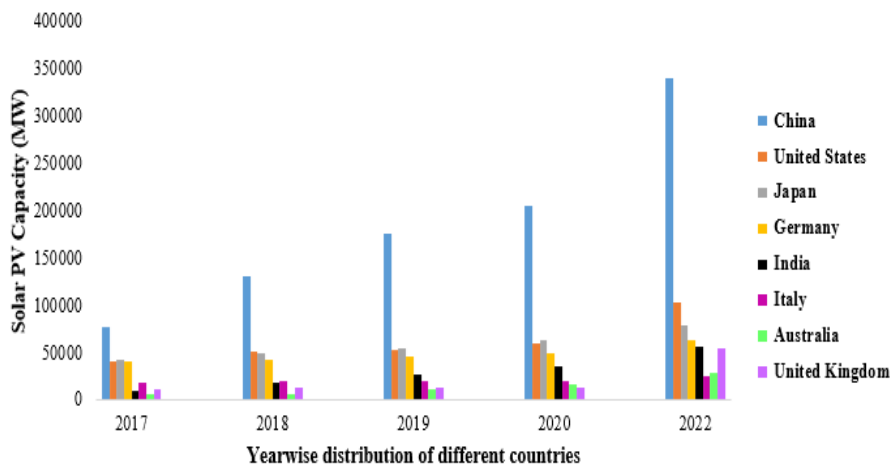
Figure 1.1: Different countries/territories total solar PV capacity (MW) for different years [2, 3]
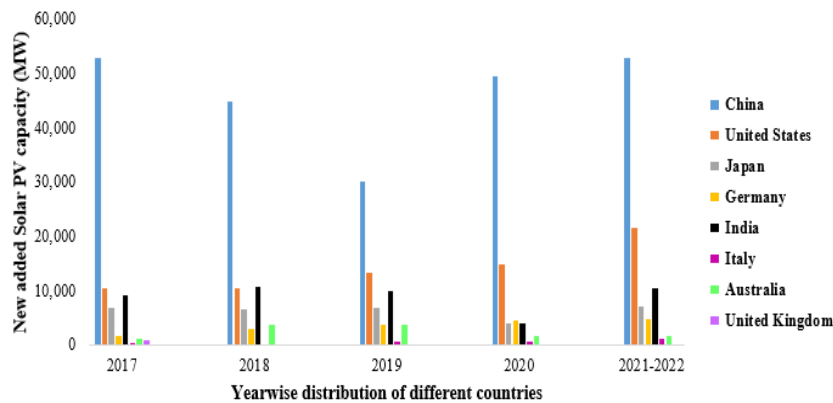
Figure 1.2: Year-by-year additions of solar PV capacity (MW) in distinct nations [2, 3]

Figures 1.1 and 1.2 depict the solar PV capacity of various countries/territories during the last five years. It clearly demonstrates the growing interest of solar energy around the world. Solar energy generation is however increasing year after year. Global warming, government policies and programmes, the economic crisis and growing scientific innovation all have driven the development of this form of energy source.

1.3 SIGNIFICANCE OF SOLAR ENERGY IN INDIA

Coal and oil contribute approximately 74% energy demand of India, necessitating it to import costlier fossil fuels. It is overly dependent on coal for energy, resulting in massive carbon dioxide emissions. As a result, there is a compelling need to generate electricity that is less

expensive, cleaner and more dependable. Furthermore, during the festive seasons, power usage and demand both increase dramatically. Despite substantial pithead reserves, the rainy season has a negative impact on coal supply. Floods wreak havoc on transportation throughout the monsoons.

1.3.1 Engrossment of Government of India

According to the Indian government, each state will have a "green city" that will be powered totally by renewable energy. Residents will have access to renewable energy, solar parks and electric transport networks. The country's power development went through different, isolated power systems. State-wise grids were developed by connecting these across time. In the 1980s, the Indian government divided the country's states into five power zones. The regional grids, have gradually been linked to form a single synchronous interconnection that spans the country. India's power grid overtook China's grid in 2014, to emerge as the world's largest synchronous grid. The initiative "National Green Energy Corridor", has prioritised the construction of renewable energy transmission network infrastructure. It is vital to incorporate share of renewable sources in order to meet the rising power requirements. India has set a goal of 500 gigawatts by 2030. India's 28 states and eight union territories govern the challenges, objectives and solutions for renewable energy integration. The bulk of renewable power generation is made up of solar and wind power.
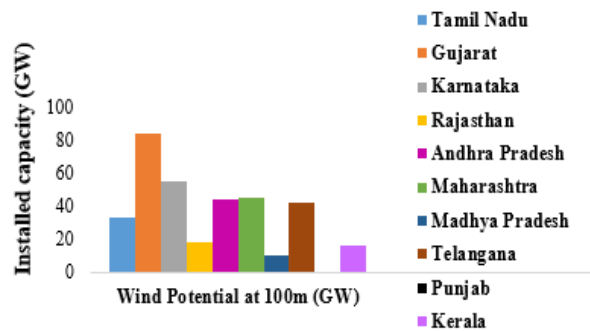
Figure 1.3: State wise Installed wind potential at 100m (GW) of India [2]

The proportions of two main renewable sources in India are depicted in Figures 1.3. Solar and wind power are important alternative energy sources in a number of states. In ten Indian states, the installed capacity and percentage shown in the descriptive statistics indicate that these sources are growing more prominent. India receives 5k trillion kWh (solar energy/year) due to its tropical and subtropical geography [2]. India possessing the largest solar power plants, has set a new objective of delivering 500 GW of energy by 2030. Renewable energy is the primary alternative for meeting emerging economies' energy needs due to its dwindling costs, increasing efficiency and reliability.

4

1.3.2 Establishment of Renewable in Ministry of India

With an emphasis on innovative and renewable energy, in 1982, the Indian state created DNES and later in 1992, it became a separate Cabinet of MNES. In 2006, was again renamed as MNRE. Solar energy was explored for power generation in India from 1961 to 1966 as a globally developing technology. In January 2010, the Government of India formed a solar quest to promote sustainable energy and accomplish a capacity of 20GW by 2022. However, in 2014, a new milestone of 100GW by 2022 was set [3]. Primary energy sources are rapidly depleting and renewable energy appears to be the most promising alternatives for meeting increasing energy needs. Its present concentration is on development of photovoltaic devices with their fabrication and applications. Indian government is focusing on energy production and access initiatives, as well as the Paris Agreement, which seeks to decarbonize and attain a 40% renewable energy capacity by 2030. The Indian government has redefined its policies and programs in order to entice international investors. Following the COVID19 outbreak, many hard obstacles remain in the way of achieving these objectives. Renewable energy projects have been praised for their speed. Eventually, it was recognized as essential services by the ministry of renewable energy and a regulation allowing project time modifications was adopted. New project bids resumed despite the lockdown [4]. Solar photovoltaic and wind energy are two low-carbon energy technologies which are presently suitable. The energy contributions of different electrical sources in India are depicted in Table 1.1.

Table1.1 The energy contribution of various electrical sources in India [3]

Source	Generation Capacity (Installed in MW)	Final Percentage share
Fossil Resources (Coal, Lignite, Gas, Diesel)	2,36,086	57.9%
Hydro	46,850	11.5%
Solar, Wind and other Renewable	1,18,080	29%
Nuclear	6,780	1.7%
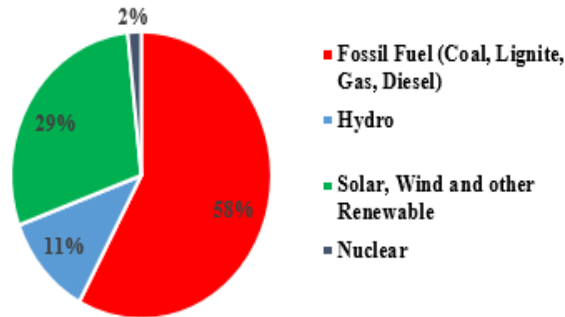
Figure 1.4: The percentage energy contribution of different sources in India [3]
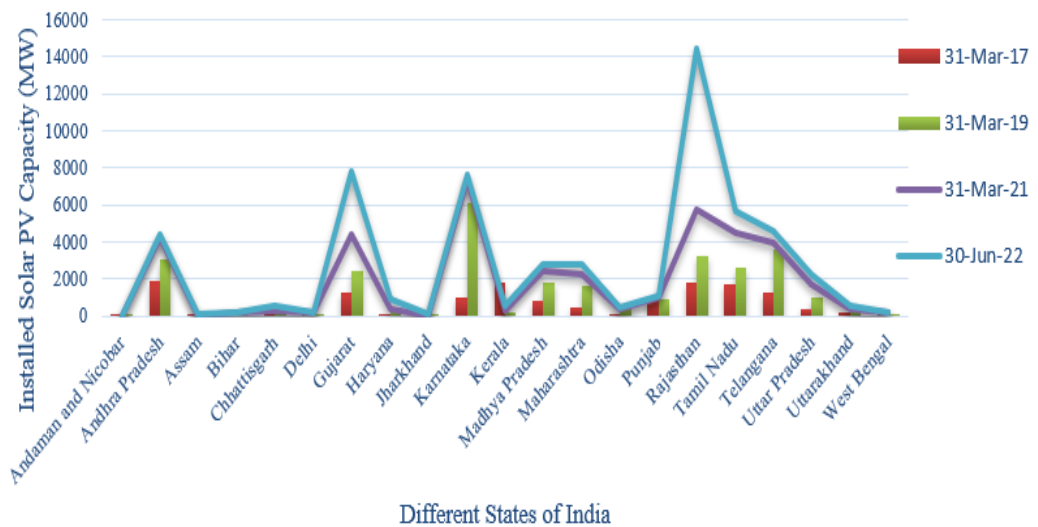
Figure 1.5: State wise Installed PV capacity of India in MW [3,5,6,7,8,9]

Figure 1.5 depicts the activated Solar Photovoltaic capacity and growing interest in a wide range of states, including remote locations experiencing power outages due to geography or local climatic factors. This is a sneak peek into India's photovoltaic future.

1.4 CATEGORIZATION OF SOLAR POWER BASED ON DISTRIBUTION

1.4.1 OFF Grid Solar Power System

These systems do not have physical access to the power grid. They incorporate batteries to store the solar energy they generate. Solar panels, battery, inverter, grid box and mounting framework make the off-grid system. During the day, the cells store solar energy and use the acquired power at night. They include locations isolated from the grid and are unreliable. Solar dwellings, lanterns, study lamps and street lights are among the most common uses, as are solar power plants. In the National Solar Mission, 2000 MW target was set for solar PV applications,

which was broken down into three phases [10]. In rural and remote places, off-grid solar panels can supply reliable and long-term power. Off-grid technologies can remove power transmission flaws like power outages. They provide power at night and in the event of a power outage and they are ideal for distant locations. The most significant benefit is the provision of continuous power during grid outages and shutdowns.

1.4.2 Grid connected Solar Power System

These systems typically generate electricity while being connected to the power grid. In these configurations, the excess electricity produced by a solar power system is distributed with the utility grid. As a result, the utility is compensated for the extra power given to it by the customers. When the sun isn't shining brightly enough, the system relies on power from the associated utility grid. India aims to have 100 GW of solar power added to the grid by 2022. India's renewable business was able to compete globally thanks to cost reductions, technological advancements and lower solar tariffs. [11]. Because grid-connected solar systems are more stable, enterprises can rely on them for their daily electricity needs. Solar energy can be generated in sufficient quantities during sunny days to power electrical appliances. Offsetting electricity bills can help businesses regain their investment costs. A solar PV rooftop system installed on a domestic or industrial building will be eligible for an Accelerated Depreciation Benefit of up to 80% per year. Additionally, customers and business owners in the home and commercial sectors may be denied access to extra energy.

1.5 SCHEMES AND POLICIES OF GOI FOR STRENGTHENING PV TECHNOLOGY

PV technology is catching up to the incentives offered by governments all around the world. The adoption of regulatory laws has expanded the PV solar interconnection research area [12-14]. India's total renewable energy capacity is 96 GW, reporting for 25.2% of the overall installed capacity. Bhadla Solar Park, the world's largest solar power plant, is situated in Rajasthan, India [15].

The Indian government has launched the following schemes to promote growth in the renewable market:

- The PM Kisan Urja Suraksha evam Utthan Mahabhiyan (KUSUM) seeks to install solar pumps for agricultural purposes.
- The Atal Jyoti Yojana (AJAY) is launched to provide LED solar lights in different states with 75% funding from MNRE and remaining 25% from MPLADS. These lights

will illuminate roadways, markets and public restrooms, among other places. It will also ensure that life in such locations is safe and secure.

- GOI also launched schemes to stir up generation of solar power. The main schemes include [10-11,16] Solar Park Scheme, Defence Scheme, Grid Connected Solar Rooftop Scheme.

1.5.1 Initiatives by Government of India

Following initiatives are taken by GOI for improving Solar Energy Sector [1,3]:

- In Khavada Gujarat, NTPC Renewable Energy Ltd. is granted a 100% subsidiary to structure a 4,750 MW sustainable energy park.
- The Indian Renewable Energy Development Agency Ltd. (IREDA) demanded bids for solar units under the Production Linked Incentive (PLI) scheme.
- Haryana has established a scheme to stimulate the use of solar energy in homes by offering a 40% subsidy for 3 KW plants.
- In the federal budget for 2021-22, MNRE was given Rs. 300 crores for the 'Green Energy Corridor' initiative.
- The government has increased funding to the Solar Energy Corporation of India (SECI) by Rs. 1,000 crores and IREDA by Rs. 1,500 crores.
- The government established a five-year PLI scheme worth Rs. 4,500 crores for the manufacturing of extremely efficient PV modules.
- The thermal power station in Rajghat, Delhi, will be closed down and converted into a 5,000 KW solar park by the Delhi government.
- Indian Railways is now contemplating energy-saving measures, with an emphasis on maximising the use of clean fuel in order to reduce emissions by 33% by 2030.

1.6 CHALLENGES WITH SOLAR PANELS IN INDIA

India imports a major portion of its solar cells and panels from Taiwan, Malaysia and China. Thus, domestic manufacture is vital. Solar panels and other associated equipment imported from other countries are expensive, making solar energy generation expensive and unaffordable. During panel research, significant issues relating to high prices charged for acquiring photovoltaic panels were discovered. The following are some of the issues that have arisen during the installation of PV panels [17, 18]:

1. Installation necessitates a huge amount of area.
2. Weather conditions are a factor.
3. The onsite testing process necessitates a large expense.

4. Panel selection among a huge number of solar panel options.

5. Thus, PV Emulators are one of the alternatives for overcoming these issues.

The basic block design in Figure 1.6 exhibits the PV Emulator under various situations, the MPPT block for rapid tracking and the converter for raising or lowering the output voltage based on the applied load. Because a PV system's output depends on arbitrary meteorological factors, the use of an actual PV panel for research, investigation of power management issues such as MPPT testing and integrating the PV power to the grid as well as load necessitates use of alternative of panel.
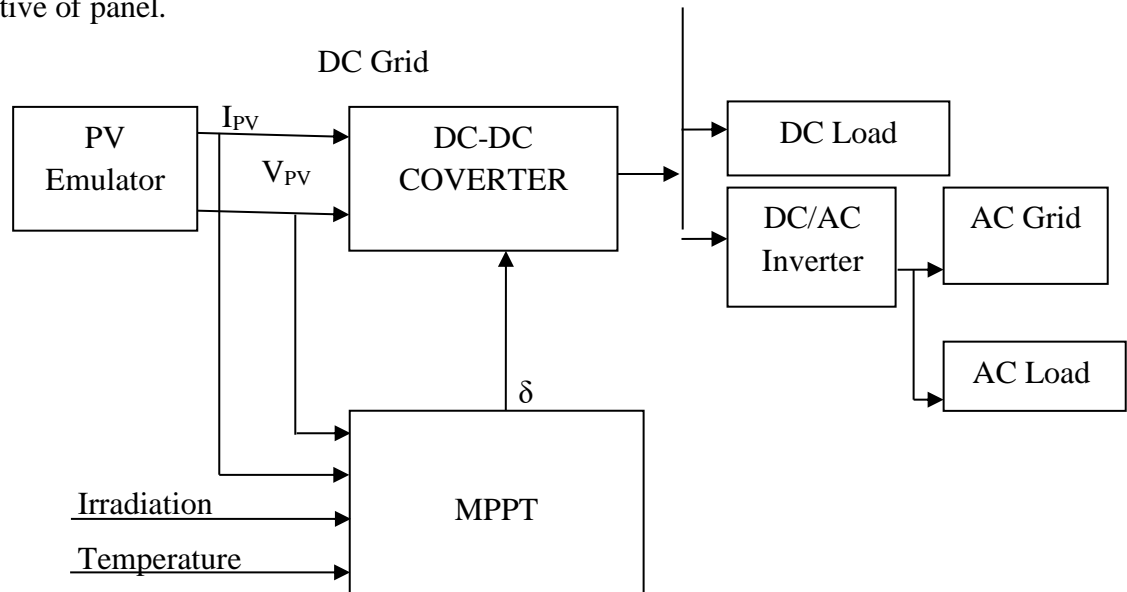
Figure 1.6 Schematic diagram of a PV system using PVE

Researchers are concentrating on PV Emulators because of these considerations. They become less bulky and offer a viable answer to the installation area issue, which has become a major concern as the world's population grows, particularly in nations like China and India.

1.7 ORGANIZATION OF THESIS

The following thesis is organized into chapters, with summaries of each chapter below:

Chapter 1 introduces the current scenario of solar power and its significance in the coming years. The worldwide contribution of solar power as reported by researchers and the schemes and policies of GOI are summarized to understand the growing popularity of solar power. The author's contribution towards Ph.D. work is presented as conclusion in the end.

Chapter 2 outlines PVE related literature review, the research needs and gaps identified on the basis of the literature review that laid the basic foundation of this research work.

Chapter 3 explains the PVE components mathematical modeling, its state space and small signal analysis with and without parasitic components. Closed loop buck converter is

described with the help of transfer function. These models provide base for designing desired PVE's circuitry.

Chapter 4 describes the major methodologies for obtaining reference PV panel values in current controlled mode. Existing lookup table and piecewise linearization are explained along with two diode and three diode models and results section covers the comparative plots obtained by their implementation in MATLAB Simulink. The plots verify the effectiveness of designed reference models for desired PVE.

Chapter 5 covers implementation of different types of control strategies on PVE. Results and discussion explain the comparative analysis of conventional, hybrid, AI-based and non-linear controllers along with their performance indices at different characteristic points. The tables conclude the performance of non-linear controllers. Finally, modeling of PVE with non-idealities is carried out to find the best modeled system.

Chapter 6 evolves around the reliability analysis of the designed PVE by part stress, State Transition Matrix, STM and Petri net method. Analysis of complete PVE based on failure rates help in the choice of best feasible reliability calculation method. Petri net comes out to be an ideal choice avoiding lengthy equations and results are verified by comparing them with the results of part stress method. Availability of designed model is evaluated considering failure and replacement rates. A comparative analysis is also carried out for dynamic and static states.

Chapter 7 gives the major conclusions based upon the research work presented in the Ph.D. thesis. Major conclusions as reported are:

- Mathematical modeling of PVE can be conveniently carried out using Signal Flow Graph, SFG method and control system basics for parasitic and non-parasitic components.
- Reference model methodologies namely two diode and three diode models are described and implemented in chapter 4 and result include performance indices for detailed insight analysis.
- New hybrid and robust controllers implemented in chapter 5 provide performance indices at relevant points of PVE characteristic curve. Comparative plots help in selection of design methodology according to desired application of solar panel.
- The non-linear behaviour of PVE is completely analysed by calculating the reliability and availability of complete PVE model in chapter 6.

- Petri net reliability method comes out to be an effective way of calculating reliability.
- To validate the findings, plots are shown in results and discussion section of chapter 4,5 and 6.

Further chapter 7 includes scope for future work and lays forth the groundwork for carrying out future research.

1.8 AUTHOR's CONTRIBUTION

After taking into consideration the above-mentioned chapters, research progress led to the following significant contributions to the Ph.D. work:

- Improvement in the mathematical modeling of PVE and its implementation using MATLAB simulation and programming with and without internal resistances of components.
- Designing PVE based on different reference models and considering performance indices at varying load conditions.
- Control of PVE by conventional, hybrid, AI based and non-linear controllers to improve their performance during dynamic conditions.
- Finding reliability of PVE considering part failure and physics of failure methods and making the system simpler and faster.
- Finding availability of system for static and dynamic states and carrying a comparative analysis.

Thus, finally obtaining overall PVE analysis by different modeling, control and reliability-availability methods.

CHAPTER 2
LITERATURE REVIEW

2.1 INTRODUCTION

A literature review is the foundation of any research study. It should aspire for the following objectives:

- A thorough examination of literature relevant to the study topic
- A summary of the insights gained
- An analysis of the research gaps identified.
- Reshaping gathered data in order to do future study

By outlining prior research work, this chapter introduces the Ph.D. work's authenticity. It describes what has been learned from others, as well as how the research undertaken provides a platform for new ideas. It also presents a methodical analysis of research publications that resulted in clarity regarding the objectives to be met.

2.2 LITERATURE SURVEY

Solar Photovoltaics (PV) refers to the transformation of photons into electricity. Bell Laboratories scientists used this concept for the first time in 1954 when they developed an operational silicon solar cell that generated an electric current when exposed to sunlight [19]. Solar cells were then used to power space satellites and small electronic devices. Matos *et al*. [20] have presented the PV cell's computational model in order to fully comprehend its design and behaviour. The datasheets for a specific PV panel hold data about V_{oc}, I_{sc} and P_m, with their maximum voltage V_m and maximum current I_m [Appendix 1]. Since onsite testing necessitates expensive and complex setups, laboratory testing with PVEs can be employed to substitute onsite testing, saving time and money. Agarwal *et al*. [21] and Ajaamoum *et al*. [22] have highlighted that a PVE lowers installation costs and eliminates onsite difficulties during irradiation and temperature variations. Grid-connected PV systems reported non-linearities such as over voltages, swells and sags, resulting in interrupted voltage and current. Further, islanding and grid synchronized tests are required for grid connected inverters. Pelin *et al*. [23] suggested emulating a grid-connected setup on a specified day in order to evaluate solar-based systems more quickly and effectively. The power converter, closed loop control approach and reference model are the three sub stages of PVE. It is found that a PVE is essential due to the following reasons:

- The PV panels actually are quite expensive [24]

- It is hard to obtain and maintain panel characteristics due to varying environmental conditions [24-26].

- It has the benefit of allowing testing to be done at night and in cloudy weather [27].

- Minor circuitry improvements allow for faster emulation of various panels with minimal effort [28]

As an outcome, extensive research is carried out to boost the quality of the emulated output. The primary goal of the PVE model is to:

- Emulate all PV panels that fall within its output limits [29].

- Emulate panels for different irradiance, temperature and partially shaded conditions [24-28].

- Develop a model with a strong dynamic response [30-31].

- To test solar equipment like inverters and maximum power point tracker [32-35]

Following categories of PVE are reported by researchers in publications.

- **Conventional PVE**: refers to PVE that employs analogue circuits and diode models. PVE based on analogue electronic circuit is described by Moussa *et al*. [36] and the suggested technique has the benefit of possessing a large bandwidth, which is critical for testing high frequency MPPT Emulators based on diode models. The performance of one diode model under different environmental factors is identified to be its primary limitation. Using a single diode model, Rana *et al*. [37] reported ripples in the current and voltage outputs with their magnitude relying on size of filter capacitor and inductor. Ishaque *et al*. [38] investigated diode model to reduce computational time and found that the designed model has high precision for low irradiance.

- **Converter-based PVE:** are found to be robust, reliable and effective [39-40]. Researchers proposed analysing converters like buck [37, 39], boost [40-41], buck-boost [42], cuk [43-44] and SEPIC [45] in order to enact them in the emulator architecture. In a boost converter, greater rms current flows from the filter capacitor, culminating the implementation of a higher rated capacitor and a higher rated inductor as compared to buck converter and buck-boost is less assumed due to polarity issues.

Zhuo *et al*. [45] proposed zero voltage and current switching (ZVZCS) with two lines mathematical approach for a convenient and simple design. Dolan *et al*. [46] explained how a buck converter based PVE can be implemented on hardware, considering DSP based control strategy and use of LabVIEW/ MATLAB for GUI. Can [47] outlined the concept and execution of a power system block set-based PVE that utilized a buck converter to imitate response of a

PV module. The literature predominantly covers articles based on buck converters as they require fewer components, which reduces cost and require simplified circuitry for control as stated by Ayop et al. [48]. The author also concluded that the resistive response of the emulator hinders the voltage response, which differs from a general buck converter, where the voltage response and response of resistor are independent of each other. Pradhan et al. [49] modeled boost converter with MPPT using P&O scheme to generate duty cycle for switch. Boost converter is generally applied for MPPT applications in PVE like Shi et al. [50] applied AI based control for MPPT using boost converter. Jenkal et al. [51] studied PVE based on diode equations and buck boost converter and validated the results by datasheet Solarex MSX-64 solar panel. Suganthi et al. [52] discuss how preferred solar panel's VI curves are inferred utilising LabView and are accomplished in hardware at a minimal price, a flyback converter-based PVE is recommended for diagnostics and academic activities. Isolated converters like Cuk, Sepic and Zeta necessitate transformers having added cost, size, complexity, total weight and converter losses, affecting overall efficiency as discussed in comparisons detailed by Suryoatmojo et al. in [53]. In [54] Parthsarathy et al. concluded that Zeta converter's operation is based on 'd' i.e. if 'd' is low, buck operation will be there and boost operation will be observed for higher 'd' values. It is also stated that buck boost converter, has higher switching and inductor current than boost mode, SEPIC converter performs only in boost operation and Cuk converter requires capacitor with larger ripple handling property. Mallal et al. [55] explained the practical testing on an experimental PVE designed with a MATLAB C MEX S-function, dSPACE board 1104 and a controlled converter. Research article by Alaoui et al. [56] implemented adaptive state feedback controller in dSPACE to obtain real-time control along with good static and dynamic performances. Azharuddin et al. [57] implemented dSPACE controller in loop with buck converter for real time control to obtain fast and accurate PVE with easy interfacing and concluded that by changing model parameter values, any solar PV characteristics can be obtained. Shahabuddin et al. [58] reviewed PVE studies with dSPACE, microcontroller and Digital Signal Controller (DSC) controllers, concluded that their efficiency, price is high and implementation is difficult when compared with conventional converter based PVEs. Andrew et al. [59] created a dynamic Wind-PV power prototype embedded model. The model is simulated with MATLAB/SIMULINK and the hybrid power system operation is handled by the TMS320F28335 controller.

Hardware In Loop (HIL) is reported as a flexible prototype tool for evaluating photovoltaic systems but Shahabuddin et al. [58] found it's hardware development complex with high pricing. Gutierrez et al. [60] developed an HIL emulator for partial shaded PV panels and the

proposed methodology allowed for the accurate modeling of systems in FPGA in loop fault detection. Rezkallah *et al*. [61] described a hardware-in-the-loop (HIL) technique of a solar PV with SMC. The findings assured voltage and frequency control ON-grid and overcurrent protection in off-grid structures. PVE implemented by Ullah *et al*. in [62] proposed a fractional order robust control method. The controller is built using the Emulator's average state space model and the outcomes are obtained by integrating MATLAB to an Arduino duo microcontroller board.

PVE characteristics are defined by researchers in terms of I_{sc}(A), V_{oc}(V), MPP (W) and the panels described in literature range from few watts to kilowatts [Appendix 1]. MPP current I_{mpp}(A) is 72-92 percent of I_{sc}, while MPP voltage V_{mpp}(V) is 70-80 percent of V_{oc}. Gour *et al*. [63] presented a model that can be implemented in any DC based converter by modifying the converter mathematics, suggesting that the design can utilised for robust loop control. To reduce the error, the second stage of PVE in closed loop, incorporates a control strategy for obtaining and comparing the desired value for converter. Based on the controlled variable, the methodologies are termed as Voltage mode control (VMC) and Current mode control (CMC) [37][60]. Kazimierczuk *et al*. [64] explained the closed-loop small-signal characteristics of the voltage-mode-controlled PWM buck converter with PI in CCM with transfer function. The hysteresis control was developed to fulfill the energy demands of transient response of load elements such as the CPU and FPGA. This technique is called a ripple control method since it accomplishes regulation by identifying ripples in the output. Variable f_{sw}, large jitter and the necessity of a capacitor possessing significantly larger equivalent series resistor (ESR) for ripple detection at output are issues with the method [65]. The current mode is reported to possess fast transient response especially in case of current sensitive loads. Reatu *et al*. [66] proposed derivation of linear equivalent circuit of boost converter and its representation in the frequency domain by CMC. The closed control loop entails a controller with error as input signal. The reference values are introduced in PVE by means of either Piecewise model, Look Up Table (LUT) or diode model.

P, PI and PID are the categorized as conventional controllers. Solaiam [67] discussed PID as commonly incorporated controller for characteristic curve modeling, implementation and the control strategy. Jindal *et al*. [68] demonstrated different classical PI tuning methods with performance parameters and indices alongside load of ideal and non-ideal buck converter. PID controllers are preferred because of their ease of operation, ease of design, low cost and efficiency. Balakishan *et al*. [69] proposed algorithm for PVE rendering use of a buck converter in CMC with PI controller. The heuristic monitors the point on the PV characteristics curve

15

under varying loads in a test bench with a 50 W buck converter with AT'mega328 as the core controller. Prusty *et al*. [70] stated that PID controllers can be used effectively if an accurate mathematical model is derived, but the restriction of existing systems is the precise and successful tuning of parameters.

Papers reported tuning of conventional controllers by hybrid and artificial intelligent methods such as by PSO, FOPID and PSOFOPID. Cech *et al*. [71] demonstrated that working with multiple process models at a given time is simple with FOPID and thus solve robust modeling techniques for basic examples of uncertainty descriptions. Sahin *et al*. [72] designed a FOPID controller for a PV resistive load circuit with PSO-tuned controller gains implemented with boost converter. The findings conclude small ITSE and POS values but same t_r and e_{ss} on applying PID and FOPID. According to Haroon *et al*. [73], the FOPI Emulator performed well within the system's nominal parameters; however, the power stage characteristics vary according to the operating settings and can be rectified by using sliding mode, back stepping and H_∞ in future. Bagyaveereswaran *et al*. [74] proposed PSO tuned control scheme resulting in high attainment rate and fast steady-state response time. Gupta *et al*. [75] explained PSO with an objective function to be minimized. A Non-minimum phase type non-linear system with lumped parameters is optimized and compared with PID and Fuzzy based system. Sowjanya *et al*. [76] used PSOPID and evaluated the system's performance by modelling its OF with ISE, IAE and ITAE. The paper also compared the performance of PID controllers using PSO and Ziegler-Nichol methods. LI *et al*. [77] explained PSO tuning by minimising ITAE as the optimal solution and then utilized to optimise PID control parameters. In terms of dynamic performance, Muftah *et al*. [78] proposed the perspective of time domain performance metrics and indicated that the PSO fuzzy FOPID outperforms the PSO Fuzzy PID controller, The addition of a fractional order controller enhanced the ruggedness of trajectory prediction and presented more flexibility in parameter selection, but tuning more parameters caused issues. In comparison to other power converters, the PV emulator implementation adopting programmable supply is straightforward because the controller is built into the programmable power supply, thus doesn't require implementation. LabVIEW is a graphic software language with fast execution. It can be implemented for the PV model as discussed by Dolan [46] and Bhise *et al*. [79]. Durago *et al*. [80] detailed a PV panel characteristic database provided by LabVIEW and utilized it to assess designed PV model. Another software used by researchers for implementation is MATLAB [81-82] MATLAB shows a popular software choice for researchers as it provides simulation, programming and GUI to researchers. Further reported controllers of PVE are based on robust SMC. Mattavelli *et al*. [83] considered

small-signal technique with SMC to evaluate impedances and transfer function. He investigated controller parameter variations effects on stability. For validation, simulated SEPIC converter results and experimental boost converter outcomes are discussed. Guldemir. [84] discussed robustness attained by SMC and the findings validate the robustness against voltage transients, as well as the response voltage's ability to transmit the load without instabilities. He. [85] envisaged SMC system based on buck converter large signal model and came to the conclusion that the scope of the variations around the operating point has no restriction on system stability. Das *et al.* [86] presented an integral SMC buck converter with PID and made comparison with basic SMC. ISMC maintained robustness against parameter perturbations and eliminated the switching frequency deviations during load and supply voltage variations. Tan [87] described fixed-frequency PWM design-based SMC operating in CCM on buck, boost and buck-boost converters and the model is tested with line and load changes using boost converter. Gambhir *et al.* [88] did rigorous review work and concluded that SMC is robust with respect to load variations and provides better dynamic response.

Other non-linear robust controllers discussed in literature are Fuzzy Logic Controllers (FLC). Raja *et al.* [89] found that fuzzy logic controllers work in close approximation to actual panels but their tuning remains a limitation in research work. Chen [90] implemented fuzzy controller to enhance the transient performance of the regulated system. He also reported that when static error and dynamic error possess different polarities then, the output of the PD like FLC is comparable to PD controller. Shaoa *et al.* [91] explained fuzzy PID control simulator that accurately simulated characteristics of a photovoltaic cell and also rapidly realized the dynamic characteristics under varying load. The results show error $< 3.6\%$, overshoot $< 3.5\%$, the ripple coefficient $< 3\%$ and the tracking time as 0.3sec. Iqbal *et al.* [92] reported buck converter with dynamic loading in closed loop with FLC and the findings conclude good steady state and dynamic stability of the PVE system. Ayop *et al.* [93] proposed a fuzzy logic PI control system to optimise the dynamic response of the Resistance Feedback Method PVE and the results show that the dynamics of the proposed PVE is 2.3 times better than the original without jeopardising accuracy. Lyapunov-based Neural Network (NN) controllers investigated by Atig *et al.* [94] show that these controllers are useful in regulation of duty cycle and are also utilised to effectively assess the stability of the system. However, NN based controllers are found to be dependent on number of inputs and outputs as stated by Miloudi *et al.* [95]. The process of collecting characteristic data from the experimental approach or the electrical circuit PV model at various loads, irradiances and temperatures has been described by Saraswathi *et al.* [96]. He described the neuron network, PV model data training in offline mode. Ayop *et al.* [97] stated

that using Artificial NN (ANN) with adaptive PI enhances the output current's dynamic performance and is recorded 80% faster than conventional controller. Swarnkar *et al.* [98] explained application of MRAC and further extended this research in [99]. The outcomes are evaluated for different adaptation mechanisms due to variations in adaptation gain. Jain *et al.* [100] concluded that MRAC responses fast with larger overshoots for large values of adaptation gain and for small values of gain slow response with small overshoot is obtained thus the gain selection is extremely important and is dependent on the signals. Sowparnika [101] demonstrated a comparison of response of PID and MPC controllers and the simulation results conclude that rise time is minimized with MPC and the converter model withstands the variation in the input voltage with different operating conditions. The basics of MPC detailed by Sultana *et al.* in [102] are beneficial for applying MPC schemes and to investigate controller's flexibility to design, analyse and implement in renewable systems. Dehghanzadeh *et al.* [103] reported that when compared to the PI controller, the continuous control MPC performed more effectively in terms of instantaneous and disturbance rejection. It also harvests higher amount of PV power due to its contribution towards improvising INC method for MPPT. Samani *et al.* [104] investigated MPC to obtain the optimal point with the help of a cost function. To attain MPPT in photovoltaic systems, a Cuk converter is studied using MPC and Fuzzy MPC. He also asserted that employing predictive equations eliminates the need for additional sensors. Pradhan *et al.* [105] presented PV modeling of grid connected system including MPC for MPPT. He concluded that MPC provides a faster MPPT response under varying conditions with improved efficiency. He also reported reduced power oscillation around MPP. The research in renewable using MPC as seen in literature is more refined to MPPT applications. Lanzon [106] proposed weight function optimization without wasting time in finding weights. The proposed method eliminates hit-trial methodology and eliminates error encountered in designing effective loop-shaping weights. Thus, the designer can concentrate on more fundamental design issues than simply finding weights. Phurahong *et al.* [107] suggested an approach for developing a robust controller for CMC buck converter, based on 2DOF H_∞ loop shaping concept. The findings also stated that the controller structure gets complicated with high order since the order of the controller is contingent to the order of the plant and weighting function. Sampaio *et al.* [108] worked on control methodology with uncertainties in buck converter and the controller gain has been obtained by using pole placement in accordance with the H_∞ constraint via linear matrix inequalities. Malik *et al.* [109] concluded that H_∞ controller is readily applicable to problems involving multivariate systems but the mathematical understanding of system needed to apply them remains a limitation. Azar

et al. [110] explains novel H$_\infty$ controller loop synthesis along with a PID controller loop shaping synthesis design procedure. Literature study on controllers concludes that controllers are be tuned based on certain defined operating range using mathematical models but they are subject to failure under changing load conditions. To guarantee the fast conversions, a controller needs be designed taking into consideration the stability of the emulator. Researchers have focused majorly on the deployment of digital CMC power converter systems. Holme *et al*. [111] explained a digital CMC divided into three subsystems: Analogue data acquisition, 16-bit DSP and a PWM. Evidently, it had significant drawbacks due to complicated hardware, high cost and low reliability. Boudreaux *et al*. [112] has considered ADC conversion, delay and resolution as non-linearity in parameters for buck converter model using 8-bit Microcontroller. Sustersic *et al*. [113] developed two-loop PI controller for the testing of the digital controller and converter with PWM in CMC. Alsumady *et al*. [114] described a simple, low-cost and efficient digital potentiometer controlled buck converter programmed for various output steps. The designed model can be utilized in hybrid power supplies for tracking pre-regulation efficiently.

Prominent reliability evaluation methods for PV applications that are covered in literature are based on "MIL-HDBK-217F [115], Monte-Carlo Simulation stated by Billinton *et al*. in [116] for complex systems, Markov Process [125-126] to improve efficiency and stability of entire system and Reliability Block Diagram (RBD) [117] concealing simulation of the PV system to gain information on system's availability/unavailability. It also reported the PV components that deteriorate at a faster rate during execution. Sykes *et al*. [118] investigated protection reliability, hidden failure, modeling and analysis, mean time to failure and failure rate data. Yao *et al*. [119] investigated two major failure mechanisms of converters. Underlying cause of component and assembly failure are thoroughly explained, as are prevention methods including quality control, soldering process control and external overstress for component reliability. Javadian *et al*. [120] calculated reliability of buck converter components and compared the P and N type MOSFETs based on reliability analysis. Components in RBD are connected in series, parallel, or a combination of these, according to Zhang *et al*. [121]. In RBD, a series configuration implies that all components should indeed work for the system to function properly, whereas a parallel configuration indicates that the system works if at least one of the components continues to work. Chavan [122] presented reliability analysis of DC-DC converter by part stress method and concluded that power switches have highest failure rates. The principle idea of reliability evaluation discussed by Gharehkoushan *et al*. in [123] is to determine failure rates that decrease PV output i.e., impact of voltage levels, power losses on

failure rates of panel components in working and out of service state. Kalaiarasi *et al*. [124] detailed reliability calculation for series system containing four components using Markov's Model and derived expression for F(t) and MTTF of the system. He concluded that as the value of t increases, R(t) decreases and F(t) increases. Gupta *et al*. [125] developed a PV-DC nanogrid with dual response converter to achieve better performance and reliability. To test the robustness in parametric variation, performance models like sensitivity and reliability models are explored. Markov reliability models have been investigated for MTTF by utilising data available in Military Handbook for Electronic Equipment Reliability Prediction (MIL-HDBK-217F). Navamani *et al*. [126] have modified structure of quadratic boost converter and calculated the reliability of model. The new model is shown more reliable than the existing model. Mohammadi *et al*. [127] described converter's reliability by relying on IGBT and diode thermal performance. The thermal interpretation is applied to measure the temperature of the switch and diode junctions. Airoboman *et al*. [128] carried out study of reliability of a network, derived mathematical model for reliability and to develop simulink model for the network. Kumar *et al*. [129] reviewed the scope for software techniques and models for evaluating Reliability, Availability and Maintainability (RAM) of complex systems. Juneja *et al*. [130] explained the reliability analysis by Fuzzy Petri net method to reduce calculation time including the dynamics of the system too. Kishor [131] discussed the thermal analysis of components and their effect on the reliability. It also addressed how f_{sw} and d affect power dissipation and T_j. Sayed *et al*. [132] investigated an improved RBD to predict the RAM performance, to monitor the critical subassemblies to enhance the availability and optimize maintenance cost. Yadav *et al*. [133] explained the reliability and availability analysis of converter subsystems using Markov's state transition modeling and the optimization is obtained by implementing GA and ANN.

These methods provide a good literature backup and ideas to fill the gaps found in previous work. Solar PV applications necessitate highly reliable component performance to circumvent risks and system failures, thereby minimising loss of life and system cost. This can be accomplished through reliability research and component significance analysis for enhancing overall system performance.

2.3 MAJOR FINDINGS AFTER LITERATURE REVIEW

The work described in the literature laid the groundwork for future research into PVE's improvement. The following findings formed the foundation for this work:

- Parasitic effects of components for PVE design can be considered to improve accuracy and study the dynamic performance of PVE.

- The scope of improving mathematical modeling using basic control and graph theory is broad.

- Only a few papers discussed SC and OC points on the VI characteristic curve, so they can be narrowed down.

- Robust controllers such as MPC, focus on MPPT rather than the entire VI characteristic curve. More robust controllers can be explored for PVE.

- There is a lack of comparison of control strategies used for designing and modeling of PVE.

- There has been little published work on reference models with parasitic effects.

- Limited work on comparing the performance of controllers for a PVE on a scale ranging from conventional to advanced controllers.

- Lack of reliability analysis of complete PVE to ensure effective designing.

- Conventional methods employed for reliability analysis focused only converter reliability.

- New computational and engineering alternatives must be devised to quickly and effortlessly assess the reliability and availability of the designed system.

The scope of modeling PVE with multiple reference models and controllers, not detailed in literature provide potential aid in a broader comparative analysis. The reliability analysis will widen the application areas of PVE and tackle availability issues also. The objective of this work is to provide a simple Emulator design by comparing conventional methods to AI-based methods and monitoring the Emulator's design constraints in case of various parameters, varying from idea to parasitic components. The aim is to obtain closest VI values for OC and SC regions. Different modeling, control and reliability techniques for PV Emulator will cover more aspects of non-linear solar panel applications.

CHAPTER 3
MATHEMATICAL MODELING OF PVE

3.1 INTRODUCTION

PVE is a closed-loop power electronic system that reproduces the properties of PV panel regardless of the surroundings. It is a DC-DC converter that is employed to evaluate PV systems since it closely mimics the reaction of a real PV panel and is unaffected by temperature or irradiation. Under these varying conditions, a PVE provides current and voltage characteristics of a solar panel. It is necessary for the following reasons:

- PV panels themselves are costly.

- Due to constantly fluctuating irradiance as well as other environmental factors, it is challenging to maintain and duplicate identical properties with PV panels.

- The PV simulator allows you to experiment with solar PV systems at night, in overcast weather and in low irradiance settings.

- By modifying the controller, it can easily reproduce the required properties of various PV panels while lowering the cost.

Accurate and reliable solar cell modeling is essential for improving the design of a solar PV system. [30]. MATLAB is a popular piece of software for simulating PV models with non-linear equations. Before putting the model into practise, simulation is necessary to ensure that it works properly [39]. The modeling of basic converters for PVE layout is covered in this chapter. It also explains how the values of the various components are determined. The methods used to calculate the converter's transfer function using both ideal and non-ideal elements are also covered in the following sections.

3.2 EMULATOR ARCHITECTURE

A converter is incorporated in PVE to convert the VI characteristic signals provided by PV model into power transmitting characteristics. The dynamic response of a competent PVE is similar to that of an actual PV panel. Because a PV panel is a nonlinear power supply, a PVE must provide power while maintaining the same nonlinear properties also like original panel. Equivalent circuit of PV generator method is one of three solutions accessible for developing a PVE, however it has the disadvantage of low quality due to dissipated power in the diode. The second technique focuses on the amplification of a basic cell, however it is only suited for lower power ratings [39].
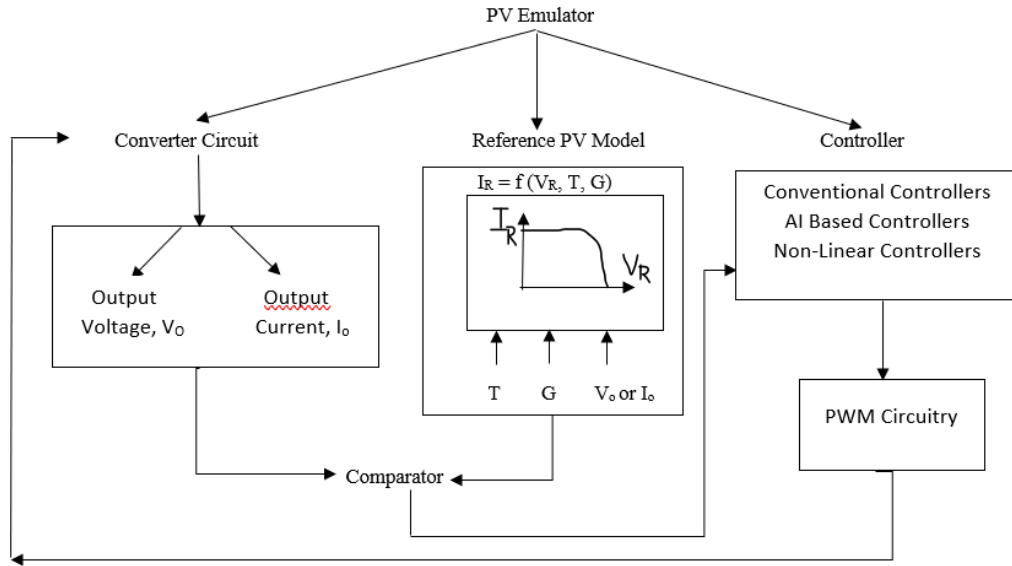
Figure 3.1 Basic Architecture of PV Emulator

A power converter is needed to transform the PV model's characteristic signal into the PVE's power transmitting signal. In power management applications, buck converter is a common converter topology. When V_{oc} is greater than the applied voltage, a buck converter is the best choice for a PVE. The interleaved buck converter has several drawbacks, including the need for complex controllers, substantial quantity of parts and sensitivity to non - symmetric duty cycle, which results in uneven current distribution across the inductor. As a result, current greater than the rated value flows through the inductors, diodes and MOSFETs, causing the converter to be ruined.

3.3 SUBSYSTEMS OF PVE

Because of the minimal number of components, simplicity of design and requirement of a lower value of V_{pv} than V_{in}, a buck converter was employed in this PVE design. Buck converters are simple devices made up of an inductor, a capacitor and switches that regulate the inductor. It alternates between integrating the inductor to the applied voltage and discharging it into the load to store energy in it. Storage elements include inductors and capacitors. As a result, they are time-dependent components. The inductor is a physical component that raises voltage. The capacitor is employed to keep the process stable. It prevents ripples, which are losses at the output.

Pulse Width Modulation (PWM) regulates the voltage applied to the LC circuit. PWM is a process for controlling modern power electronics circuits [134-135]. Based on the t_{on} and t_{off} of a cycle period, this voltage is separated into two halves. For the remainder of the cycle period, the voltage supplied to the LC circuit for t_{on} is V and the input voltage is zero. A power

switch performs in the cut-off and saturated regions of the power supply, causing small power loss at the switch. As a result, SMPS is employed to produce a very efficient PVE. Switched power supply, unlike linear regulators, can increase or decrease the input voltage. The energy retained by the inductor and capacitor can be repurposed to output voltages that are boost, reduced or passed through a transformer to provide electrical isolation from the input. The power switch requires a PWM to generate pulses. The goal is to regulate 'd' so that the load receives a controlled voltage. To prevent the LC filter from following each individual switching event, high f_{sw} is fixed.

3.4 TOPOLOGIES OF DC-DC BUCK CONVERTER

The functions of converter are:

- Line-load variations, circuit parameter variations and disturbance are all taken into account while regulating the output voltage.
- Using different topologies to convert dc input voltage to acceptable output dc levels.
- Invariably used for input source and load isolation in some cases.
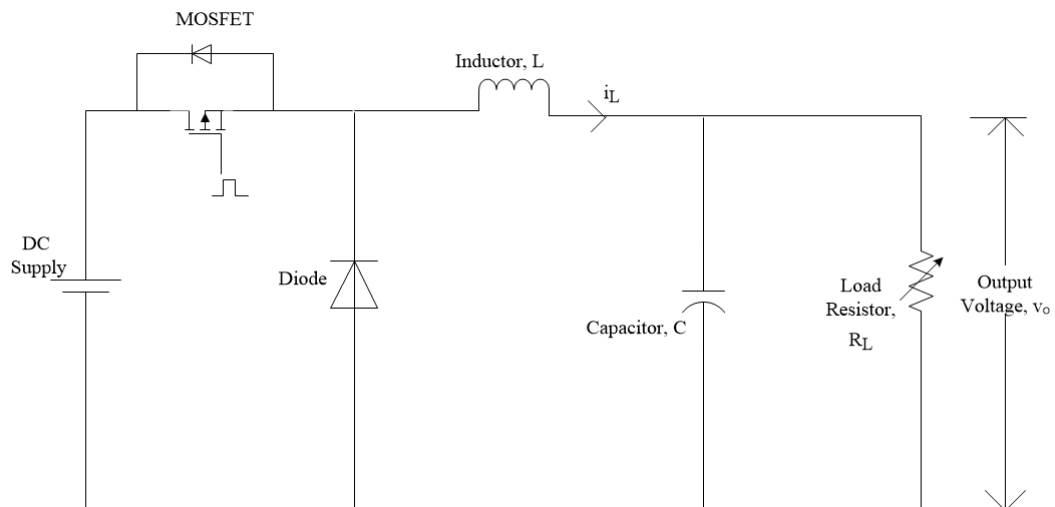
Figure 3.2: Ideal Buck Converter Circuitry

Figure 3.2 illustrates an ideal buck converter circuit with a voltage source and a pulse generator for the MOSFET's gate signal. The output is subjected to a resistive load. The following subheadings go through each of these components in further depth.

Value of L; $\qquad L = \dfrac{d(1-d)V_{in}}{f\Delta i_L}$ mH $\qquad\qquad$ (3.1)

Critical L value; $\qquad L_c = \dfrac{(1-d)R_L}{2f}$ $\qquad\qquad$ (3.2)

24

Value of C;
$$\Delta V_o = \frac{d(1-d)V_{in}}{8f^2 LC}$$

$$C = \frac{d(1-d)V_{in}}{8f^2 L\Delta V_o} \ \mu F \tag{3.3}$$

Critical C value;
$$C_c = \frac{(1-d)}{16f^2 L_c} \tag{3.4}$$

So, Duty ratio, $d = \frac{V_o}{V_{in}}$ (3.5)

3.4.1. Switch for PVE

In the actual world, semiconductor devices such as MOSFETs are used to make the switch. The switch toggles between open and closed positions at a high f_s and d. When switch S is ON, the input voltage is intrigued to the low pass filter; when switch S is OFF, the inductor retains its current flow, causing the diode to operate and current to flow through it. By adjusting the duty cycle with PWM and a closed loop circuit, a controllable voltage is achievable. Table 3.1 compares BJT and MOSFET devices for a better understanding of the devices for a certain application.

Table 3.1: Comparison of BJT and MOSFET

S.No.	BJT	MOSFET
1	Current Controlled device	Voltage Controlled device
2	Its switching time is high so, it generates more switching losses.	It functions better as compared to BJT while switching
3	Because the forward voltage drop resistance $R_{D\ (on)}$ is so low, BJTs perform well in conduction.	The forward voltage drop resistance $R_{D\ (on)}$ is higher in MOSFET.
4	It has a low input impedance, thus it requires a lot of current. As a result, it will require a huge amount of power to drive.	Less power is needed to drive it.

Table 3.2. shows comparison of power electronic switch devices based on their speed. And according to a particular application, choice can be made for efficient results.

Table 3.2: Comparison between BJT, IGBT and MOSFET

Parameters	BJT	IGBT	MOSFET
Switching Period	Slow	Medium	Fast
$R_{D\,(on)}$ forward voltage loss	Low	Low	Large
Gate driver/ Power Requirement	High	Low	Low

3.4.2. Operating Frequency for PVE

Higher efficiencies are achieved by using semiconductor switches having high switching frequencies and energy storage devices for dc-dc conversion. High f_{sw} permits lesser passive components while offer a sustainable transient performance. As the f_{sw} increases, the overall size and value of the components decline. There is a frequency limit beyond which the inductor or switching losses diminish the system's efficiency. At higher frequencies, the output capacitor is also smaller. As a result, f_{sw} is chosen depending on: D_1T

a. Minimum ON time (t_{on})
b. Maximum Input voltage

$$f_{sw} \leq \frac{1}{t_{on(min)}} \left(\frac{V_{output}}{V_{in(max)}} \right) \tag{3.6}$$

If the converter's min t_{on} is exceeded, it will skip pulses, modify the f_{sw}, or cause the output to become unregulated. t_{on}, on the other hand, fluctuates with temperature and load. Power semiconductors that are frequently turned on and off monitor the flow of energy in power supplies.

3.4.3. Diode for PVE

Since the inductor current does not vary sharply, the diode provides a channel at t_{off}. This diode gives direct current flow and ensures the current flow through the inductor. This is pivotal that the diode turns off quickly so, it permits conversion of the inductor's stored energy to load. As a result, the efficiency improves. When the switch is OFF, the current drops linearly and when the switch is ON, the current rises linearly.

3.4.4. Modes of Operation in DC-DC Converters

DC-DC converters operate in two distinct modes [134-135]:

- Continuous conduction mode (CCM)

  During operation, the inductor current is greater than zero in this mode of operation.

The CCM waveform of an inductor in buck converter is shown in Figure 3.3.
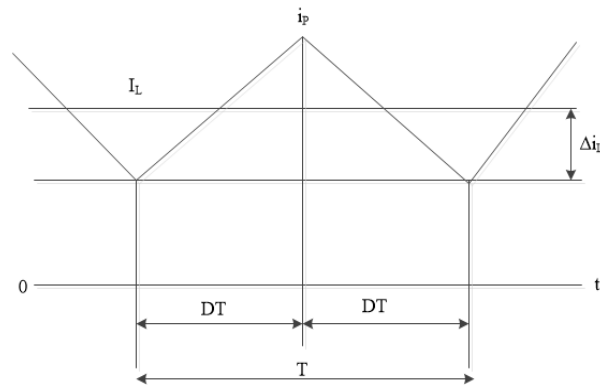
Figure 3.3: Waveform representing current in CCM

- Discontinuous conduction mode (DCM)

The inductor current becomes and remains zero for a fraction of the 'OFF' duration in this mode of operation as shown in Figure 3.4. This operation's inductor waveform is shown below:
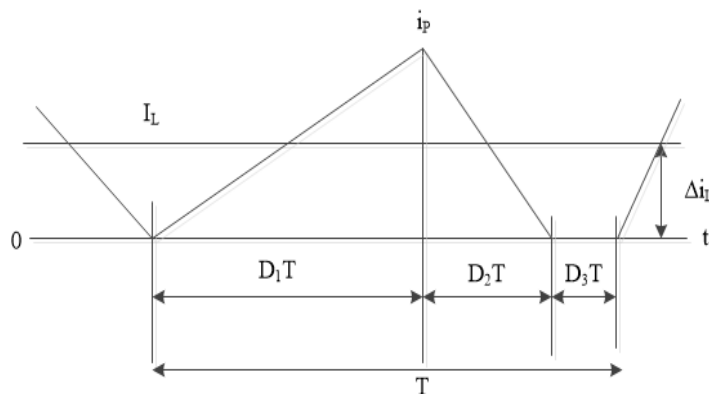
Figure 3.4: Waveform representing current in DCM

3.4.5. Small Signal Analysis

Small signal analysis involves circuit averaging, state space averaging, or PWM switch modeling and is the most popular method of modeling [63, 134,136]. Buck converters are examined in this chapter, as they are one of the most fundamental converters. The state-space descriptions for each switching state are substituted for a single state-space description, which eliminates the switching process and utilises them to represent the average of the switched networks during the operating cycle.
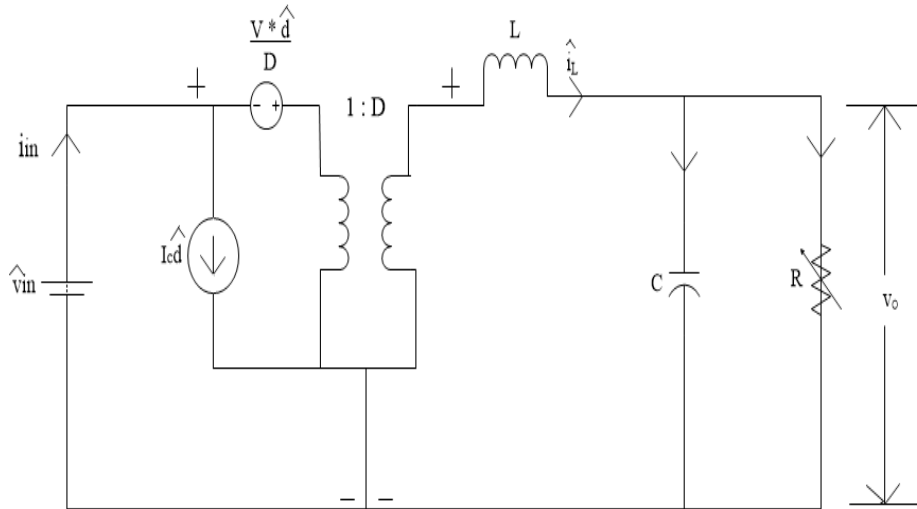
Figure 3.5: Small signal circuit of buck converter [134]

Figure 3.5 describes the small signal form with PWM for Buck converter. The system is simplified further by reconfiguring the average system and afterwards linearizing in the proximity of the steady-state values. The system input and output impedance and thus the transfer functions are derived after matrix operations. In the state-space averaging approach, the derivative of the i_L and v_c is explained by utilising network theory and are then averaged over a cycle. Figure 3.5 shows the computation of small signal analysis.

3.5 TRANSFER FUNCTION OF BUCK CONVERTER

To provide closed-loop transfer functions, the open-loop transfer function model is closed with voltage/current feedback from the output voltage/current. Various methods are applied in this work to obtain the transfer function.

3.5.1 Ideal Model of Buck converter for PVE model

Ideal model consists of ideal components operating in ideal conditions with negligible losses.

3.5.1.1 KCL and KVL approach

To evaluate the converter's transfer function, the ideal model of converter is explored [137-138]. The switch has two states ON and OFF as described in detailed in figures 3.6 and 3.7.

a. **Buck Converter (ON state)**
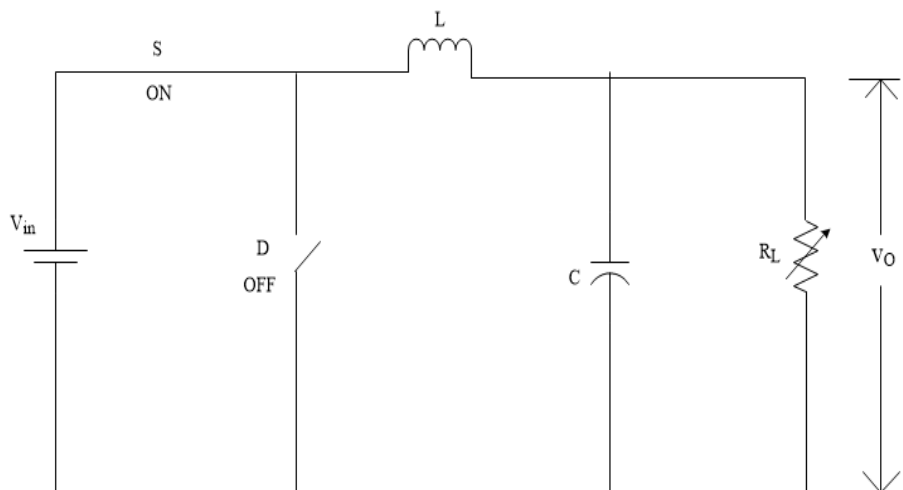
Figure 3.6: Buck converter with switch (S) in ON state

$$L\frac{di_L}{dt} = -v_0 + V_{in}$$

$$C\frac{dv_o}{dt} = i_L - \frac{v_0}{R} \tag{3.7}$$

b. **Buck Converter (OFF state)**
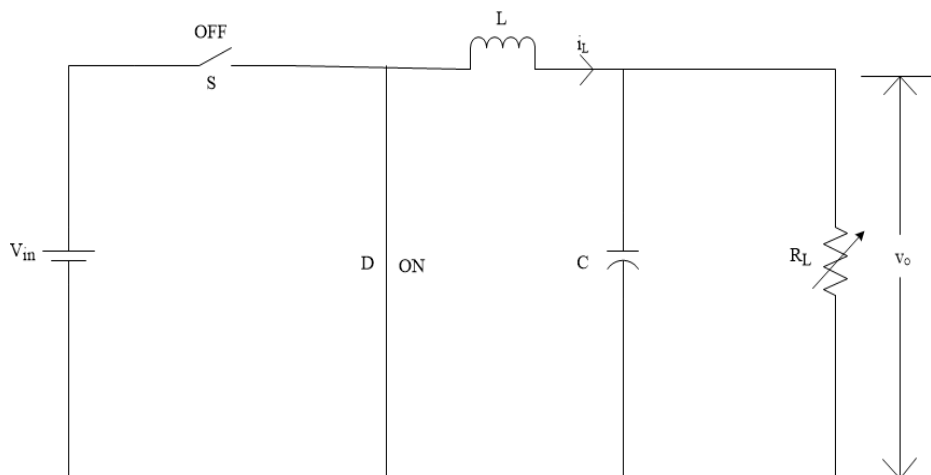
Figure 3.7: Buck converter with switch (S) in OFF state

$$L\frac{di_L}{dt} = -v_0$$

$$C\frac{dv_o}{dt} = i_L - \frac{v_0}{R} \tag{3.8}$$

Averaging above equations (3.7) and (3.8)

$$L\frac{\overline{di_L}}{dt} = -\overline{v}_0 + \overline{d_1}\,\overline{V_{in}} \tag{3.9}$$

$$C\frac{\overline{dv_o}}{dt} = \overline{I_L} - \frac{\overline{V_0}}{R} \tag{3.10}$$

Small Signal Analysis of average equations (3.9) and (3.0) gives:

$$sL(\tilde{\imath}_L + \overline{I_L}) = -(\widetilde{v_o} + \overline{V_0}) + (\overline{D_1} + \widetilde{d_1})(\widetilde{v_{in}} + \overline{V_{in}})$$

$$sL\tilde{\imath}_L + sL\overline{I_L} = -\widetilde{v_o} + \overline{V_0} + \overline{D_1}\,\widetilde{v_{in}} + \widetilde{d_1}\,\widetilde{v_{in}} + \overline{D_1}\,\overline{V_{in}} + \widetilde{d_1}\,\overline{V_{in}}$$

Taking AC components, we get:

$$sL\tilde{\imath}_L = -\widetilde{v_o} + \overline{D_1}\,\widetilde{v_{in}} + \widetilde{d_1}\,\widetilde{v_{in}} + \widetilde{d_1}\,\overline{V_{in}} \tag{3.11}$$

$$\frac{C\overline{dv_o}}{dt} = \overline{I_L} - \frac{\overline{V_0}}{R}$$

$$sC(\widetilde{v_o} + \overline{V_0}) = (\tilde{\imath}_L + \overline{I_L}) - \left(\frac{\widetilde{v_o}}{R} + \frac{\overline{V_0}}{R}\right)$$

$$sC(\widetilde{v_o}) = (\tilde{\imath}_L) - \left(\frac{\widetilde{v_o}}{R}\right) \tag{3.12}$$

From Average equations;

$$L\frac{\overline{di_L}}{dt} = 0$$

Therefore, we get $0 = -\overline{V_0} + \overline{D_1}\,\overline{V_{in}}$

So, we get the duty cycle; $\frac{\overline{V_0}}{\overline{V_{in}}} = \overline{D}_{in}$ \hfill (3.13)

Also; $sC(\overline{V_0}) = \overline{I_L} - \frac{\overline{V_0}}{R}$

$$0 = \overline{I_L} - \frac{\overline{V_0}}{R}$$

$$\overline{I_L} = \frac{\overline{D_1}\,\overline{V_{in}}}{R} \tag{3.14}$$

Small Signal Analysis of equation (3.11) and (3.12) gives;

$$sL\tilde{\imath}_L = -\widetilde{v_o} + \overline{D_1}\,\widetilde{v_{in}} + \widetilde{d_1}\,\widetilde{v_{in}} + \widetilde{d_1}\,\overline{V_{in}}$$

$$s\tilde{\imath}_L = \frac{1}{L}\left[-\widetilde{v_o} + \overline{D_1}\,\widetilde{v_{in}} + \widetilde{d_1}\,\widetilde{v_{in}} + \widetilde{d_1}\,\overline{V_{in}}\right]$$

$$s\tilde{\imath}_L = \left[-\frac{\tilde{v}_o}{L} + \frac{\overline{D_1}}{L}\widetilde{v}_{in} + \tilde{d}\frac{\overline{V_{in}}}{L} \right] \qquad (3.15)$$

$$sC\widetilde{v_o} = \tilde{\imath}_L - \frac{\widetilde{v_o}}{R}$$

$$s\widetilde{v_o} = \frac{\tilde{\imath}_L}{C} - \frac{\widetilde{v_o}}{RC} \qquad (3.16)$$

The expression for $\frac{\widetilde{V_o}}{\tilde{d}}$ of buck converter is:

$$\frac{\widetilde{V_o}}{\tilde{d}} = \frac{\frac{V_{in}}{LC}}{s^2 + \frac{1}{RC}s + \frac{1}{LC} + \frac{V_{in}}{LC}} \qquad (3.17)$$

3.5.1.2 Signal Flow Graph Method

SFG is a graphical way of calculating a control system's transfer function. The primary benefit of this method is that it provides a simplified approach for evaluating the transfer function without having to redraw the system multiple times. It decreases the number of components by substituting nodes and loops for them. Mason's Gain formula is used to compute the overall system's transfer function [139-140].

Using equations (3.15) and (3.16) following signal flow graph Figure 3.8, is obtained
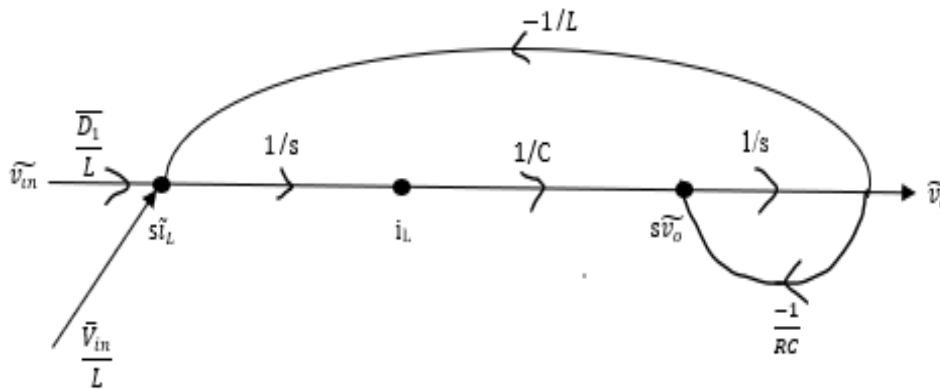
Figure 3.8: Signal Flow Graph of ideal buck converter

Figure 3.8 describes ideal buck's SFG plot obtained using above derived equations.

Solving above SFG by Mason's Gain Formula:

Forward Path Gain $= \frac{\overline{D_1}}{L} * \frac{1}{s} * \frac{1}{C} * \frac{1}{s}$

Loop Gains; $L_1 = \frac{-1}{sRC}$; $L_2 = \frac{-1}{s^2RC}$

$$\Delta_1 = 0$$

$$\Delta = 1 + \frac{1}{sRC} + \frac{1}{s^2RC}$$

Transfer function; $\frac{\widetilde{V_o}}{\widetilde{v}_{in}} = \frac{\widetilde{d}}{RLCs^2 + Ls + R} * R$ (3.18)

$$\frac{\widetilde{V_o}}{\widetilde{d}} = \frac{v_{in}}{LC(s^2 + \frac{1}{RC}s + \frac{1}{LC})}$$ (3.19)

3.5.2 Buck Model with Non-ideal components

A buck converter having non-ideal components is shown in Figure 3.9. This block is used to describe equations governing the behavior of the converter in both the ON and OFF states.
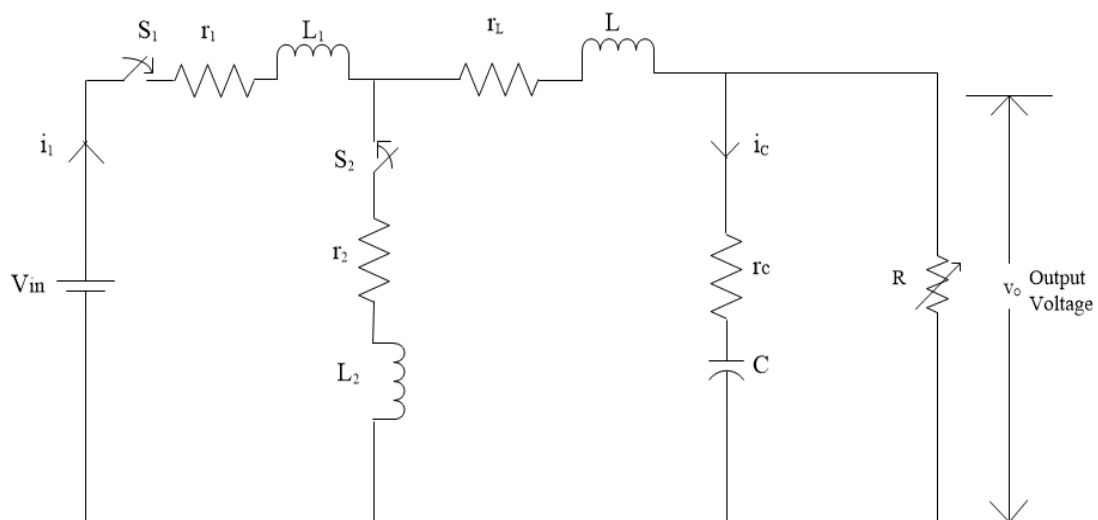
Figure 3.9: Model with non ideal components

L_1, r_1 represent MOSFET; L_2, r_2 represent Diode; L, r_L represent Inductor; C, r_C represent Capacitor

3.5.2.1 KCL and KVL approach

a. Buck converter (ON state) with non-ideal components
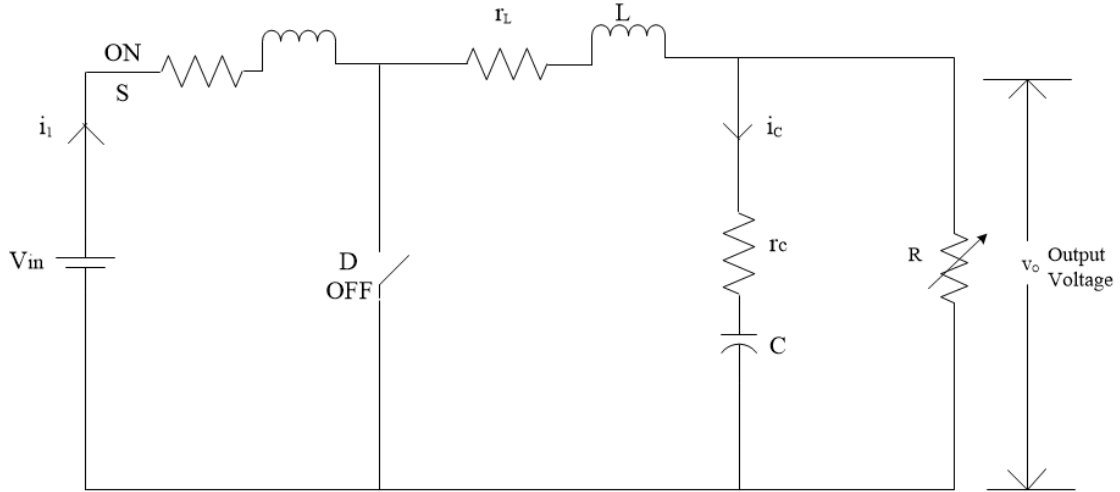
Figure 3.10: Buck converter with switch (S) ON with non-ideal components

By KVL;

$$V_{in} = L_1\frac{di_1}{dt} + i_1 r_1 + L\frac{di_1}{dt} + i_1 r_L + i_1 R_1 \tag{3.20}$$

By KCL;

$$i_1 = C\frac{dv_c}{dt} + i_0 + \frac{v_0}{R} \tag{3.21}$$

$$V_0 = v_c + r_c C\frac{dv_0}{dt} \tag{3.22}$$

(3.20) implies; $V_{in} - i_1 r_1 - i_1 r_L + i_1 R_1 = L_1\frac{di_1}{dt} + L\frac{di_1}{dt}$ (3.23)

(3.21) implies; $i_1 = i_c + \frac{v_0}{R} + i_0$

(3.22) implies; $i_c = \frac{Cdv_c}{dt} + \frac{R}{R+r_c} i_1$

$$L_1\frac{di_L}{dt} + L\frac{di_L}{dt} = V_{in} - i_1 r_1 - i_1 r_L + i_1 R$$

(3.24a)

$$i_1 = C\frac{dv_c}{dt} + \frac{R}{R+r_c} i_1 + \frac{v_0}{R} + i_0 R$$

$$\frac{Cdv_c}{dt} = i_1 - i_0 - \frac{R}{R+r_c} i_1 - \frac{v_0}{R} \tag{3.24b}$$

33

b. Buck Converter (OFF state) with non-ideal components
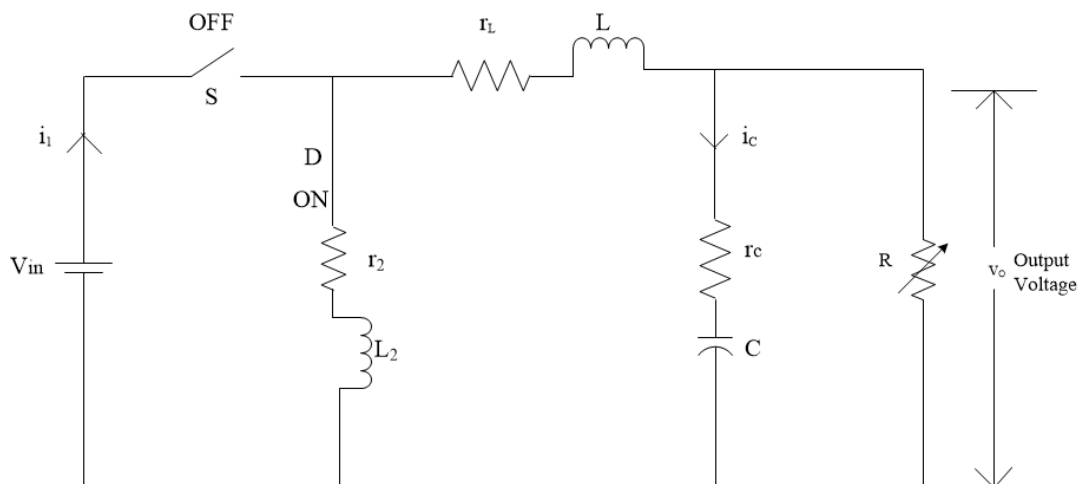
Figure 3.11: Buck converter with switch (S) OFF with non-ideal components

On applying KVL in Figure 3.11 gives;

$$0 = L_2 \frac{di_1}{dt} + L \frac{di_1}{dt} V_{in} - i_1 r_2 - i_1 r_L + i_1 R \qquad (3.25a)$$

By KCL;

$$i_1 = C \frac{dv_c}{dt} + \frac{R}{R + r_c} i_1 + \frac{v_o}{R} + i_o$$

$$\frac{C dv_c}{dt} = i_1 - i_o - \frac{R}{R + r_c} i_1 - \frac{v_0}{R} \qquad (3.25b)$$

3.5.2.2 Signal Flow Graph Method

Considering $\overline{d_1}$ = ON mode and $\overline{d_2}$ = OFF mode; Averaging (ON state) from above equations:

$$\overline{d_1} L_1 \frac{\overline{di_1}}{dt} + \overline{d_2} L_2 \frac{\overline{di_1}}{dt} + L \frac{\overline{di_1}}{dt} = \overline{d_1} \overline{V_{in}} - \overline{d_1}(\bar{\imath}_1 r_1) - \overline{d_1}(\bar{\imath}_1 r_L) - \overline{d_1}(\bar{\imath}_1 R) - \overline{d_2}(\bar{\imath}_1 r_2) -$$

$$\overline{d_2}(\bar{\imath}_L r_L) - \overline{d_2}(\bar{\imath}_L R) \qquad (3.26)$$

Averaging (OFF state) from above equations:

$$\frac{C\overline{dv_c}}{dt} = \overline{d_1}\bar{\imath}_1 - \bar{\imath}_0 - \overline{d_1} \frac{R}{R+r_c} \bar{\imath}_1 - \overline{d_2} \frac{R}{R+r_c} \bar{\imath}_L - \frac{\overline{v_o}}{R} \qquad (3.27)$$

Small Signal Analysis of average equations (3.26) and (3.27) gives:

$$sL_1(\tilde{\imath}_1 + \overline{I_1})(\tilde{d}_1 + \overline{D_1}) + sL_2(\tilde{\imath}_1 + \overline{I_1})(\tilde{d}_2 + \overline{D_2}) + sL(\tilde{\imath}_1 + \overline{I_1}) = (\tilde{v}_{in} + \overline{V_{in}})(\tilde{d}_1 +$$

$$\overline{D_1}) - r_1(\tilde{\imath}_1 + \overline{I_1})(\tilde{d}_1 + \overline{D_1}) - r_L(\tilde{\imath}_1 + \overline{I_1})(\tilde{d}_1 + \overline{D_1}) - R(\tilde{\imath}_1 + \overline{I_1})(\tilde{d}_1 + \overline{D_1}) - r_2(\tilde{\imath}_1 +$$

$$\overline{I_1})(\tilde{d}_2 + \overline{D_2}) - r_L(\tilde{\imath}_1 + \overline{I_1})(\tilde{d}_2 + \overline{D_2}) - R(\tilde{\imath}_1 + \overline{I_1})(\tilde{d}_2 + \overline{D_2}) \qquad (3.28)$$

$$s\,\tilde{\imath}_1\,[\,L_1\,\overline{D_1}\,+L\,] = \tilde{d}_1\,\overline{V_{in}} + \overline{D_1}\,\tilde{v}_{in} - r_1\overline{D_1}\ \tilde{\imath}_1 - r_2\overline{D_2}\tilde{\imath}_1 - r_L\overline{D_1}\tilde{\imath}_1 - r_L\overline{D_2}\tilde{\imath}_1 - R\overline{D_1}\tilde{\imath}_1 -$$

$$R\overline{D_2}\tilde{\imath}_1 \qquad (3.29)$$

$$sC\tilde{v}_c = \overline{D_1}\,\tilde{\imath}_1 - \tilde{\imath}_0 - \overline{D_1}\,\frac{R}{R+r_c}\,\tilde{\imath}_1 - \overline{D_2}\,\frac{R}{R+r_c}\,\tilde{\imath}_1 - \frac{\overline{V_o}}{R}(\overline{D_1}\,\overline{D_2})\frac{R}{R+r_c}\,\tilde{\imath}_1 \qquad (3.30)$$

c. Signal Flow with Parasitic effect

Using above equations, following signal flow graph is obtained with parasitic components.
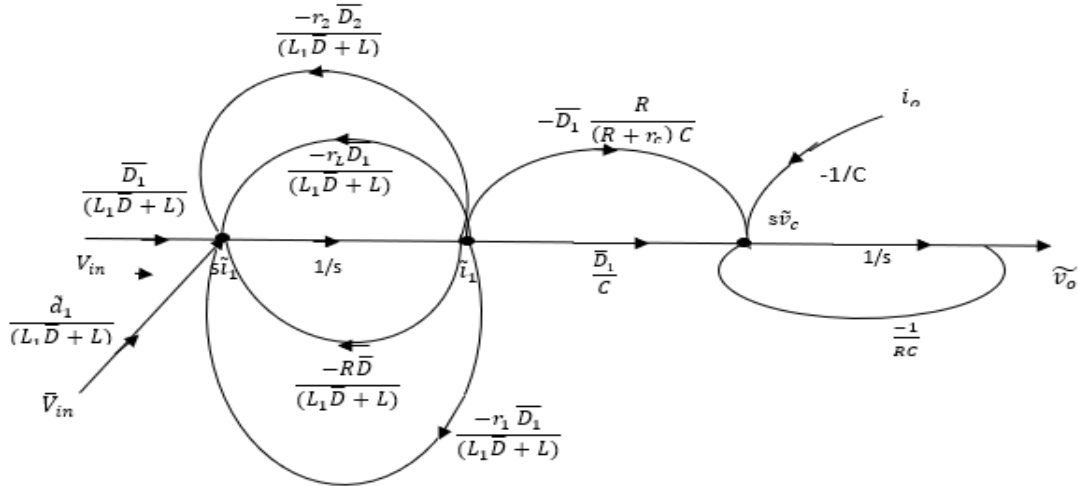
Figure 3.12: Signal Flow Graph of buck converter with Parasitic effect

Figure 3.12 illustrates the SFG of a Buck converter with the parasitic effect computed using the calculations above. Mason's Gain formula is also used to determine the transfer function.

Forward Path Gain = $\dfrac{\overline{D_1}}{(L_1\overline{D}+L)} * \dfrac{1}{s} * \dfrac{\overline{D_1}}{C} * \dfrac{1}{s}$

Loop Gains; $L_1 = \dfrac{1}{s} * \dfrac{-R\overline{D_1}}{(L_1\overline{D}+L)}$

$L_2 = \dfrac{1}{s} * \dfrac{-r_1\overline{D_1}}{(L_1\overline{D}+L)}$

$L_3 = \dfrac{1}{s} * \dfrac{-r_L\overline{D}}{(L_1\overline{D}+L)}$

$$L_4 = \frac{-r_2\overline{D_2}}{s(L_1\overline{D}+L)}$$

$$L_5 = \frac{1}{sRC}$$

$$\Delta = 1 + \left[\frac{R\overline{D}+r_1\overline{D_1}+r_L\overline{D}+r_2\overline{D_2}}{s(L_1\overline{D}+L)}\right] + \frac{1}{sRC} + \frac{R\overline{D_1}}{s^2RC(L_1\overline{D}+L)} + \frac{r_1\overline{D_1}}{s^2RC(L_1\overline{D}+L)} + \frac{r_L\overline{D}}{s^2RC(L_1\overline{D}+L)} +$$

$$\frac{r_2\overline{D_2}}{s^2RC(L_1\overline{D}+L)}$$

Pair of Non-touching loops are L_1L_5, L_2L_5, L_3L_5 and L_4L_5

Transfer function; $\frac{\widetilde{V_o}}{\widetilde{v}_{in}} =$

$$\frac{\frac{\overline{D_1^2}}{s^2C(L_1\overline{D}+L)}}{1+\left[\frac{R\overline{D}+r_1\overline{D_1}+r_L\overline{D}+r_2\overline{D_2}}{s(L_1\overline{D}+L)}\right]+\frac{1}{sRC}+\frac{R\overline{D_1}}{s^2RC(L_1\overline{D}+L)}+\frac{r_1\overline{D_1}}{s^2RC(L_1\overline{D}+L)}+\frac{r_L\overline{D}}{s^2RC(L_1\overline{D}+L)}+\frac{r_2\overline{D_2}}{s^2RC(L_1\overline{D}+L)}} \tag{3.31}$$

$$\frac{\widetilde{v_o}}{\tilde{d}} = \tilde{v}_{in}\left[\frac{1+sr_cC}{1+s\left(r_cC+\frac{Rr_L}{R+r_L}C+\frac{L}{R+r_L}\right)+s^2LC\left(\frac{R+r_c}{R+r_L}\right)}\right]$$

3.6 CONCLUSION

This chapter covered PVE mathematical modeling required for a variety of applications. PV cell modeling with software has become an important tool for researchers. The ability to generate quick and cost-effective solutions is an essential aspect of this work. The important conclusions of this chapter are:

- PVE simulation must be accurate and dependable to enhance the designing aspect of a PV system.
- Modeling the system before implementing it, is cost-effective and reliable in terms of design and development.
- The modeling and selection criteria for buck converter components for PVE design are explained in this chapter.
- The transfer functions for ideal and non-ideal components are derived by different methods to precisely tune controllers in close loop circuitry. The derived methods were implemented to determine the transfer function from output voltage to input voltage and output voltage to duty ratio. This helped in finding parameter ratio for the transfer function depending on the applications without attempting to solve complex circuits.

- The equations obtained by solving the SFG's help in calculating transfer function in a simpler way. The implementation of non-ideal components will help in overall modeling which is replica of actual PV panel. These equations form the fundamental base for designing the reference models and various controllers as discussed in further chapters.

CHAPTER 4
REFERENCE MODEL TOPOLOGIES AND THEIR IMPLEMENTATION

4.1 INTRODUCTION

PV panels are made up of interconnected non-linear PV cells to obtain electricity from solar energy [20]. The experimental data of characteristics curves for varying irradiance and temperature is available on the data sheets provided with PV panels, necessitating the use of a lookup table or diode models to provide reference values.

4.1.1 Feedback Loop Architecture

In PVE modeling, the main purpose of lookup tables or diode models is to store VI characteristics of the emulated panel and provide the reference value. The architecture employed in the PVE can be described by two models.

- Electrical circuit model
- Interpolation model

The characteristic equation is obtained using KVL and KCL and the final electrical model is actually the PV modeling rendered as an electrical circuit. This model, often called as the analytical model, is frequently used in PVE implementations. Electrical circuit models are divided into three types:

- 1D model
- 2Dmodel
- 3D model

4.2 DIRECT CALCULATION METHOD

The reference model is fed into emulator's controller using direct calculation method. A popular PV reference model is diode model [141-144].

4.2.1 One diode (1D) model

Researchers have studied a variety of solar cell models. [145- 147]. Figure 4.1 shows 1D model with two resistors, also known as the 1D-2R model. Here one diode as well as series and shunt resistances R_{sh}, are considered.

When a model needs to be reused repeatedly for different panels, modeling is a simple and quick approach. V_{oc}, I_{sc}, MPP are important points on the PVE reference curve.
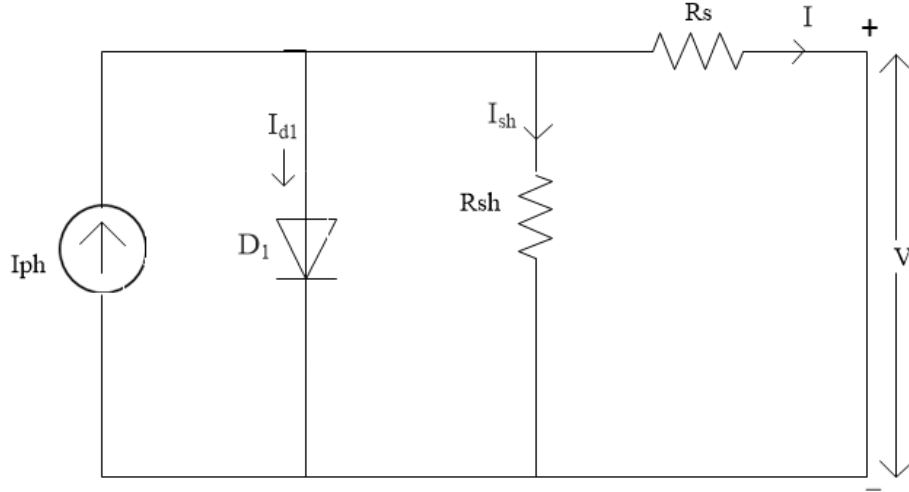
Figure 4.1 One diode model (1D2R)

Variable irradiance influences the I_{sc}, while temperature influences the V_{oc}. The following equations vividly show the relationships between these terms. Because of its simplicity and reasonable accuracy, 1D model is the most popular model for PV module modeling. Simple techniques can also be used for finding 1D model parameters.

Mathematical Modeling

a. Photo Current; $I_{ph} = [I_{sc} + k_i (T\text{-}298)] \frac{G}{1000}$ (4.1)

b. Saturation Current; $I_o = I_{rs} (\frac{T}{T_n})^3 \exp [\frac{qE_{go} (\frac{1}{T_n} - \frac{1}{T})}{nk}]$ (4.2)

c. Reverse Saturation Current; $I_{rs} = \dfrac{I_{sc}}{[\exp^{\left(\frac{qV_{oc}}{nN_s kT}\right)-1}]}$ (4.3)

d. Current through shunt resistor; $I_{sh} = \dfrac{(V+IR_s)}{R_{sh}}$ (4.4)

e. Output Current; $I = I_{ph} - I_o [\exp^{\left(\frac{q(V+IR_s)}{nN_s kT}\right)-1}] - I_{sh}$ (4.5)

For the required system, MATLAB simulation has advantages like graphical user interface, a block diagram implementation, platform to construct appropriate functions and integrate program code in a direct way. The basic block layouts of diode model based on the preceding equations are shown in the following figures. To have a better knowledge of each current component, a set of macro models for sub-blocks is drawn. The leakage current at the p-n junction is depicted by parallel resistor. It influences the V_{oc} and has no effect on I_{sc}. In the constant current area, an increase in parallel resistance decreases the V_{oc} and increases the slope

of the PV module's VI characteristic curve. If the slope of the VI characteristic curve at the I_{sc} = 0, the parallel resistance is believed to be infinity. Because the irradiance is frequently increasing, 1D methodology is best suited to PV modules with amorphous silicon fabrication. However, it's not effective for small irradiance circumstances as the model ignores the effects of recombination of space charge.
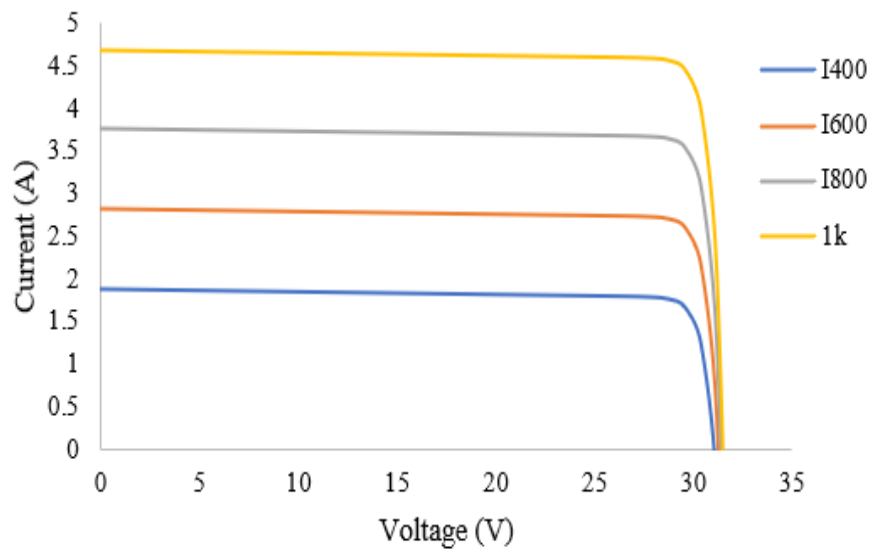
(a)
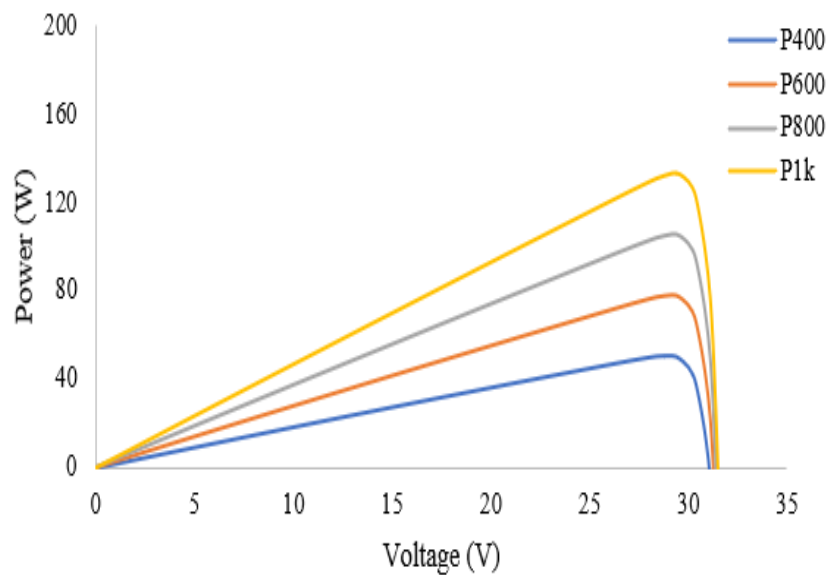
(b)

Figure 4.2(a): Typical characteristics of PV panel for varying irradiance (W/m²) (a-b)
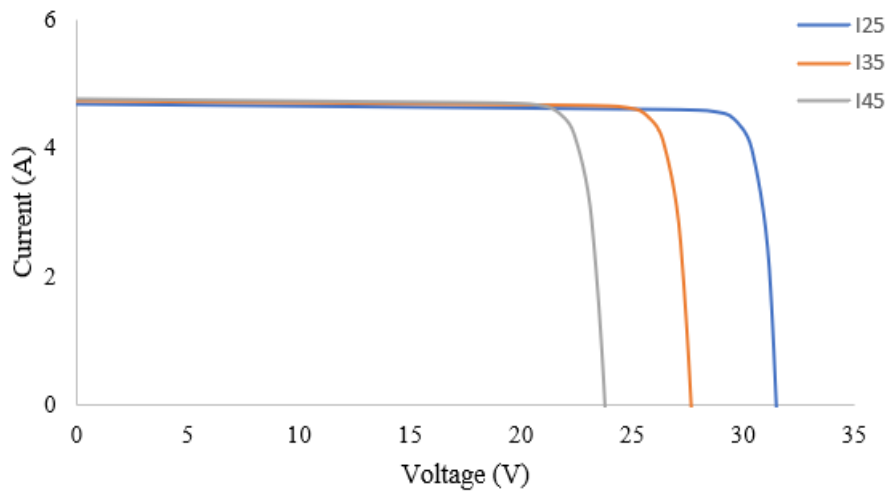
(a)
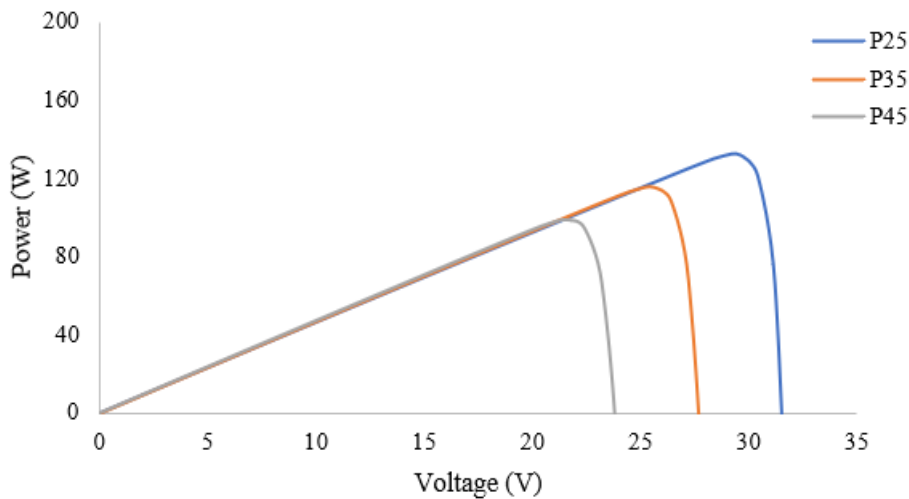
(b)

Figure 4.2(b): Typical characteristics of PV panel for varying temperature (˙C) (a-b) of 115W PV panel.

Figure 4.2(a) and Figure 4.2(b) demonstrate the typical characteristics of PV panel for irradiance varying from 400 to 1000 W/m² and temperature varying from 25 degrees to 45 degrees for 115W PV panel respectively. Various reference models are designed to follow these characteristics in close approximation for effective modeling of PVE. Following sections cover various reference model schemes adopted for designing of required PVE.

4.2.2 Two Diode (2D) model

The PV power producing unit is built around a PV cell. It's a semiconductor converting solar energy into voltage. Modules are formed by connecting these cells. To create a complete PV system, these modules are connected to the components. The type N semiconductor in a solar

cell is illuminated by the sun, while the type P semiconductor stays in the solar cell's back [20]. When adopting the PV electrical circuit model, another aspect to consider is the ideality factor. The ideality factor = 1, in ideal conditions. In actuality, however, this number fluctuates relying on the junction behaviour's non-ideality. Depending on the fabrication technique, the ideality factor ranges from 1 to 2 [148]. It is a function of voltage across the device in the preceding one diode calculations, but it is a dependent on voltage across the device in actuality. The surfaces control the combination in the device at higher voltages, therefore the ideality factor approximates 1. At small voltages, on the other hand, the junction combination is already controlled, hence the ideality factor is set to two. An extra diode connected in parallel with the previous diode is used to model this junction combination. The two-diode cell model's functioning is described by the equations below.
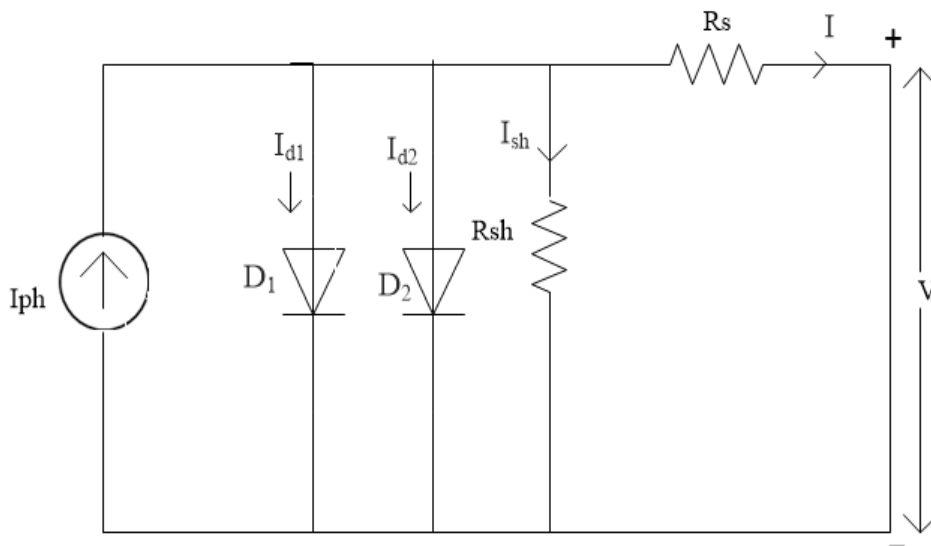
Figure 4.3: Two Diode model of a Solar cell

$$I = I_{ph} - I_{o1} \, e[^{\frac{(V+IR_s)}{a_1 VT_1}} - 1] - I_{o2} \, e[^{\frac{(V+IR_s)}{a_2 VT_2}} - 1] + \frac{(V+IR_s)}{R_{sh}} \qquad (4.6)$$

4.2.3 Three Diode model

For the above models, an increase in quantity of diodes results in reduction in V_{oc} and maximum power drawn, despite the change in ideality factors. In all three models, I_{sc} is much the same [149-150]. The following are the equations that define the cell model:

$$I = I_{ph} - I_{d1} - I_{d2} - I_{d3} - I_{sh} \qquad (4.7)$$

$$I_{ph} = I_{sc} + k_i \, (\Delta T) * \frac{G}{1000} \qquad (4.8)$$
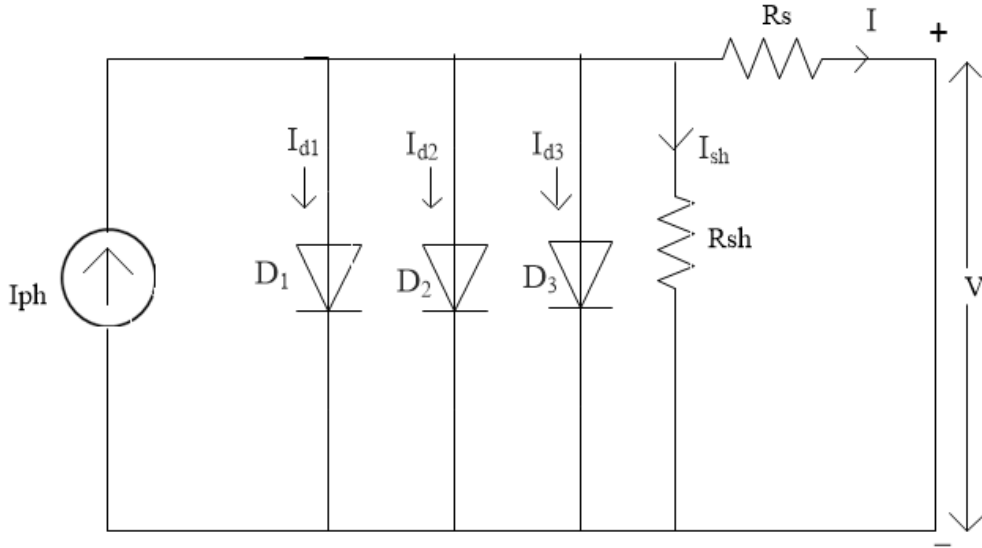
Figure 4.4: Three Diode model of a Solar cell

$$I_{sh} = \frac{(V + IR_S)}{R_{sh}} \qquad (4.9)$$

$$I_{d1} = I_{o1}\,e\left[\frac{(V+IR_S)}{a_1 VT_1}\right] \qquad (4.10)$$

$$I_{d2} = I_{o2}\,e\left[\frac{(V+IR_S)}{a_2 VT_2}\right] \qquad (4.11)$$

$$I_{d3} = I_{o3}\,e\left[\frac{(V+IR_S)}{a_3 VT_3}\right] \qquad (4.12)$$

Because of its precision under low irradiance conditions, two and three diode models are better for simulating partial shading conditions. This approach is also applicable to panels made of monocrystalline silicon or polycrystalline silicon. This approach is implemented in PVE to avoid overheating of diodes and thus increase the reliability and availability of the system.

Under varying irradiance and temperature conditions, these models produced faster results. It was simple to adapt the models to various external parameters and even different panel ratings. By acquiring reference values matching to the panel to be emulated, factors like accuracy and stability can be attained efficiently.

4.3 LOOK UP TABLE METHOD

An extensively utilized strategy in emulator is the look-up table (LUT) method [151-152]. The VI characteristic of the PV are depicted using diverse look-up table methods [153].

LUT's response is mainly applied as the reference signal to PV emulator's loop converter circuit [154]. LUT's circumvent the constraints of the simple look-up table and thus table has

been enhanced as V-R table. Because the input is entered by dividing the voltage and current response. The R_{pv} is taken as the table's input and V_{pv} act as the table's output. For VI-R LUT having R_{pv} as input and V_{pv} along with I_{pv} as output, the reference signal is generated according to the output resistance.

4.4 PIECEWISE LINEAR METHOD

The piecewise linear method is a curve estimating method that uses various subdivided straight lines to follow the PV characteristic curve in simplest manner for PV emulator [155].

$$V = (-0.0096)\ I^2 + (0.211)\ I + 4.037 \tag{4.13}$$

represents the second order equation for above linearization curve with $R^2 = 0.899$ using excel.

In general; $V = a_2\ I^2 + a_1\ I + a_0$ (4.14)

$V_{OC} = a_0$ (as at Open Circuit, I will be zero) (4.15)

$V_p = a_2\ I_p^2 + a_1\ I_p + a_0$ (at MPP, $I = I_p$ and $V = V_p$) (4.16)

$0 = a_2\ I_{sc}^2 + a_1\ I_{sc} + a_0$ (at Short-circuit, $I = I_{sc}$ and $V = 0$) (4.17)

Data sheet of panels provide values of V_{OC} , I_{sc} , V_p and I_p thus, a linearized plot can be obtained easily by solving above equations by matrix algebra.

$$\begin{bmatrix} V_{OC} \\ V_p \\ 0 \end{bmatrix} = \begin{bmatrix} 1 & 0 & 0 \\ 1 & I_p & I_p^2 \\ 1 & I_{sc} & I_{sc}^2 \end{bmatrix} * \begin{bmatrix} a_0 \\ a_1 \\ a_2 \end{bmatrix} \tag{4.18}$$

Substituting values of a will provide an equation $V = f\ (I)$ and thus the reference values can be obtained at different points.

Another method of obtaining linear equations in two parts shown in above figure are derived by standard slope intercept equation $y = mx + c$. From part I of above graph we get

$$(I - I_{SC}) = \frac{(I_P - I_{SC})}{(V_P - 0)} * (V - 0) \tag{4.19}$$

$$(I - I_P) = \frac{(0 - I_P)}{(V_{OC} - V_P)} * (V - V_P) \tag{4.20}$$

Using equation (4.19); $I = -0.0156*V + 4.7$ (4.21)

Using equation (4.20); $I = -0.7133*V + 19.10$ (4.22)

Thus, the piecewise linear model equation can be derived in two distinct ways. The first method is to apply the module's selected point. The chosen points are I_{sc}, V_{oc} and MPP, given in the PV panel's datasheet. This model can only generate the VI characteristic curve @STC because the manufacturer provides these three points at STC. This technique, however, is optimised by the addition of functions which adjust the three selected values based on irradiance and panel temperature [156]. The second method is to show the correlation precisely on the PV curve's I-V characteristic. The minimum number of straight lines required for this strategy in the PVE are two and the maximum lines for this approach are five. Each drawn line's slope and y-axis intersection are graphically determined. There is no restriction on the number of lines that can be deployed to fit characteristics. The limitation is that during the PVE operation, the irradiance and panel temperature could not be modified [157].

4.5 RESULTS AND DISCUSSION

Various reference model topologies and methods are described in this chapter. These methods were applied to closed loop buck converter to get results matching the actual PV panel. Following plots were obtained on applying these reference models to different controllers to show the effectiveness of results.
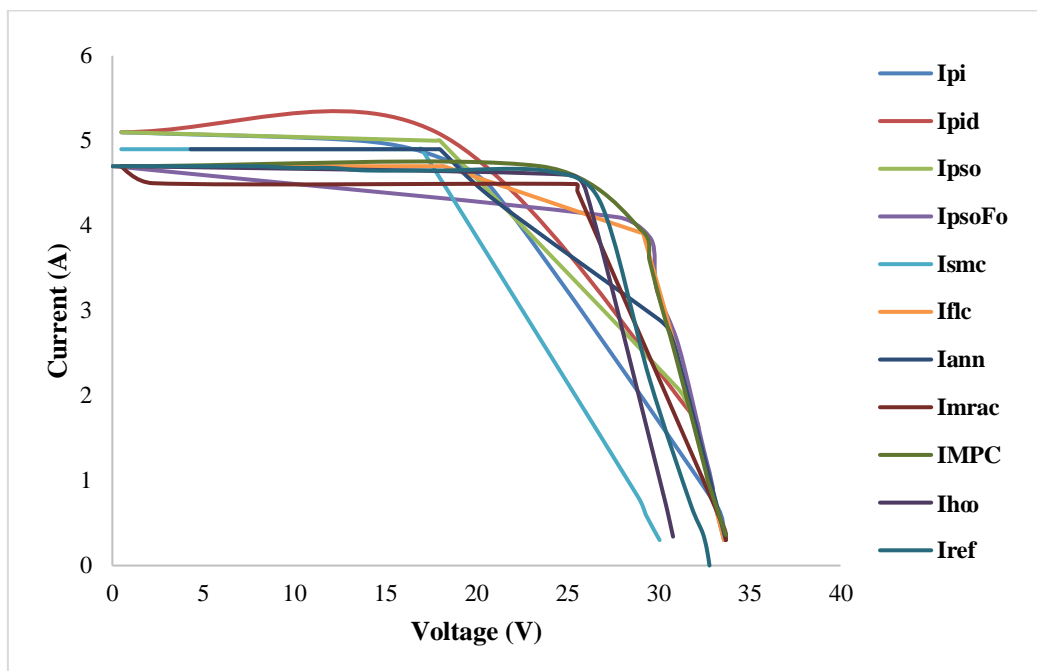
Figure 4.5: VI characteristics using 1D reference model
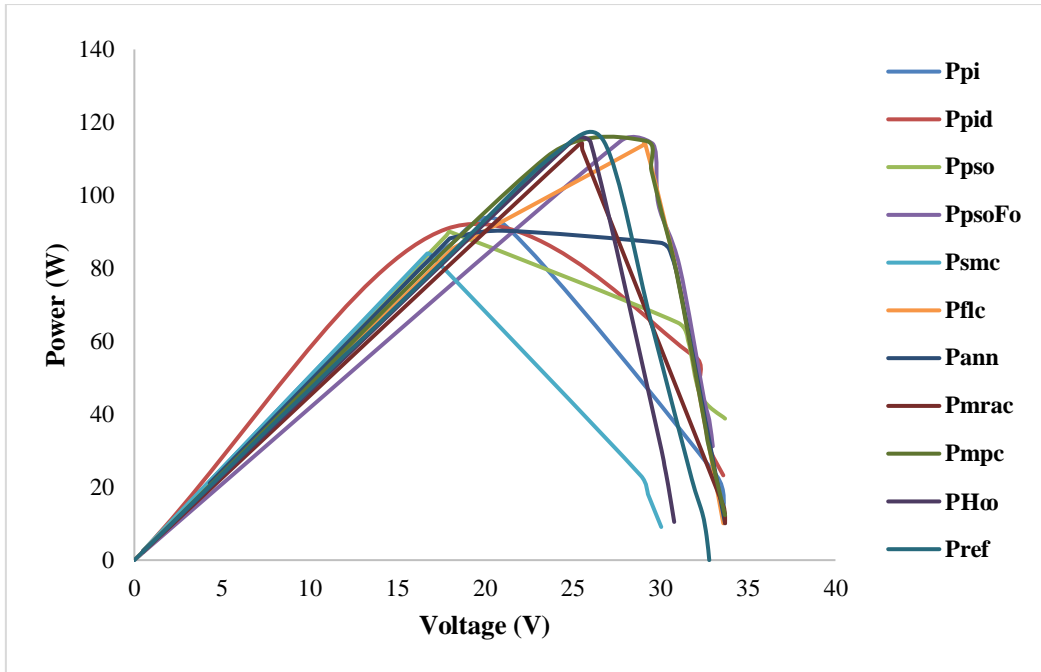
Figure 4.6: PV characteristics using 1D reference model

Figure 4.5 shows comparative analysis of VI characteristics and Figure 4.6 shows comparative analysis of PV characteristics of PVE using 1D reference model with different controllers in feedback loop. The plots are following reference values of PVE characteristics.
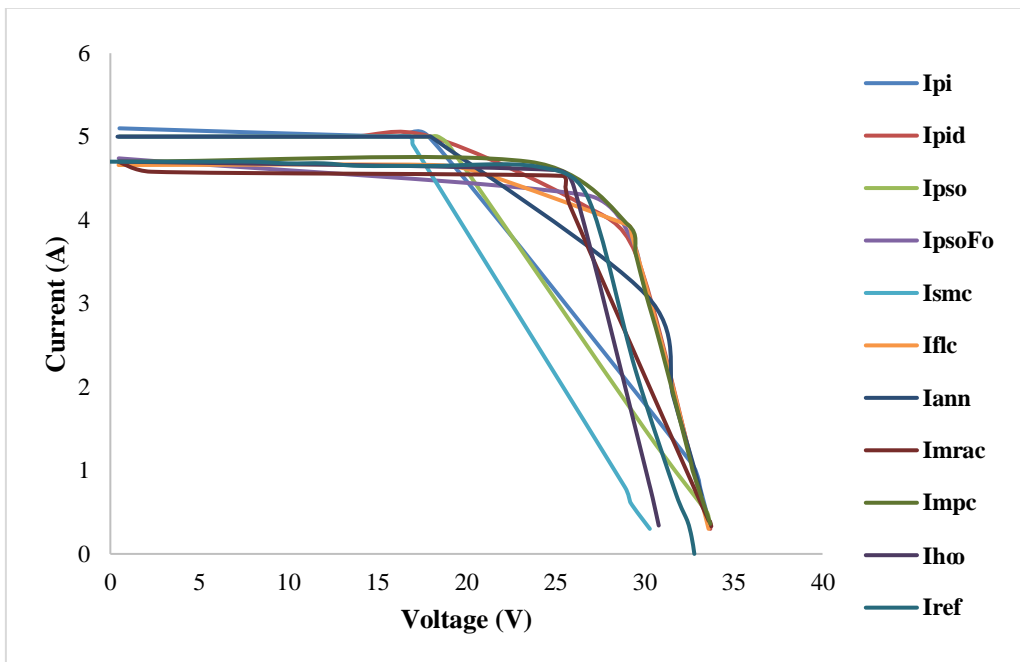
Figure 4.7: VI characteristics using 2D reference model
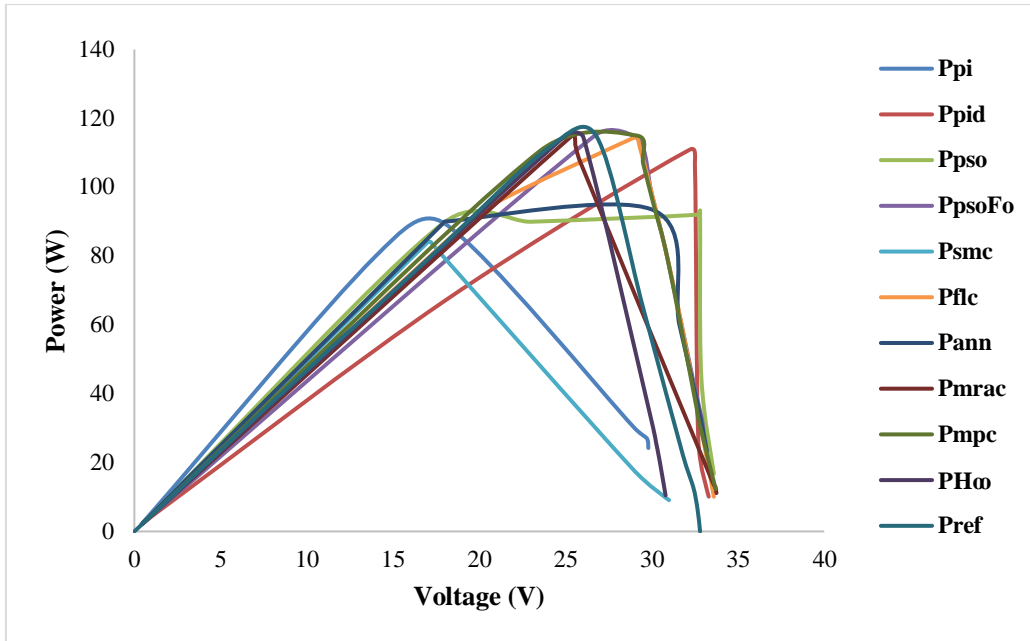
Figure 4.8: PV characteristics using 2D reference model

Figure 4.7 shows comparative analysis of VI characteristics and Figure 4.8 shows comparative analysis of PV characteristics of PVE using 2D reference model with different controllers in feedback loop. The results are better than 1D near SC and OC as more controllers are able to reach the desired reference values. Comparative analysis is carried out at three main points i.e SC, MPP and OC point.
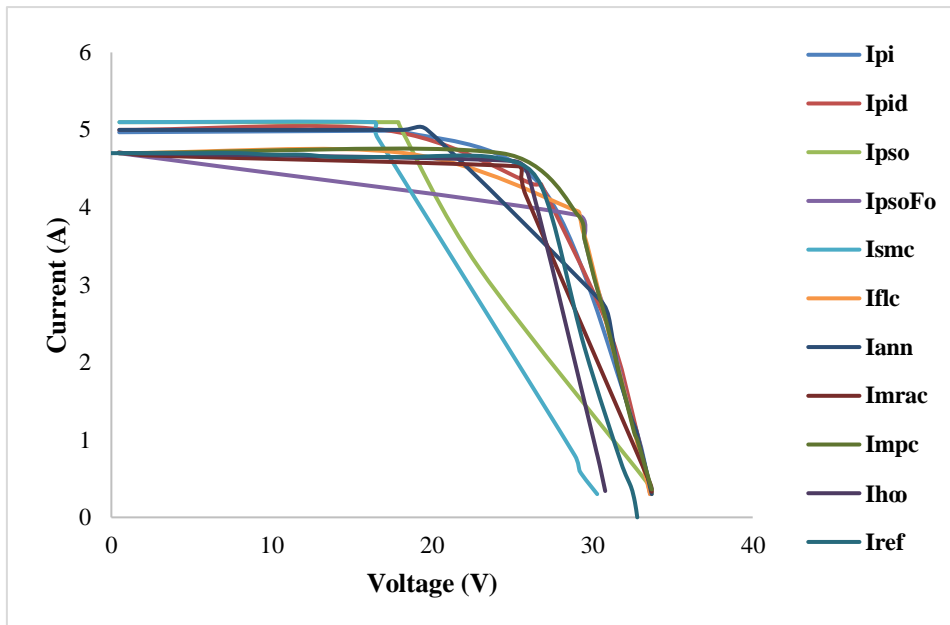
Figure 4.9: VI characteristics using 3D reference model
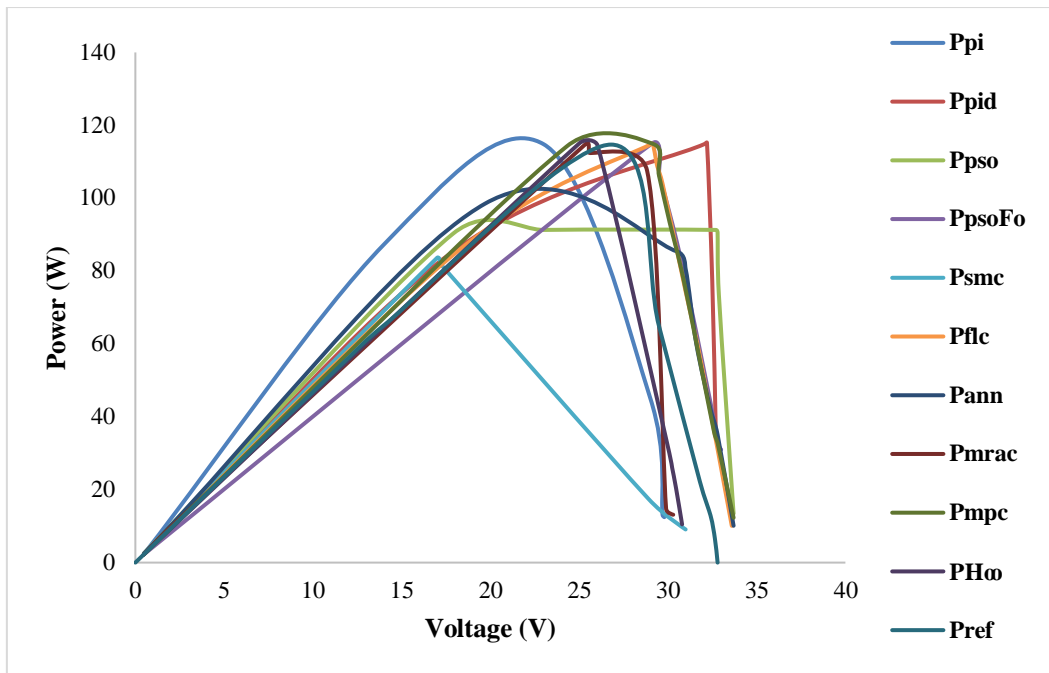
Figure 4.10: PV characteristics using 3D reference model

Figure 4.9 shows comparative analysis of VI characteristics and Figure 4.10 shows comparative analysis of PV characteristics of PVE using 3D reference model with different controllers in feedback loop. When compared with results of 1D and 2D models, the results of 3D reference model are best in overall frame. The overshoot seen near SC in 1D model is also eliminated. The comparison concludes that all reference models have similar behaviour near OC but near to SC 3D reference model has shown refined performance.
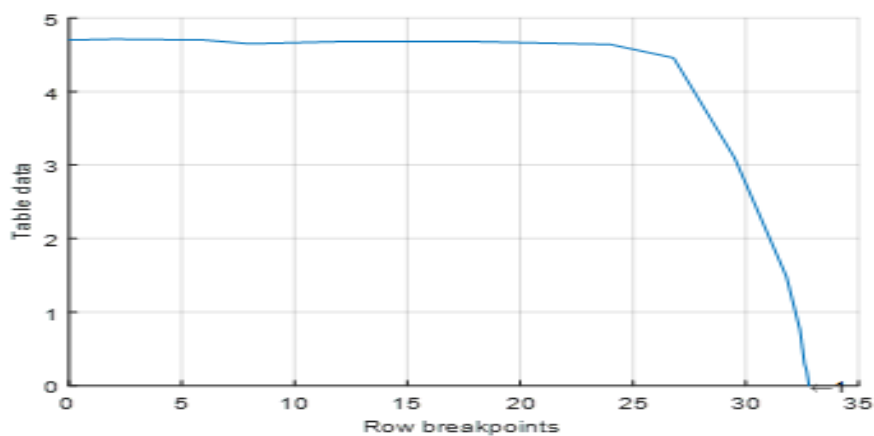
Figure 4.11: 1D LUT for VI characteristics at STC

Figure 4.11 shows VI characteristics with voltage (V) in volts on x-axis (Row breakpoints) and current (I) in amperes on y-axis (Table data) for one dimensional look-up table.
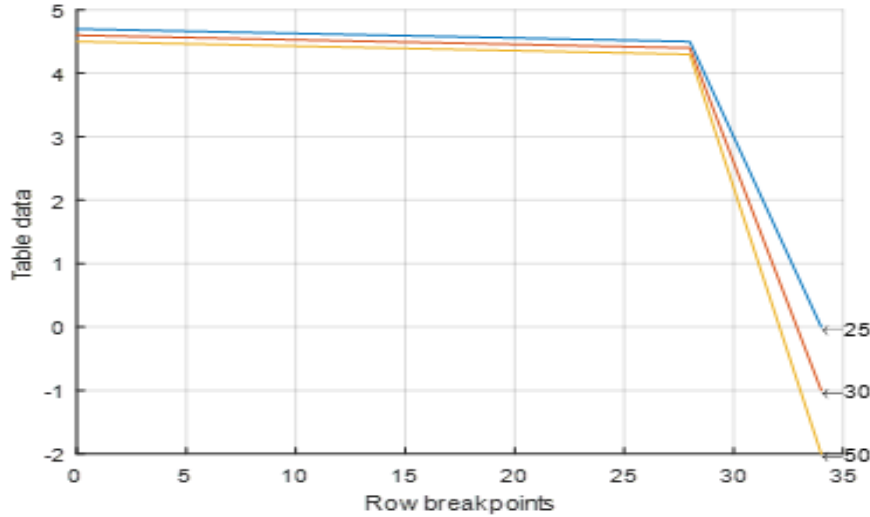
Figure 4.12: 3D LUT for VI characteristics at varying temperature but constant irradiance

Figure 4.12 depicts 3D LUT with voltage (V) in volts on x-axis (Row breakpoints) and current (I) in amperes on y-axis (Table data) for three-dimensional look-up table with varying temperature ranging from 25 degrees to 50 degrees with constant irradiance.

The IV or VI look-up table is perhaps the most basic version reported in papers. In IV LUT, Vpv, is used as the table's input and the PV current, Ipv, is used as the table's output (as shown in above plots). The VI LUT, on the other hand, has I_{pv} as its input and V_{pv} as its output.
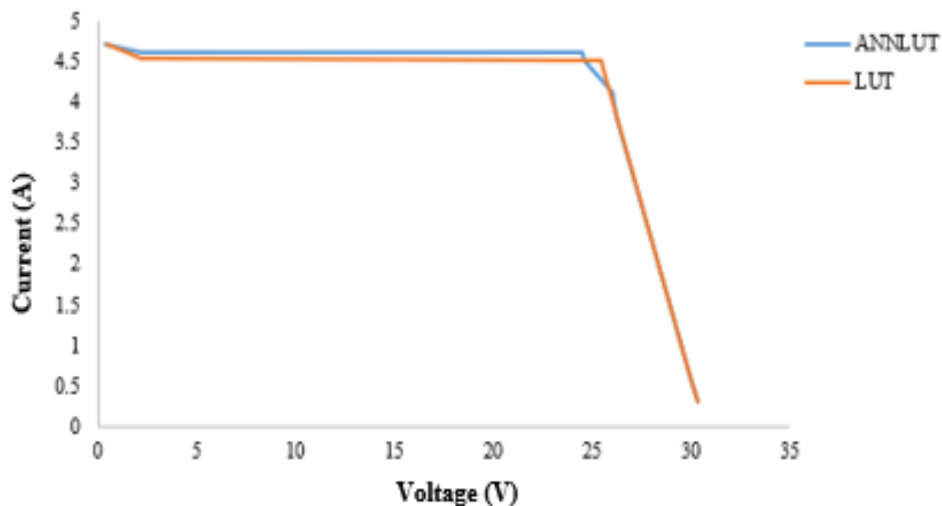
Figure 4.13: VI characteristics using ANN for reference model design

Figure 4.13 represents characteristics of PV panel obtained by applying ANN to design reference model for PVE. The comparison is made with manual LUT and ANN based LUT.
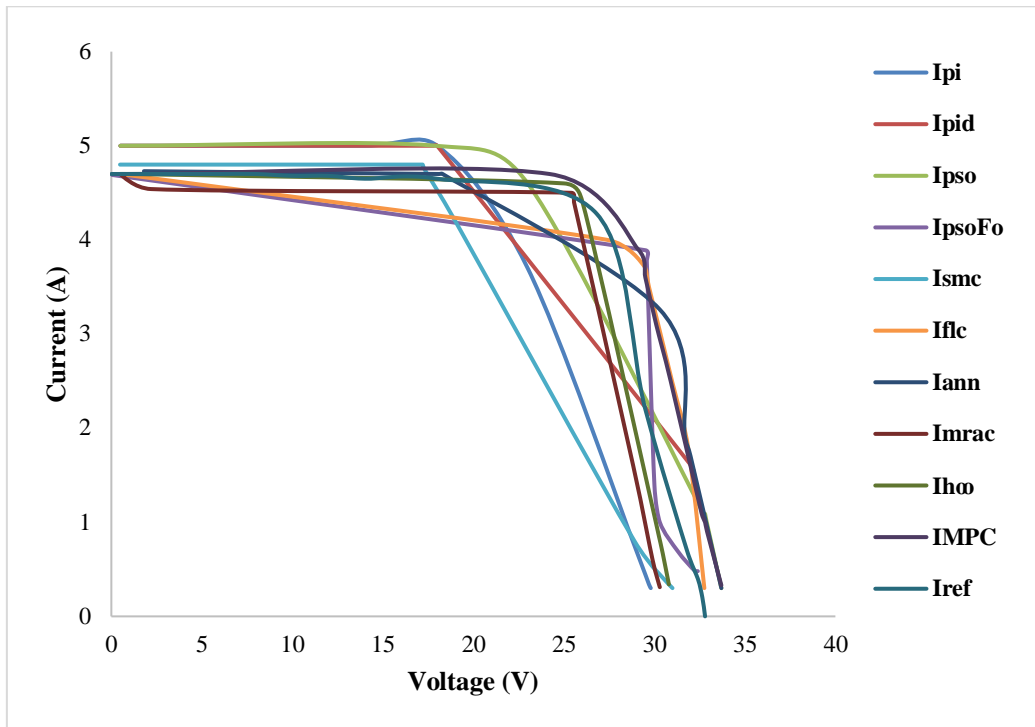
Figure 4.14: VI characteristics using LUT reference model
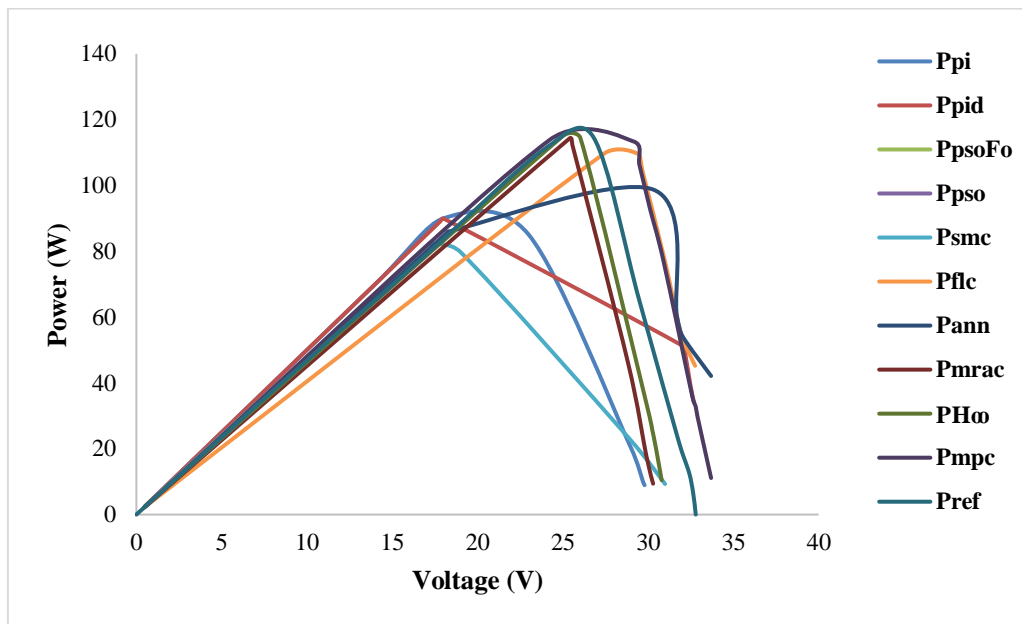
Figure 4.15: PV characteristics using LUT reference model

Figure 4.14 illustrates comparative analysis of various controllers using LUT as reference model and Figure 4.15 depicts comparative analysis with LUT reference model. The overall characteristics are found to be acceptable in LUT. When reference diode model and reference LUT results are compared, MPP point is closely followed by LUT.
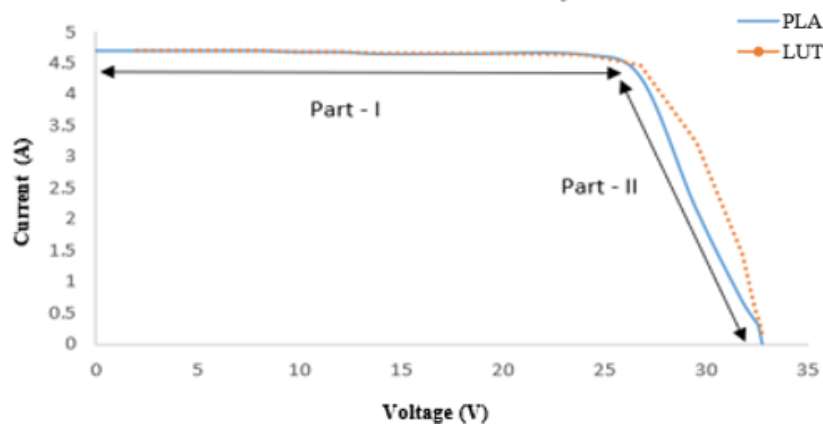
Figure 4.16: VI characteristics of PV panel for PLA

For the considered panel, $V_{oc} = 32.8V$; $V_p = 26.8V$; $I_p = 4.28A$, $I_{sc} = 4.7$

Figure 4.16 shows the mathematical approach of reference model design. This approach can be implemented using MATLAB code/ programming tool. The parameters given in datasheet are required for the piecewise reference model approach.

3D model results are shown in Figure 4.9 and Figure 4.10 and the results are found to be the best among 1D, 2D and LUT reference models in terms of overall characteristics and dynamics. Figure 4.16 shows PLA as reference model, which allows modeling by linear equations dividing characteristics plot in sub-parts. Results of comparative analysis show that the selection of reference model can also be made as per particular application of solar panel to be emulated. Further various controllers are implemented to select the reference model based on controller response.

4.6 CONCLUSION

This chapter covered the hierarchies involved in reference models forming a closed loop with buck converter and concludes:

- Reference system modeling implementing one, two and three diode models for best comparative results.

- LUT is explained with 1-dimension and 3-dimension structure. Piecewise Linear Analysis is further explained as an alternative to obtain PV reference values if three main points: I_{sc}, MPP and V_{oc} are known.

- The difference between actual and reference values are the values that govern how controllers work as well as how the PVE is structured.

- It is also concluded that modeling of the reference model is vital for efficient controller performance. So, in the further chapter, this analysis act as base for controller design & reliability analysis and are implemented in MATLAB to find out the best suited application of these methods in PVEs.

CHAPTER 5

PVE CONTROL STRATEGIES AND THEIR IMPLEMENTATION

5.1 INTRODUCTION

Controller in a control system aims at minimizing the difference between the system's actual output and its desired output. Controllers are an integral part of power systems and are reported in all advanced systems too.

Controllers are beneficial for a number of purposes, specifically:

- To increase steady-state accuracy by minimizing steady-state error.
- To effectively reduce the unintended offsets.
- To control maximum overshoot.
- To reduce the system's noise signals.
- To speed up an overdamped system's response.

5.2 CONTROL STRATEGY FOR EMULATOR

In PVE, closed loop control is implemented to regulate 'd' provided to the switch. The reference mathematical models explained in Chapter 4 provide the desired current, comparable with the converter's feedback current as its in Current Control Mode (CCM). The generated error is present as input to the controller. Here the main objective of the controller design for PV emulator is to generate pulses with 'd' such that the DC voltage response is equal to the reference voltage. The output voltage regulation should be maintained despite variation in operating conditions such as load resistance, temperature and irradiance. This is achieved by varying 'd' but keeping f_{sw} constant. For this purpose, Pulse Width Modulation (PWM) technique is employed. Therefore, the controller has to continuously monitor this duty cycle so that the proper switching pulses are generated. CMC is used along with suitable controller. In literature, many control design techniques ranging from conventional PI, PID controllers to AI based controllers are found as summarized in literature review (Chapter 2). This work focused on implementing:

- Conventional Controllers: PI and PID
- Hybrid Controllers: PSOPID and PSOFOPID
- AI based Controllers: FLC and ANFIS
- Non-Linear and Robust Controllers: SMC, MRAC, MPC and H_∞.
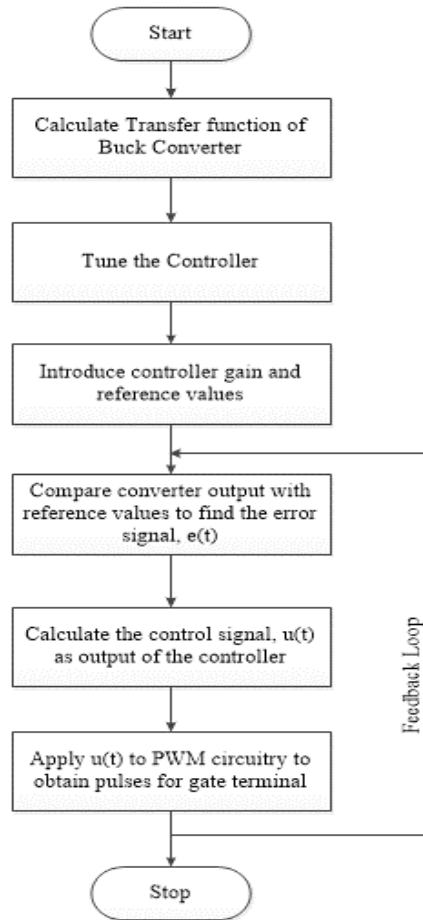
Figure 5.1: Flowchart depicting significance of a controller in PVE

Figure 5.1 describes the significance of controller in closed loop circuitry of PVE. The aim of controller is to reduce the difference between the output values and reference model values to reduce the error and provide pulses to trigger gate of switching device.

5.3 CONVENTIONAL CONTROLLERS

The control strategy required for any controller requires good mathematical modeling of the system. Previous chapters 3 and 4 have described the mathematical modeling of converter and the reference models for providing input to the controller. Following tuning methods are applied for implementation in converter's closed loop circuitry to make it function as a PVE.

5.3.1 PI and PID controllers

Selection of P, I and D parameters dependent on plant, so the plant dynamics are modeled before controller tuning. The optimum settings of controller to find the best values of the controller parameter is known as tuning. The two widely used conventional tuning methods reported for controller tuning are Ziegler Nichol's continuous cycle method and Cohen Coon's

process reaction curve method [158-159]. The parameters in PVE modeling are chosen so that response, speed, t_s and POS guarantee the system stability.
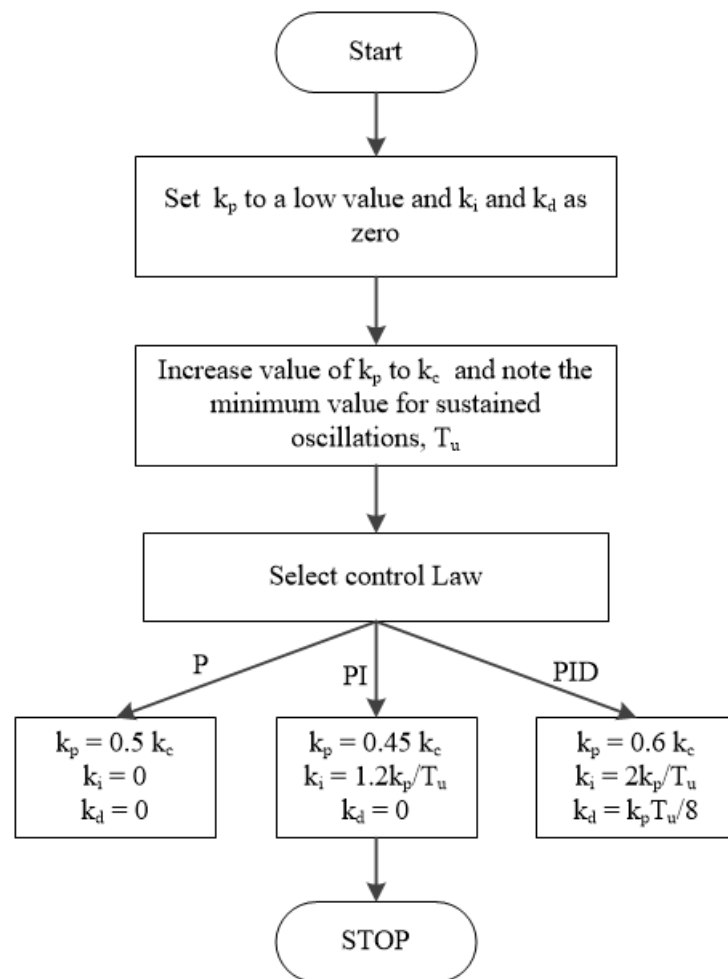
Figure 5.2: Flowchart representing P, PI and PID tuning methodology

The tuning methodology of P, PI, and PID controllers for any loop control is depicted in Figure 5.2. This approach is used to obtain PVE results based on conventional control strategies, which will serve as a good comparative base for characteristics plotted by other controller implementations.

$$G(s) = k_p + \frac{k_i}{s} + k_d s \qquad (5.1)$$
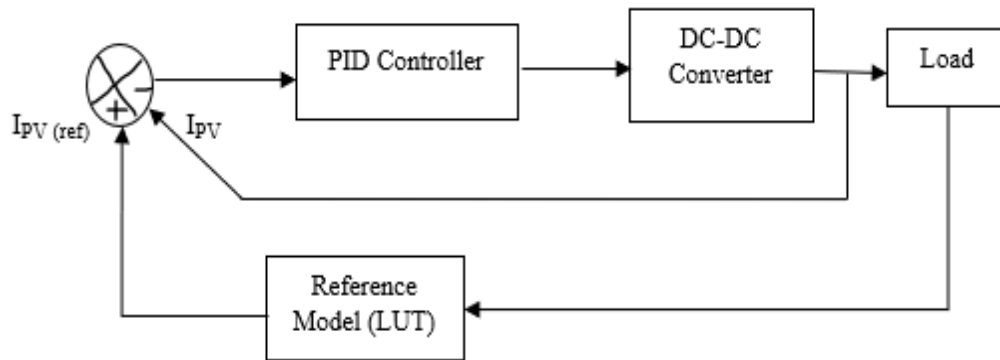
Figure 5.3: Block diagram of PID controller implemented in PVE

Figure 5.3 shows the block diagram description of conventional controllers. The PID controller's proportional component seeks to decrease error response to disturbance. The integral term of error eradicates steady-state error and the derivative term of error diminishes the dynamic response, improving system stability. The criteria for selection in PVE is to have minimal settling time with a small or no overshoot. For a wide range of practical models, this tuning approach works quite well [68, 160]. So, modifications in traditional controller can be achieved by introducing more tuned parameters i.e. by involving order of integral (λ) and order of derivative (μ) in fractions by FOPID controller [161-163]. The new G(s) is then represented by:

$$G(s) = k_p + \frac{k_i}{s^\lambda} + k_d s^\mu \tag{5.2}$$

This implementation of FOPID is made in hybrid mode with PSO as discussed in next section to obtain results on wider range.

5.4 HYBRID CONTROLLERS

The advancement in software computational methods have offered modified ways to tune the parameters to find best performance. Heuristic methods have been proposed over the years to tune PID controllers. One opted for the PID parameter tuning hybrid approach for PVE in this analysis is the particle swarm optimization (PSO). The methods discussed in 5.2.1 used the tuning rules proposed by Ziegler and Nichols.

The Key features important for PVE are as follows:

- The scheme is outcome of findings of swarm in contrary to dynamics in PV system.
- It is simple to implement and possess a stable convergence characteristic as well as high computational efficiency.

It is ascertained and discovered that assessing optimal or near optimal PID parameters with the Z-N formula is complicated [164-166]. For these reasons, it is critical to improve the system performance of PID controllers by integrating new features including performance indices, error indices etc. It is also realized that the issues related to dynamic performance and transient loading are improvised by using hybrid-mode controlled methods [167]. PSOPI and PSOPID [168-169] controllers are thus designed to minimize rise time and settling time along with error component of the system. An objective function is thus formed with the above parameters to obtain tuned value of gains k_p, k_i and k_d, thereby resulting in faster and easy process for PVE controller tuning action.
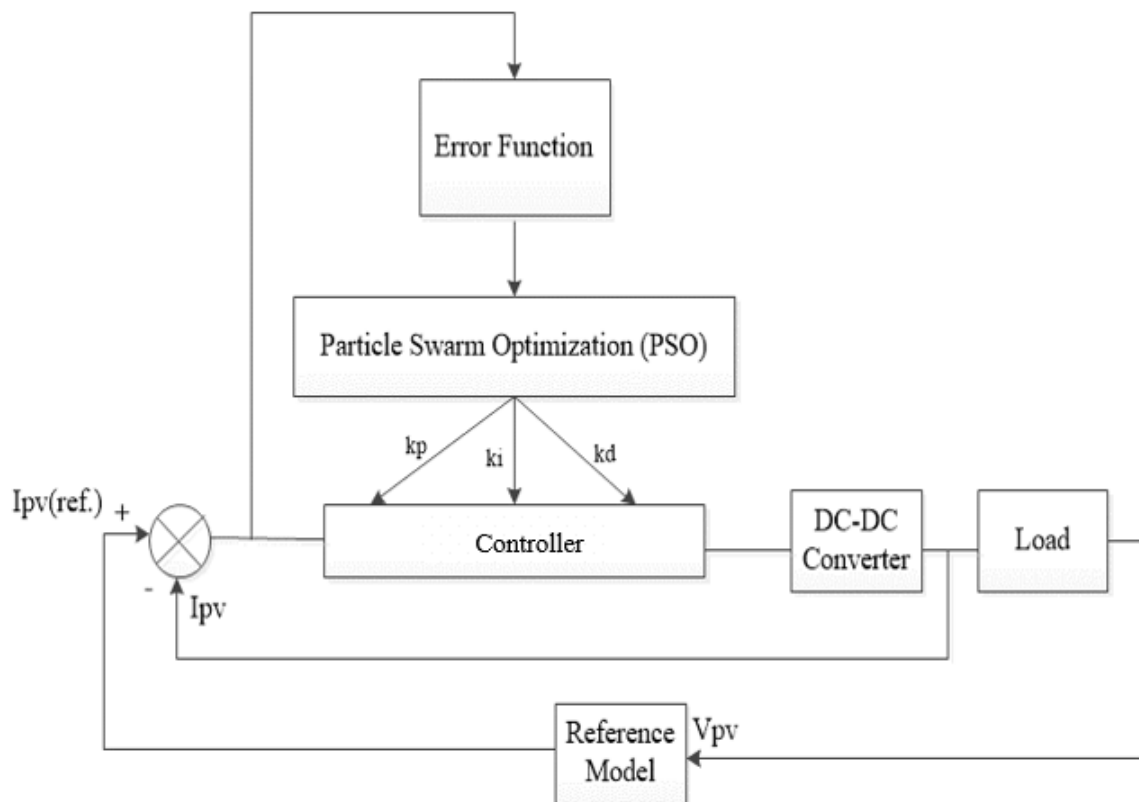
Figure 5.4: Block diagram of PSO tuned PVE

Figure 5.4 represents block diagram of PSO tuned PID controller implemented in PVE. The tuning problem of conventional controllers can somehow be made easier by these algorithm-based models. Figure 5.5 shows a flowchart of the step-by-step implementation of PSO tuning for PID for a deeper understanding of the PVE system.
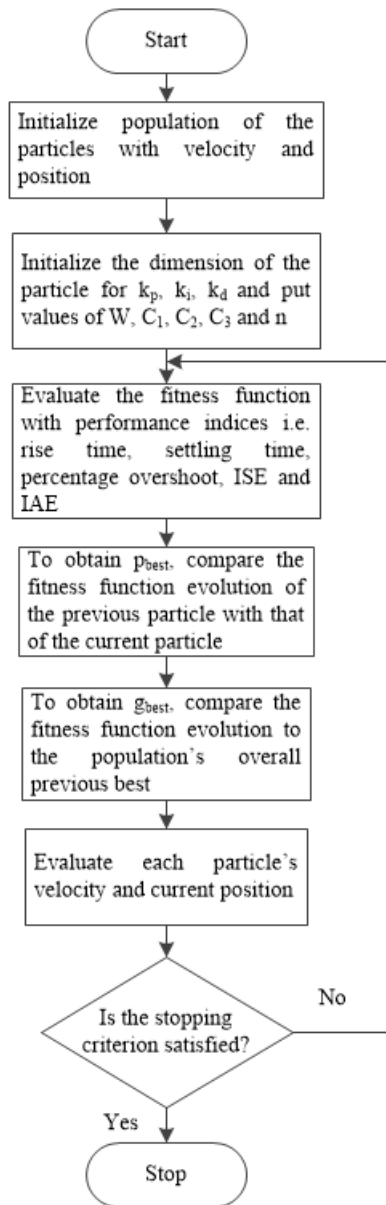
Figure 5.5: Flowchart of PSO implementation

FOPID has several advantages over the traditional PID controller such as a simplified structure, better tracking and a wider ability to handle model uncertainties in nonlinear applications. Because of the presence of two extra parameters, tuning the FOPID controller becomes complex, so a hybrid PSOFOPID [75-78,170] is implemented for efficient tuning. By incorporating the benefits of PSO methodology, the algorithmic-based tuning made the process faster than traditional FOPID.

5.5 AI BASED CONTROLLERS

Many artificial intelligence (AI) methodologies are utilized to optimise performance of controller over broad range of parameter variation alongside maintaining the basic properties

of PVE. For tuning of PID parameters, AI techniques like fuzzy system and neural-fuzzy logic have been extensively used. The prime features of AI based controllers are:

- To provide a complete control proportional to the error signal (like k_p) by all-pass gain factor.
- Equivalent to k_i, minimising steady-state errors via low-frequency compensation.
- Enhancing dynamic response by using high-frequency compensation similar to a differentiator.
- Shortening the time required for gain adjustment.

5.5.1 Fuzzy Logic Controller

Fuzzy logic based tuning method converts the user supplied human rules into their mathematical equivalents. High accuracy, reliability, robustness, good range, less maintenance and high performance are the primary requirements PVE controller. A proper controller must be selected in order to bring all of the above-mentioned qualities. There is a trade-off between the desired response and ease of the controller design. Therefore, the selection of controllers has drawn increasing attention from research and industry applications. The model is implemented in MATLAB simulation to bring out more simplicity in result analysis [41,89, 160]. Fuzzy controllers' control laws vary from traditional controllers in that they do not use precise mathematical descriptions. Figure 5.6 shows the basic input-output blocks of FLC implemented in PVE model. Error and change of error are taken as inputs.
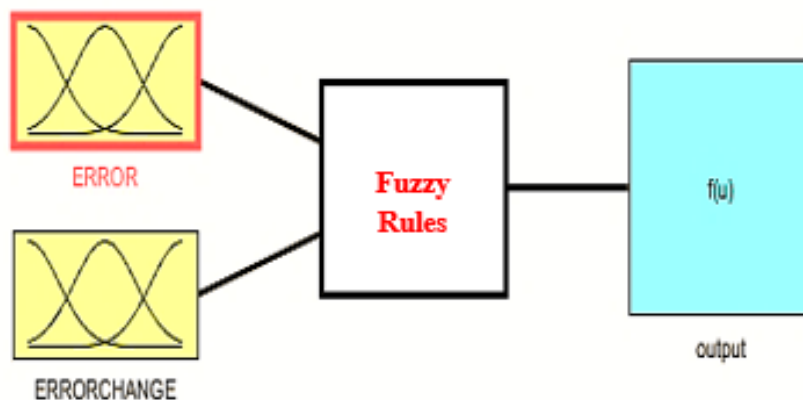
Figure 5.6: Block diagram of FLC structure of PVE
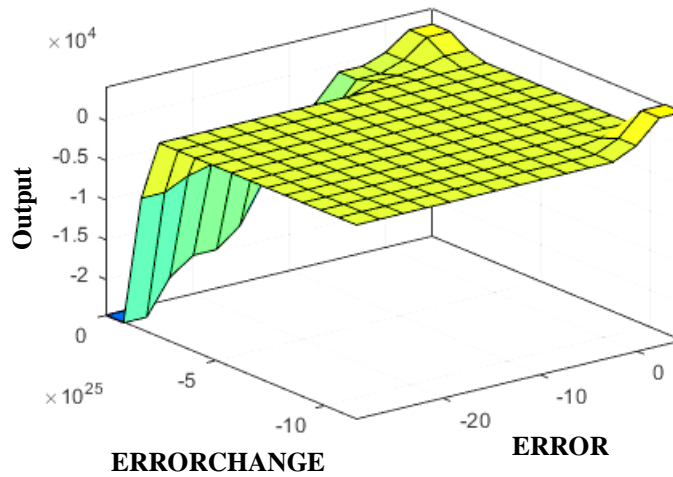
Figure 5.7: Surface view of FLC structure of PVE

Figure 5.7 depicts the surface view of FLC, which includes input membership functions as error and change of error, as well as output membership function as output. The output is a reduced error that is fed into PWM for gate pulse generation.

5.5.2 ANFIS Controller

Fuzzy logic controllers are often combined with neural networks to frame ANFIS controllers. When applied to nonlinear systems with changing characteristics, this kind of controller offers significant advantages over conventional PID [97, 171].
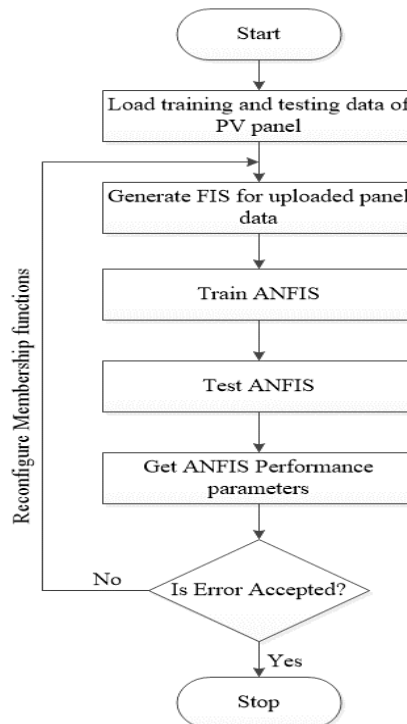
Figure 5.8: Flowchart for ANFIS based PVE

Figure 5.8 shows the flowchart explanation of ANN based implementation on PVE. Tuning of membership functions remains a cumbersome task in FLC. These factors compliment use of Adaptive Neuro-Fuzzy Inference System (ANFIS) controller for PV Emulator design. It is AI system based on the Takagi-Sugeno Fuzzy Inference System, also known as an Artificial Neural Network (ANN). It incorporates the concepts of NN and FLC [172-174] to provide the benefits of both methods within one approach.
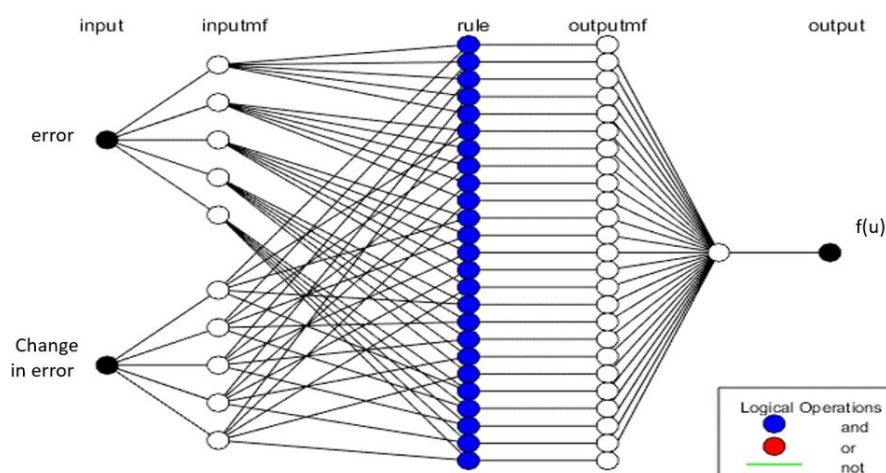
Figure 5.9: ANFIS internal structure of PVE model

Figure 5.9 presents the internal structure of applied ANN using back propagation to PVE with input membership functions, their rules, logical operations and output structure. It provides accurate predictions for the highly nonlinear systems. The membership functions are assigned to linguistic variables using subsets: FSC, SC, MP, OC, COC for inputs error and error change.

5.6 NON-LINEAR AND ROBUST CONTROLLERS

Nonlinear control approaches are investigated in order to maintain stability and effective control in massive signal conditioning, as well as to increase the model's dynamic response or robustness.

5.6.1 Sliding Mode Controller, SMC

SMC provides robustness and quick reaction to fluctuations in supply, load and circuit parameters. SFG is used to construct a PWM-based SMC buck converter in this work. At the simulation level, a new set of mathematical representations is used to construct similar duty cycles that are independent of load variation. The controller can be constructed using expressions that have fewer components. It is construction of a surface as per its control law to steer the trajectory of state variables to the desired origin on coinciding [84, 175-176]. PV

emulator configuration uses a converter in loop with SMC and diode model. T and d are the switching interval and duty cycle, respectively. The SMC design is divided into two categories:

- To build a sliding surface such that there is a desired system response to the plant confined to the sliding surface. This implies that the plant dynamics states variables are constrained to satisfy another set of equations describing the switching surface.
- To create the switched feedback gains needed to push the state trajectory of the plant to the sliding surface (as shown in Figure 5.10). The control signal switches between two structures when the 'S' is very close to zero.
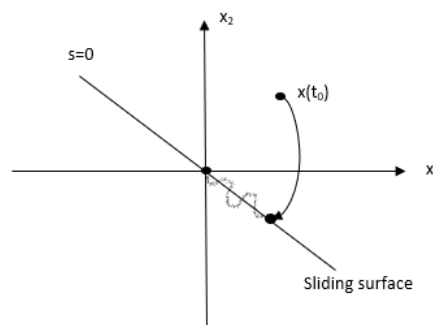
Figure 5.10: Description of Sliding surface in SMC

The goal of PVE's control strategy is to properly follow PV model signals, decrease processing load, generate reliable emulator output and simulate a range of PV modules without having to rethink the entire control strategy and influencing the power converter system and load. The equations defining ON and OFF state of Buck can be written as:

$$L\frac{di_L}{dt} = -v_0 + V_{in} \tag{5.3}$$

$$L\frac{di_L}{dt} = -v_0 \tag{5.4}$$

***Detailed description is derived in Chapter 3

From above equations (5.3) and (5.4)

$$\dot{X} = f(X, t, d) \tag{5.5}$$

Also, $v_0 = [0 \quad 0 \quad 0 \quad ....0 \quad 1] * X^T$ (5.6)

When the system approaches the sliding surface, the controller aims for the output to reach the desired value (given by either a diode model or a LUT). Partial or complete state variables can

reach this surface [83, 85, 178]. A new portion akin to an integral with a constant is added to the surface equation to minimize the error between the actual and intended value. As a result, the new sliding surface, S:

$$S = ai_n + bv_o + m\int_0^t edt = 0 \tag{5.7}$$

signal or the difference between desired (v_r) and actual value (v_o). $S > 0$ in open state and $S < 0$ in closed state.

In steady state, when the system is kept on sliding surface, the derivative of S becomes zero and the stable point is when e = 0, $v_r = v_o$. So, sliding surface equation (5.7) becomes;

$ai_n = - bv_o$.

For buck converter;

$$\dot{S} = [a \quad b] * \dot{X} + m\int_0^t e \, dt = 0 \tag{5.8}$$

$$\dot{S} = [a \quad b] * \begin{bmatrix} \dot{x}_1 \\ \dot{x}_2 \end{bmatrix} + m\int_0^t (x_2 - v_r)dt = 0 \tag{5.9}$$

This concludes that the system on new surface is represented by:

$$\dot{X} = f(X, t, d_{eq}) \tag{5.10}$$

and if time is taken as zero; the system represents a steady state.

The term d_{eq} is equivalent duty ratio of the sliding surface. Substituting above equations in equation (5.10), the value of d_{eq} can be derived as follows: $\dot{X} = \begin{bmatrix} \dot{x}_1 \\ \dot{x}_2 \end{bmatrix}$.

$$\dot{x}_1 = \frac{v_i}{L} d_{eq} - \frac{x_2}{L}$$

$$\dot{x}_2 = \frac{x_1}{C} - \frac{x_2}{RC} \tag{5.11}$$

By placing equation (5.11) into (5.10), the equation becomes

$$0 = a\left[\frac{v_i}{L} d_{eq} - \frac{x_2}{L}\right] + b\left[\frac{x_1}{C} - \frac{x_2}{RC}\right] + m(x_2 - v_r)$$

And placing $\dot{S} = 0$;

$$d_{eq} = \frac{aRCx_2 - Lb(x_2 - Rx_1) + RLC\ m(V_r - x_2)}{aRCV_i} \qquad (5.12)$$

The system equation on sliding surface is obtained from equations (5.3), (5.4) and (5.12) as:

$$\dot{X} = \begin{bmatrix} \frac{-b}{ac} & \frac{b - mRCL}{aRC} \\ \frac{1}{C} & \frac{-1}{RC} \end{bmatrix} X + \begin{bmatrix} \frac{mV_rL}{a} \\ 0 \end{bmatrix} \qquad (5.13)$$

For above defined system to be stable; $v_0 = v_r$, the error must be zero. And $v_0 = x_2$

therefore $v_0 = v_r = x_2$

Also, $i_c = x_1 - \frac{x_2}{R} = i_L - \frac{v_o}{R}$ and $d_{eq} = \frac{v_r}{V_i}$

Equation (5.12) and (5.13) gives a new control input which is independent of load, R. The new control equation is represented below:

$$d_{eq}(t) = \frac{x_2(aC - LCm) + Lbi_c + LCm(V_r)}{aCV_i} \qquad (5.14)$$

With deq, the system's closed loop dynamics converge towards a sliding surface. The system reaches the sliding surface in defined time if s = 0. For parametric uncertainties, a deq estimate is available. The Routh Hurwitz criterion and the characteristic equation of (5.13), described are used to find the values of unknown a, b and m in order to determine the value of equation (5.14) as shown in (5.15) below.

$$\det (A - \lambda I) = 0$$

$$\lambda^2 + \left[\frac{b}{ac} + \frac{1}{RC}\right]\lambda + \frac{m}{ac} = 0 \qquad (5.15)$$

5.6.2 Model Reference Adaptive Controller, MRAC

"To adapt" is defined as making an adjustment to a changed environment. When the parameters change over time, standard controllers cannot be used. Therefore, adaptive controllers are necessary. An adaptive system can alter itself in response to system inputs while taking system uncertainty into account. The term "adaptive parameters" refers to variables that can be changed, while "adaptive law" refers to the mathematical equations that describe how these variables can be changed. MRAC is used to create closed loop controllers that dynamically modify system variables by contrasting plant output with a predetermined reference response. Figure 5.11 shows a simplified block architecture of MRAC. There is an inner loop along with

an outer loop [179]. The output of plant is compared to a desired signal and the generated difference signal is received by the outer loop for a dynamic controller parameter adjustment system.
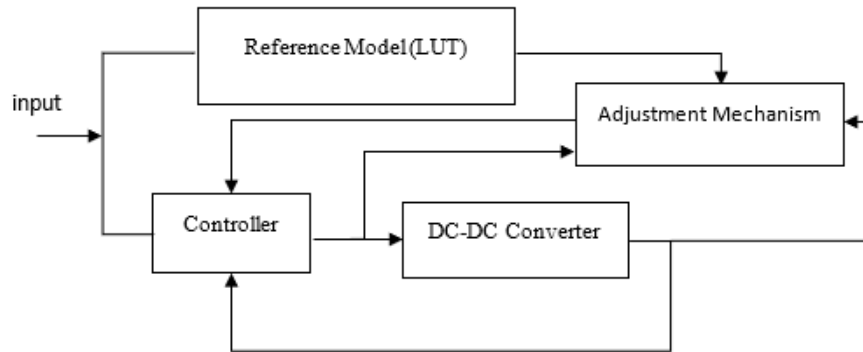
Figure 5.11: Block diagram of MRAC in PVE

The system adapts to the error signal in case of direct control MRAC. Adaptive law modifies the control system's parameters. The purpose of direct MRAC techniques is to create a common control system that does not require analysis in the control loop even while improving the control system's performance and quality in comparison to a constant gain system. On the other hand, the technology automatically adjusts in indirect control by correlating plant output and online basic reference. The parameter's value is derived by evaluating formulas in linear algebra that relate to the plant's online model at each moment.

The MRAC model comprises of following components:

- Controller: The control law can be explained using a set of variables that are changeable in this scenario.
- Adjustment Mechanism: It is implemented to adjust the system's parameters to compare present system and the reference model. Tools for creating adjustment mechanisms include the Lyapunov theory, the MIT rule and the theory of enhanced error.
- Reference Model: It offers a baseline for assessment of the output.

The primary method for solving MRAC is the MIT rule [100]. A closed system that can be modified by the parameter theta is required to implement MRAC. A tracking methodology can be established because an adjustment mechanism is required to reduce the error between the model and plant. A cost function, according to this rule, is a function of the error between the

outputs and reference model and specifications of the controller are revised to minimise this cost function.

MRAC will compute "u" control input. MIT rule aims at minimizing the cost function J. Here

$$J = \frac{1}{2}e^2 \quad \text{e is the error signal} \tag{5.16}$$

$$e = y(t) - y_m(t) \tag{5.17}$$

$$y = I_{pv\,(ref)} \ \& \ y_m = I_{pv\,(load)}$$

To decrease J, a negative gradient of J is obtained as:

$$\frac{d\theta_1}{dt} = -\gamma\frac{\partial J}{\partial\theta_1} = -\gamma e\frac{\partial e}{\partial\theta_1} \tag{5.18}$$

$$\frac{d\theta_2}{dt} = -\gamma\frac{\partial J}{\partial\theta_2} = -\gamma e\frac{\partial e}{\partial\theta_2} \tag{5.19}$$

If the main model is represented as:

$$\frac{dy}{dt} = -ay + bu \tag{5.20}$$

with y as output of the system and a, b as unknown values and the reference model is represented as:

$$\frac{dy_m}{dt} = -a_m y_m + b_m u_c \tag{5.21}$$

where u_c is reference model input and a_m and b_m being known values.

$$u(t) = \theta_1(t)u_c(t) - \theta_2(t)y(t) \text{ i.e difference between desired and actual values} \tag{5.22}$$

θ_1 and θ_2 are adaptive control parameters that are found by considering $y(t)$ close to $y_m(t)$ for a selected $u_c(t)$.

Putting (5.22) in (5.20) we get:

$$\frac{dy}{dt} = -ay + b(\theta_1 u_c - \theta_2 y)$$

$$\frac{dy}{dt} = -y(a + \theta_2) + b(\theta_1 u_c) \tag{5.23}$$

Comparing reference equation (5.21) with (5.23):

$$\theta_1 = \theta_1^* = \frac{b_m}{b} \quad \text{and} \quad \theta_2 = \theta_2^* = \frac{a_{m-a}}{b} \tag{5.24}$$

θ_1 should converge to θ_1^* and θ_2 to θ_2^*

Using derivative operator, p and equation (5.23); $y = \frac{b\theta_1 u_c}{p+a+b\theta_2}$ (5.25)

Using equation (5.25); error equation becomes:

$$e = \frac{b\theta_1 u_c}{p+a+b\theta_2} - y_m \tag{5.26}$$

taking partial derivative of above equation:

$$\frac{\partial e}{\partial \theta_1} = \frac{bu_c}{p+a+b\theta_2} \tag{5.27a}$$

$$\frac{\partial e}{\partial \theta_2} = \frac{-by}{p+a+b\theta_2} \tag{5.27b}$$

From equation (5.24); $a_m = a + b\theta_2^* \simeq a + b\theta_2$ and $p + a + b\theta_2 \simeq p + a_m$ (5.28)

So, equations (5.27) can be rewritten as:

$$\frac{\partial e}{\partial \theta_1} = \frac{bu_c}{p+a_m} \tag{5.29a}$$

$$\frac{\partial e}{\partial \theta_2} = \frac{-by}{p+a_m} \tag{5.29b}$$

Substituting equations (5.29) in equation (5.18) and (5.19);

$$\frac{d\theta_1}{dt} = -Y\frac{a_m\, u_c\, e}{p+a_m} \tag{5.30a}$$

$$\frac{d\theta_2}{dt} = Y\frac{a_m\, y\, e}{p+a_m} \tag{5.30b}$$

Here Y = control gain in adaptive control

Equations (5.30) and (5.25) describe the dynamics of closed loop system. In time domain, these are represented as:

$$\ddot{\theta}_1 = a_m\, \dot{\theta}_1 = -Y\, a_m\, u_c\, y + Y\, a_m\, u_c\, y_m \tag{5.31}$$

$$\ddot{\theta}_2 = a_m\, \dot{\theta}_2 = Y\, a_m\, y^2 - Y\, a_m\, y_m y \tag{5.32}$$

$$\dot{y} = -a\, y + b\theta_1 u_c - b\theta_2 y \tag{5.33}$$

with $u_c(t)$ simulation of reference model is done to get $y_m(t)$.
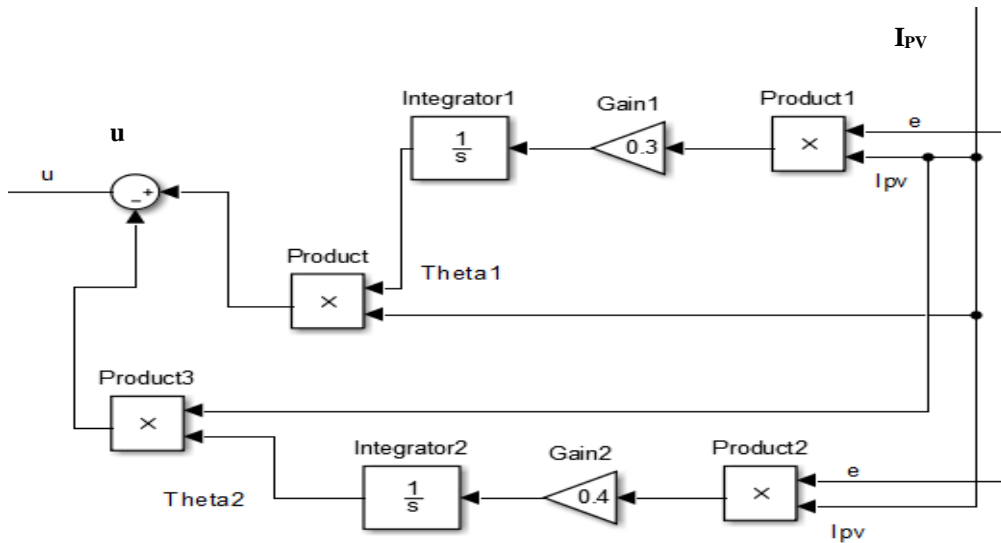
Figure 5.12: MRAC simulation model obtained from derived equations

Figure 5.12 implements MRAC design as derived in above equations since conventional PID controller cannot change in response to changes in plant parameters. In PVE designing parameters like load variation, temperature and irradiance can vary.

5.6.3 Model Predictive Controller, MPC

MPC handle multi-input and multi-output systems i.e. they are multivariant. So, they are defined as multivariant controllers that control the output simultaneously considering the interactions between systems such as PVE variables (load variation, conditions other than STC etc). The reasons for implementing MPC is their capability to handle constraints, preview capability like feedback correction, incorporation of future reference information to improve the controller's performance.
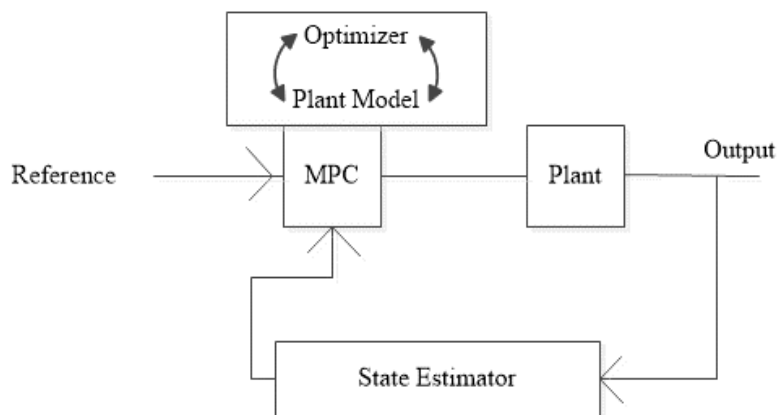
Figure 5.13: Block diagram representation of MPC

From Figure 5.13, it is clear that the controller is expected to calculate the plant's input so that the output is similar to a desired reference offered by reference models such as LUT or Diode models. MPC accomplishes this by predicting the future, i.e. it incorporates a plant model to forecast future output and an optimizer to monitor the desired reference. The trackpad conditions are unmeasured and must be estimated, which is fulfilled by default settings because the command employs a steady-state Kalman filter that derives them from the state estimator. MPC controller thus involves state Estimator:

- To predict the virtues of unmeasured states which are permitted for future predictions.
- To predict the impact of suggested manipulated variable (MV) tweaks on future plant output.
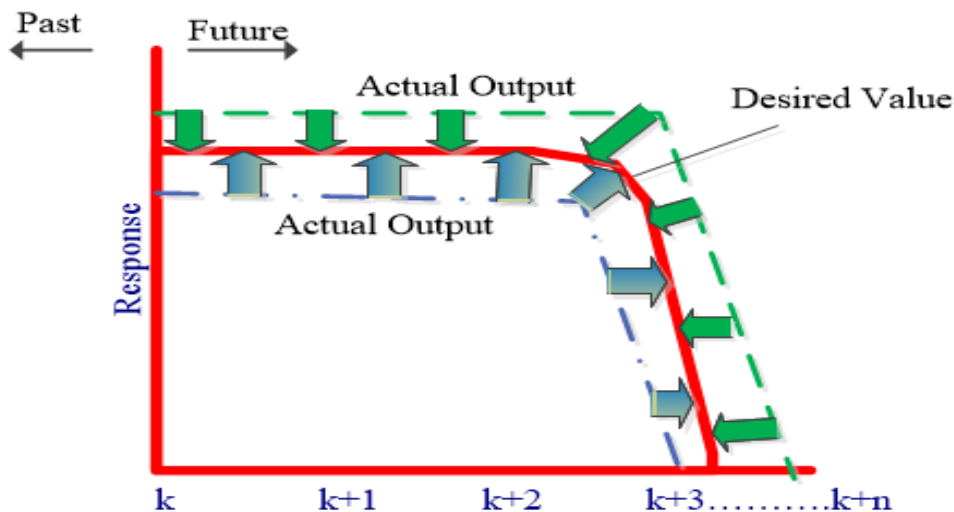
Figure 5.14: Representation of predictive nature of response in MPC

Figure 5.14 shows the desired response by red line and the actual output either as green or blue line tries to follow the red line for perfect modeling. The purpose of implementation of MPC in PVE is to predict the performance by a non-linear robust controller and obtain the required performance indices without compromising on the actual state or ignoring the practical factors like noise and disturbances. As the PVE represents a lab. Testing system at designing stage, MPC will provide a best insight into the ON- field prediction of systems.

5.6.4 H$_{infinity}$ Controller, H$_\infty$

A MATLAB-based H$_\infty$ controller has been implemented in this research for a PWM-based DC-DC buck converter. The controller is evaluated for robustness in the presence of varying load.

The objective of implementing H_∞ controller is to obtain effective and robust stability as it is capable of resisting excessive disturbance in a system [180]. The convex optimization approach can also be used to address this type of problem, Moreover, the LMI approach is a highly effective design tool for H_∞ controllers [181]. In this case, the desired voltage and sensor noise belong to exogenous input vector (w). The duty ratio is the control input (u). The outputs consist of measured response and the controlled output (z) and (y) respectively. The steps involved in controller designing are:

- Obtaining PVE model.
- Forming mathematical model of the selected PVE.
- Linearization of obtained parameters after modeling.
- Choosing weighting filters, tuning parameters.

  Minimization of error, control of input (u) are prime considerations.

$$w = [r] = \text{disturbance, noise} \tag{5.34}$$

$$u = [u] = \text{control signal} \tag{5.35}$$

$$z = \begin{bmatrix} e \\ u \end{bmatrix} = \text{error and control signal} \tag{5.36}$$

$$y = [e] = \text{error signal} \tag{5.37}$$
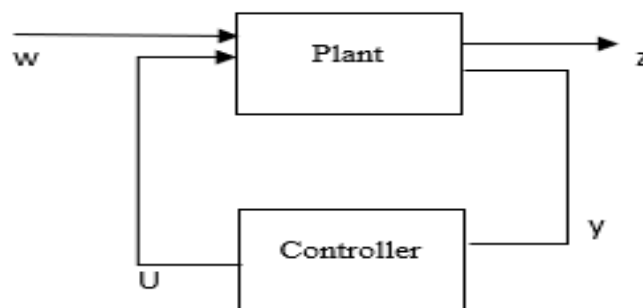
Figure 5.15: Control-Plant model of H_∞ controller
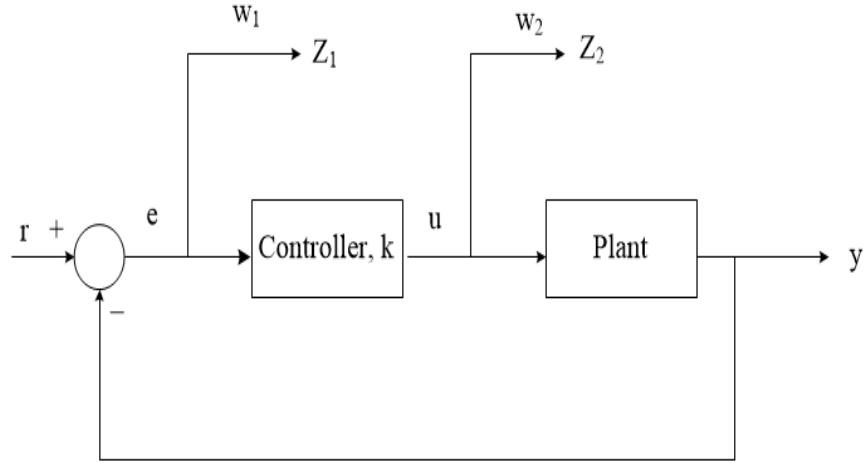
Figure 5.16: H∞ block diagram

Figure 5.15 and 5.16 represent basic block diagram and a closed loop block diagram respectively of stabilizing H∞. Controller for a partitioned plant P represented can be as:

$$P = \begin{bmatrix} A & B_1 & B_2 \\ \begin{bmatrix} C_1 \\ C_2 \end{bmatrix} & \begin{bmatrix} D_{11} & D_{12} \\ D_{21} & D_{22} \end{bmatrix} \end{bmatrix} \tag{5.38}$$

P is partitioned with inputs of B_1 as disturbances, while B_2 with control inputs. The errors are outputs of C_1, that needs to be minimum and the statistical output measures provided by the controller are responses of C_2. The plant's controller, k [182] that stabilises it is represented as:

$$k = \begin{bmatrix} A_k & B_k \\ C_k & D_k \end{bmatrix} \tag{5.39}$$

(5.39) is targeted to be minimized.

So, for the minimization;

$$\| P_{11} + P_{12} (I - k * P_{22})^{-1} k * P_{21} \|$$

$$\left\| \begin{bmatrix} \begin{bmatrix} A & 0 \\ 0 & A_k \end{bmatrix} + \begin{bmatrix} B_2 & 0 \\ 0 & k \end{bmatrix} \begin{bmatrix} I & -D_k \\ -D_{22} & I \end{bmatrix} \begin{bmatrix} 0 & C_k \\ C_2 & 0 \end{bmatrix} & \begin{matrix} B_1 + B_2 D_K * Q * D_{21} \\ B_k * Q * D_{21} \end{matrix} \\ [C_1 \quad 0] + [D_{12} \quad 0] \begin{bmatrix} I & -D_K \\ -D_{22} & I \end{bmatrix}^{-1} \begin{bmatrix} 0 & C_k \\ C_2 & 0 \end{bmatrix} & D_{11} + D_{12} * D_k * Q * D_{21} \end{bmatrix} \right\| \tag{5.40}$$

$$Q = (I - D_{22} * D_k)^{-1} \tag{5.41}$$

$$u(t) = D_k * y(t) \text{ (static output feedback)} \tag{5.42}$$

$$\begin{bmatrix} z \\ y \end{bmatrix} = \begin{bmatrix} P_{11} & P_{12} \\ P_{21} & P_{22} \end{bmatrix} \begin{bmatrix} W \\ U \end{bmatrix} \tag{5.43}$$

$$P = \begin{bmatrix} A & B_1 & B_2 \\ \begin{bmatrix} C_1 \\ C_2 \end{bmatrix} & \begin{bmatrix} D_{11} & D_{12} \\ D_{21} & D_{22} \end{bmatrix} \end{bmatrix} = P = \begin{bmatrix} A & B_1 & B_2 \\ \begin{bmatrix} 0 \\ I \end{bmatrix} & \begin{bmatrix} D_{11} & D_{12} \\ 0 & 0 \end{bmatrix} \end{bmatrix} \tag{5.44}$$

y(t) = state of the system = x(t); Put A_k, B_k, D_{21}, $C_2 = I$ and $D_{22} = D_{11} = 0$ (5.45)

The selection of a weighting function is vital in the robust control design technique and it is well known that the disturbance effect is indeed very dominant in the low frequency band. Because the weighting function is inversely proportional to the sensitivity, it serves as a low pass filter. The low frequency gain is selected inversely proportional to the desired steady-state error and the high frequency gain for limiting overshoot. Overshoot is reduced by boosting damping at the cost of response speed, resulting in a performance trade among overshoot and response speed. The sensitivity weight's high frequency gain should be kept between 0.1 to 0.5 to efficiently control overshoot and attain quick response. The weight is chosen to compensate for the unmodeled dynamics expected worst-case magnitude. It is essential to comprehend that the best weighting strategies for H_∞ control are problem-dependent and necessitate assessment skills.

Closed Loop state space $S(p,k) = \begin{bmatrix} \left| \begin{array}{c|c} A+B_2F & B_1 \\ \hline C_1 + D_{12}+F & D_{11} \end{array} \right| \end{bmatrix} = w$ (using equation (5.40))

$w_1 = 0.1 \left(\frac{s}{100s+1} \right)$; $w_2 = 0.1$;

The implementation of H_∞ control for PVE discovered that it cannot be used to control a system with an incorrect mathematical model. The controller will produce worse results than the other controllers if the mathematical model of the system is incorrect. Some non-linear conditions, such as saturation, are too difficult for this technique to manage. But in this work proper mathematical modeling as shown in chapter 3 and 4 was carried out to ensure an accurate model analysis and then the above stated controller was implemented in PVE. The results were obtained for open loop and closed loop conditions as shown in the following table. The results show that the performance indices were improvised and thus justify the effectiveness of the designed controller.

5.7 MODELING OF PVE WITH NON-IDEALITIES

These controllers are becoming a viable and competitive option, particularly in switch mode power converter systems, as their functionality is expanding and price is decreasing. Simulation

functions are simple to apply in them. Few modified controllers like Fuzzy Logic Control, Optimal Control etc. are best suitable for digital control. They are more design-flexible, easy to modify by changing the software and are reported to be less sensitive to environmental variation. These days there are numerous approaches for digital controllers such as microprocessors, DSPs, FPGAs and specially made IC designs. 8-bit microcontrollers play vital role in the modernization of electronics since the early 1980s. Despite the fact that 8-bit microcontrollers will be phased out sooner or later, there is no evidence of a drop in 8-bit usage and they remain relevant. They remained relevant into modern life due to the functionality of this technology as well as the decreasing costs of electronics. PIC18 microcontrollers, for example, are 8-bit microcontrollers with a rich set of peripherals, comparable amounts of memory and small packages. AVR 8-bit microcontroller family is similar to the PIC18 family and the ATmega328 powers the well-known Arduino Uno. If a device does not require internet connectivity, has minimal security requirements then an 8-bit microcontroller can be used.

A digitally controlled PVE system consists of an ADC accompanied by a control strategy and digitally implemented PWM. To handle the limited bandwidth or large gain variability inherent in traditional analogue controllers, digital controllers can be used in isolated DC-DC converters. To achieve better dynamic responses, advanced control methods can be used. A sampler detects continuous analogue signals at discrete time points in the system. A digital compensator improves system's performance. The closed loop system includes a filter for noise reduction and buffering ADC input. The converter sensitivity, calculation time delay and numerical precision hinder performance of the control system.
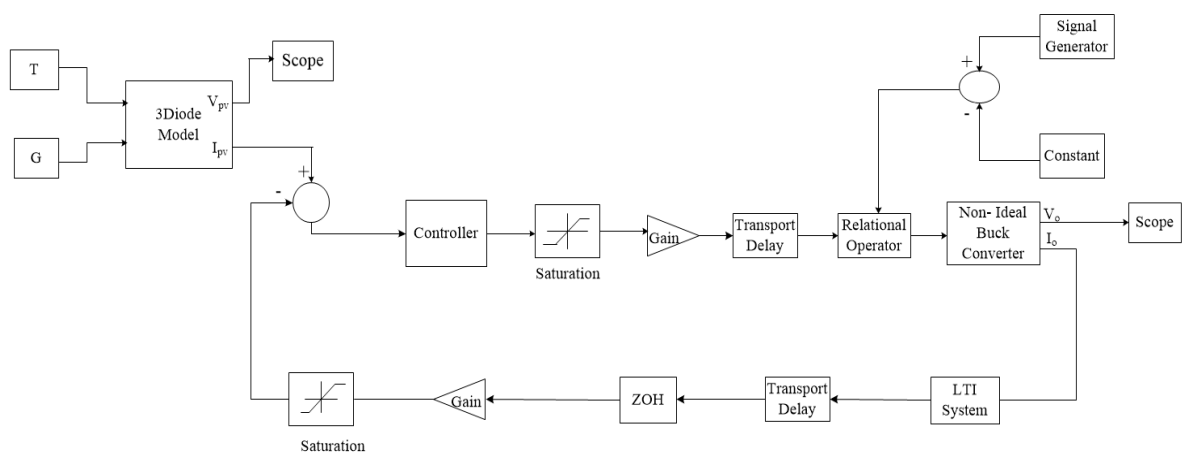
Figure 5.17: Block diagram of PVE with Non-Idealities

Figure 5.17 shows block diagram of PVE with ADC conversion and time delays. Thus, a digital simulation model for PVE is established and it provides a platform to implement different controllers, reference models with delay. As a result, while designing a digital controller, feasible aspects like ADC resolution-sampling frequency, PWM resolution and operational computation delays are considered. The dynamic response of a digital system's ADC prefers V_o to follow V_{ref} at load dynamics or input transients. To obtain input without errors using zero-order hold, the f_{sw} is kept twice the system's bandwidth. To decrease phase delay, a sampling frequency 10 times the system bandwidth is identified, resulting in a phase delay of sampling frequency/10. As a result, an ADC converter is employed to represent the error signal, improving resolution and mandating very few ADC converter bits. This simulation's goal is inclusion of non-idealities like ADC conversion. Because an 8-bit microcontroller is being considered, d is limited from 0 to 255, the value is then rounded to the closest integer and turned to a number between 0 and 1.

Researchers have focused majorly on the deployment of digital CMC power converter systems. Holme and Manning [111] investigated a digital CMC, which is divided into three subsystems: Analogue data acquisition, 16-bit DSP and a PWM. Evidently, it had significant drawbacks due to complicated hardware, high cost and low reliability. CMC is considered superior for high-performance power applications due to the fast inner current loop. Any variation in input voltage or response load is immediately sensed as i_L in a CMC power converter. CMC power converters, as a result, typically respond faster than VMC power converters.

5.8 RESULTS AND DISCUSSION

Once all controllers are designed and incorporated in the PVE model, the system performance indices and accuracy are compared. The performance index implies the quantitative measure of the system to understand system specifications. The time response parameters are taken in msec. The innate objective is to track error at transient load conditions and to explain performance of PVE. Integral square error (ISE) and integral absolute error (IAE) are performance indices that are used in objective functions as they produce minor overshoot. For time domain performance settling time t_s, rise time, t_r and percentage overshoot, POS are taken in the objective function with weight values to improve optimization performance.
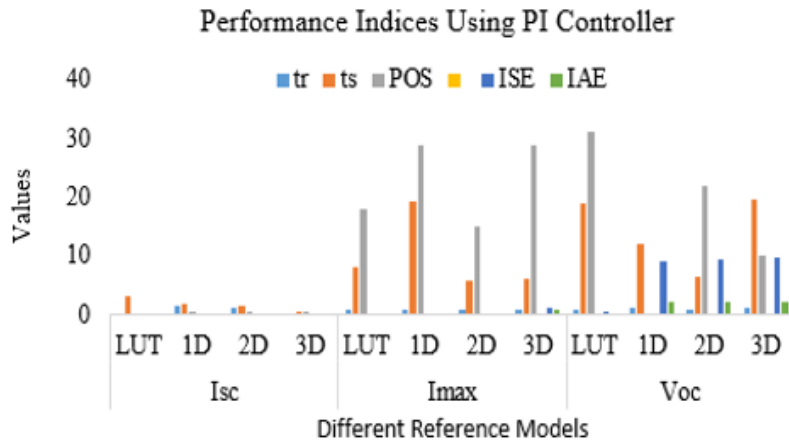
Figure 5.18: Histogram showcasing performance of PI with different reference models

Figure 5.18 concludes that the performance with 3D models shows better results with PI in I_{sc} and I_{max} region whereas 1D has better performance near V_{oc}.
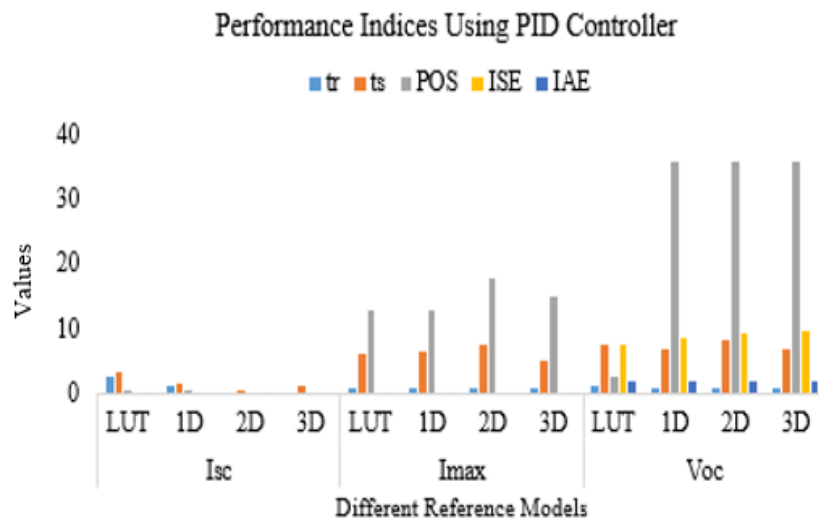
Figure 5.19: Histogram showcasing performance of PID with different reference models

Table 5.1: Summarized rise time and settling time using PI and PID controllers

Controller	Current Point	t_r (msec)	t_s (msec)
PI	SC	0.32	0.6
	MPP	0.89	5.7
	OC	0.9	6.3
PID	SC	0.28	0.38
	MPP	0.88	5
	OC	0.9	6.9

Figure 5.19 demonstrates that the performance with 3D models shows better results with PID in I_{sc} and I_{max} region whereas LUT has better performance near V_{oc} and Table 5.1 summarizes comparative results of rise time and settling time. For CMC PVE the results are acceptable at SC however to improvise the values further controllers are implemented.

Figure 5.20 shows the transient response of PID controlled PVE with different reference models. The results show that conventional controllers tend to produce a high overshoot. However, they are widely used because of their simple structure. Unfortunately, it is found to be quite difficult to properly tune the gains of PID controllers because PVE are often burdened with problems such as load dynamics, partial shading and operation other than STC.
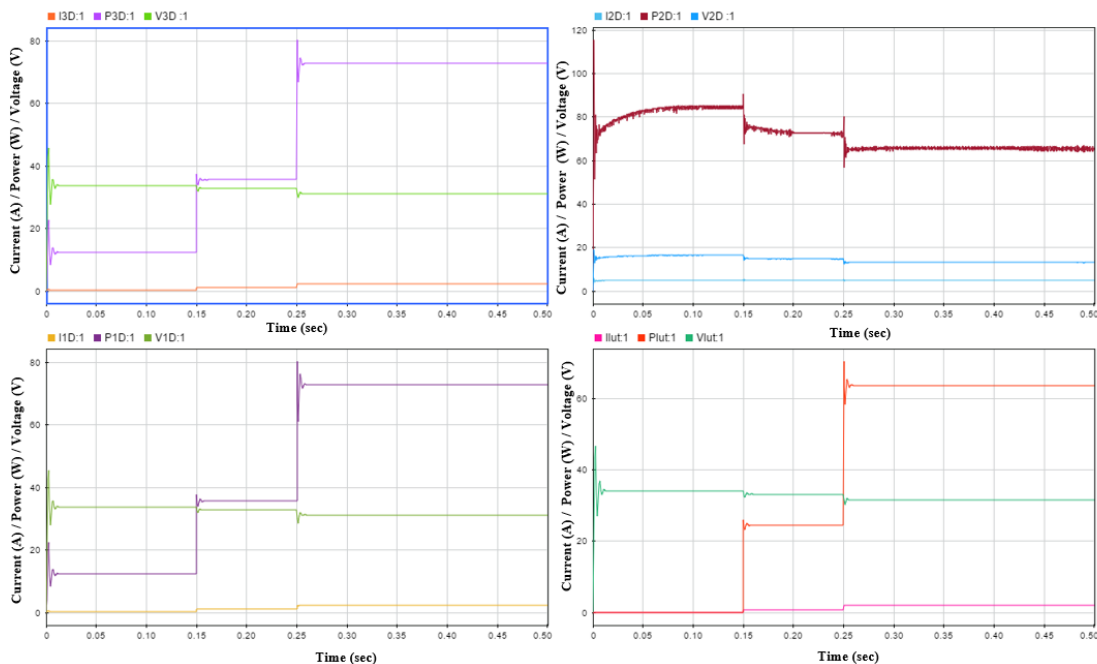
Figure 5.20: Dynamic response of PID controlled PVE

Table 5.2: Effect of increasing parameter variations

Controller Parameter	Tr	Ts	POS	Stability
k_p	Decreases	Increases	Less altered	Degrades
k_i	Decreases	Increases	increases	Degrades
k_d	Unaffected	Decreases	decreases	k_d can improve if kept small

Table 5.2 displays the importance of each gain parameter in terms of transient time. It will be useful in the later stages of designing hybrid controllers. An objective function is required in the case of algorithm-based controllers to represent the final objective in terms of a mathematical equation. One of the important parameters in forming the objective function of controllers is the selection of weights. As a result, Table 5.3 displays the various values obtained by varying the weights for minimizing the objective function, F.

$$F = \min \left(w_1(t_r) + w_2(t_s) + w_3(POS) + w_4(ISE) + w_5(IAE) \right) \qquad (5.46)$$

Table 5.3: Selection criteria for weights in objective function

S.No.	w_1	w_2	w_3	w_4	w_5	F
1	0.6	0.1	0.1	0.1	0.1	1.4
2	0.5	0.2	0.1	0.1	0.1	1.7
3	0.2	0.2	0.1	0.4	0.1	1.5
4	0.2	0.1	0.1	0.5	0.1	1.3
5	0.1	0.1	0.1	0.6	0.1	1.3
6	0.4	0.1	0.1	0.2	0.2	1.2
7	0.5	0.1	0.1	0.2	0.1	1.5
8	0.5	0.1	0.1	0.1	0.2	1.3
9	0.1	0.3	0.1	0.3	0.2	1.8
10	0.1	0.1	0.2	0.2	0.3	1.8
11	0.1	0.1	0.1	0.1	0.6	1.3
12	0.1	0.1	0.1	0.2	0.5	1.3
13	0.2	0.1	0.1	0.2	0.4	1.3
14	0.2	0.2	0.1	0.2	0.3	1.5
15	0.5	0.1	0.2	0.1	0.1	2.1

The Table 5.3 is summarized by taking weights that result in F approximate to a value 2.
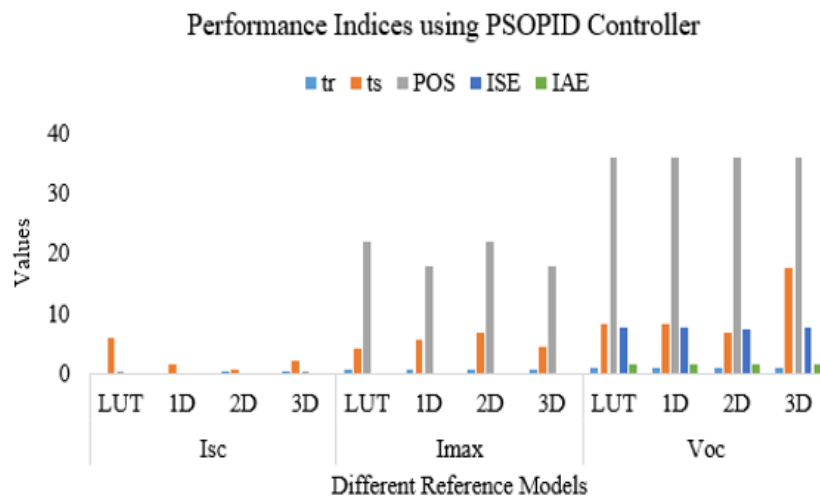
Figure 5.21: Comparative analysis of PSOPID based on different reference models

Figure 5.21 summarizes the comparative analysis of performance indices of PSO tuned PID based on different reference models. The histogram shows good results in I_{sc} region with all diode models. MPP region has good results with 1D and near V_{oc} the problem of overshoot is prominent as the selection criteria was based on settling time. So, 2D shows best results in that region with PSOPID.
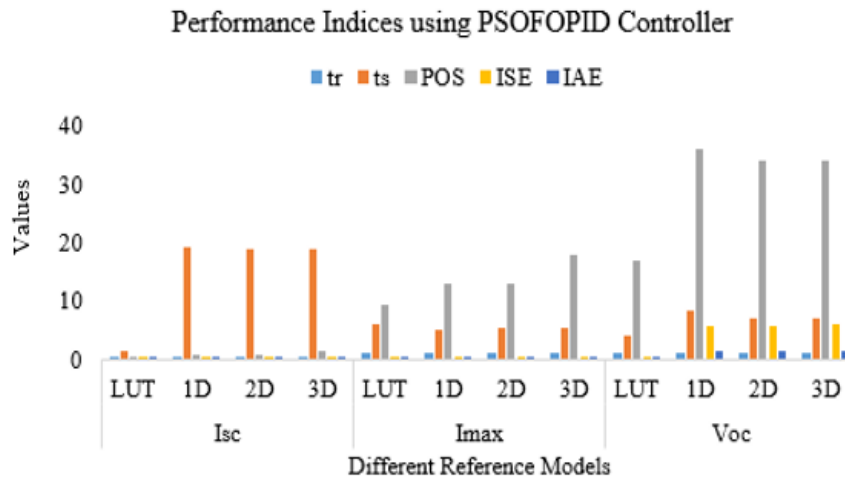
Figure 5.22: Comparative analysis of PSOFOPID based on different reference models

Table 5.4: Summarized rise time and settling time using PSOPID and PSOFOPID controllers

Controller	Current Point	t_r (msec)	t_s (msec)
PSOPID	SC	0.3	0.6
	MPP	0.6	4.2
	OC	0.9	6.9
PSOFOPID	SC	0.35	19
	MPP	0.88	5.2
	OC	0.86	3.9

The results of tuning in Figure 5.22 show that the proposed PSOFOPID controller with different reference models outperformed conventional controllers in terms of set point tracking and smooth controller response. And Table 5.4 gives a comparative summary of rise time and settling time using PSOPID and PSOFOPID based PVE. The results seem to be better than table 5.1 values for rise time.
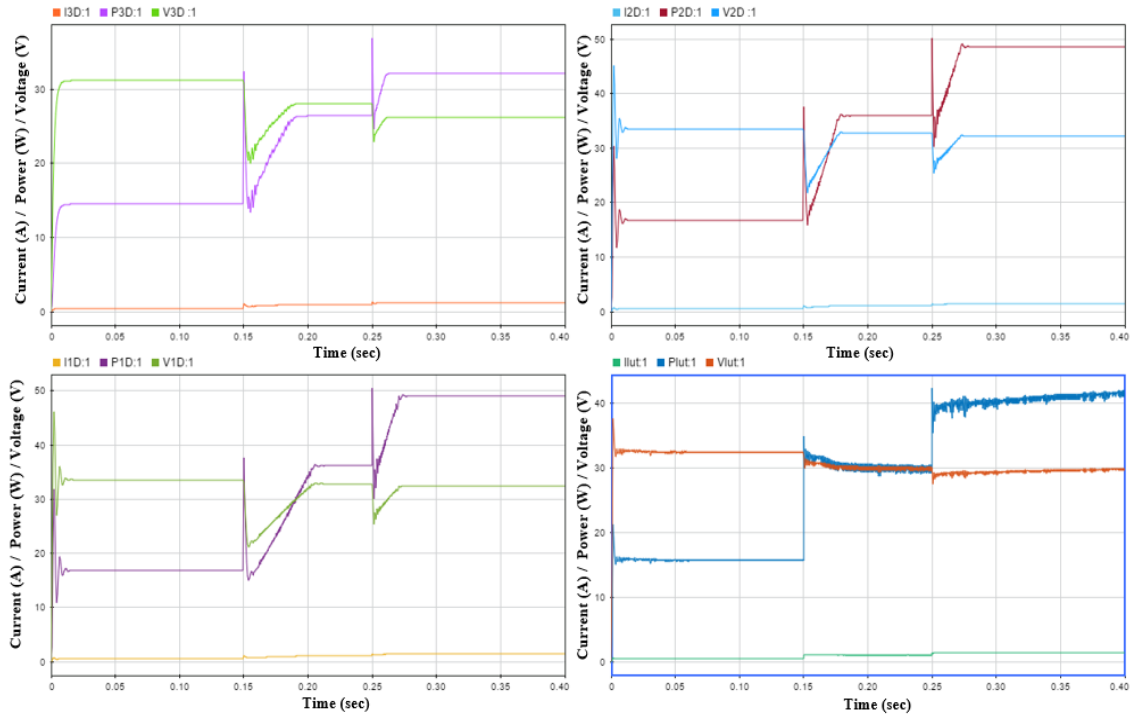
Figure 5.23: Dynamic response of PSOFOPID controlled PVE

Figure 5.23 shows the dynamics obtained by implementation of PSOFOPID controller in PVE model. Transient response with 3D reference model seems to be acceptable.
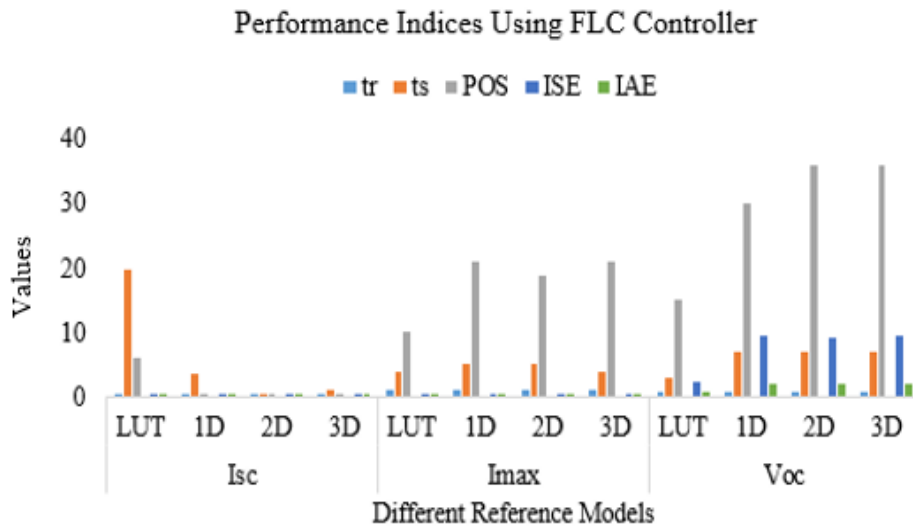
Figure 5.24: Performance Indices based comparison of different reference models in FLC implemented PVE

Figure 5.24 demonstrates the performance indices-based comparison of different reference models in FLC implemented PVE. 2D and 3D based models show fine results in I_{sc} region. 3D shows better results in I_{max} but LUT has finest performance near V_{oc}.
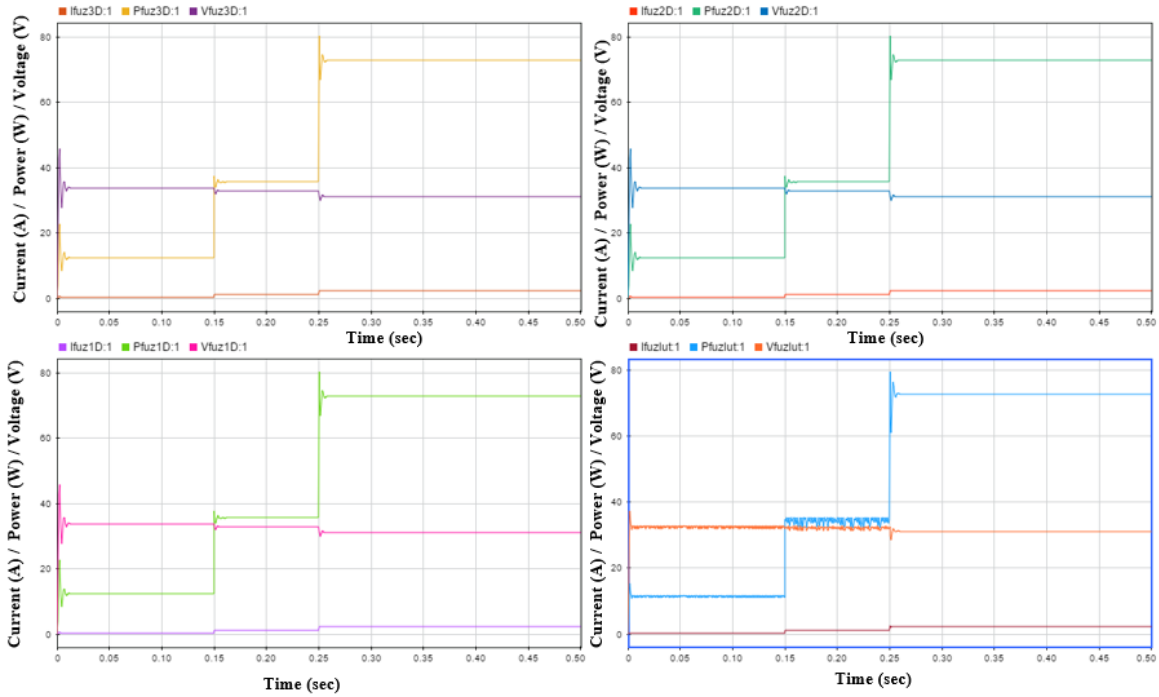
Figure 5.25: Dynamic response of FLC controlled PVE

Figure 5.25 concludes the transient behaviour of PVE based on FLC and it is found that it performs well in all diode-based models. However, LUT shows transients in power region.
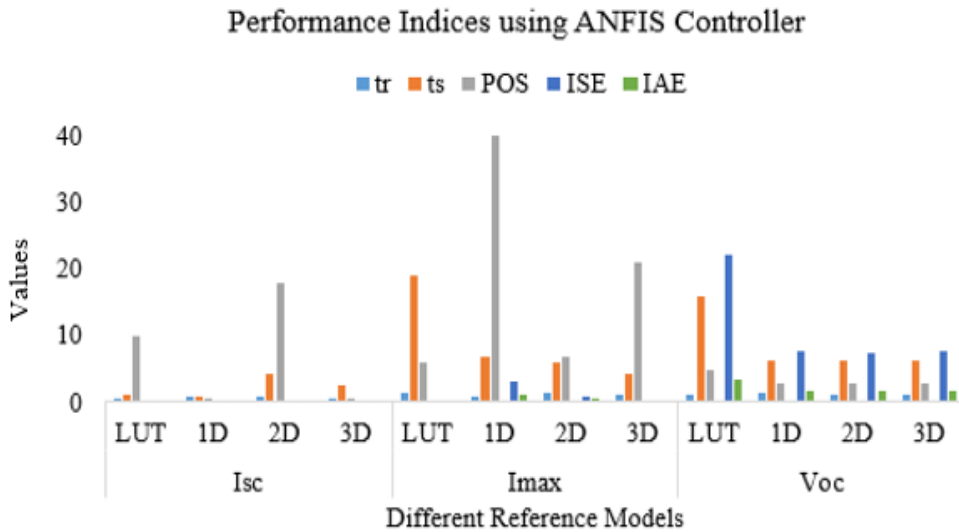
Figure 5.26: Performance Analysis of ANFIS based reference models in PVE

Figure 5.26 concludes that 1D performs well in I_{sc} region, 2D near MPP and every diode model show satisfactory results near V_{OC}. Figure 5.26 concludes the transient response of ANFIS based PVE and it is found that diode reference model results are comparable and acceptable.

Table 5.5: Summarized rise time and settling time using FLC and ANFIS controllers

Controller	Current Point	t_r (msec)	t_s (msec)
FLC	SC	0.4	0.5
	MPP	0.9	3.9
	OC	0.8	3
ANFIS	SC	0.4	1.0
	MPP	0.8	6.9
	OC	1.2	6.2

Table 5.5 depicts the comparison of rise time and settling time using FLC and ANFIS. The results show improvement in case of settling time as compared to table 5.4
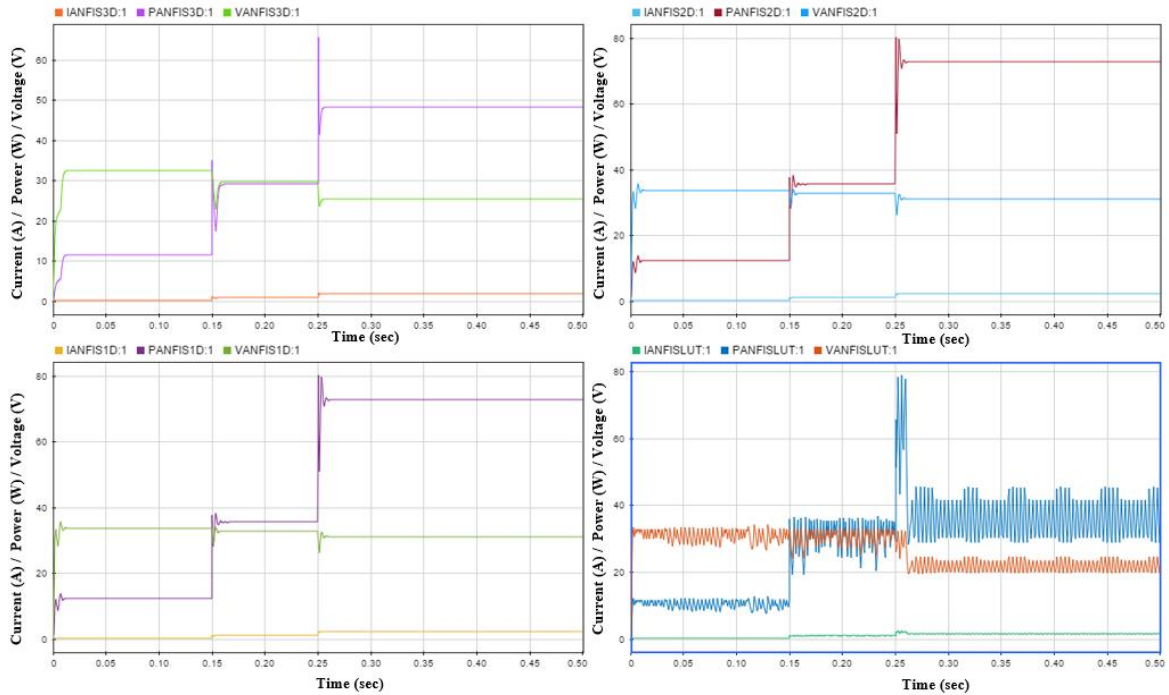
Figure 5.27: Dynamic response of ANFIS controlled PVE
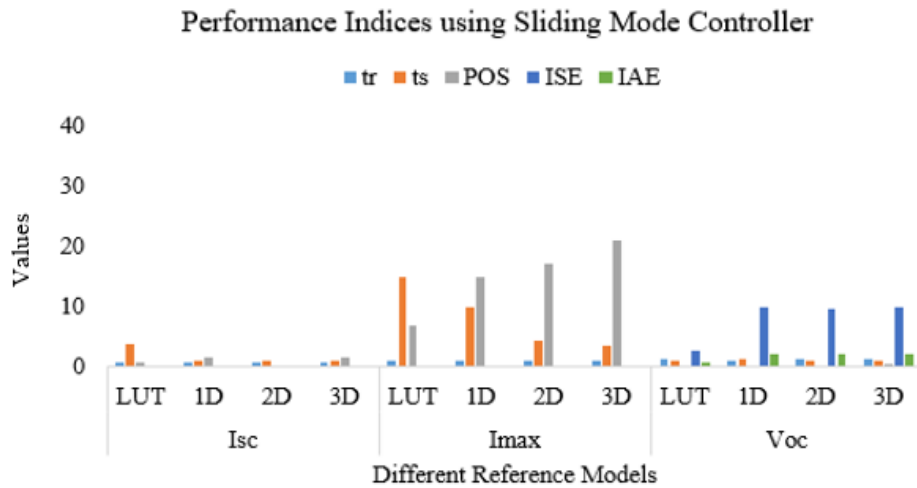
Figure 5.28: Performance analysis using SMC in different regions of PVE

Figure 5.28 presents performance analysis using SMC in different regions of PVE by different reference models. 2D model is best in Ist region, 3D has fine performance in IInd and IIIrd region of operation of PVE.

Table 5.6: Values of amplifiers using a, b, m in SMC modeling

S.No	Calculated values for simulation
1	$aC = 726 \times 10^{-6}$
2	$mCL = 19.14 \times 10^{-6}$
3	$Lb = 0.00029$

Table 5.2 summarizes the values calculated and assigned to parameters of SMC model. These values are required to find the stability of the system. Figure 5.29 depicts the transient behaviour of PVE based on SMC. The robust controller shows its robustness in all reference models with its constant behaviour over dynamic loading.

Table 5.7: Summarized rise time and settling time using SMC

Controller	Current Point	t_r (msec)	t_s (msec)
SMC	SC	0.6	0.9
	MPP	1	4.4
	OC	1.2	0.9

Table 5.7 depicts that SMC controller gives fastest settling time of 0.9 msec. The other time values are also acceptable for PVE operations.
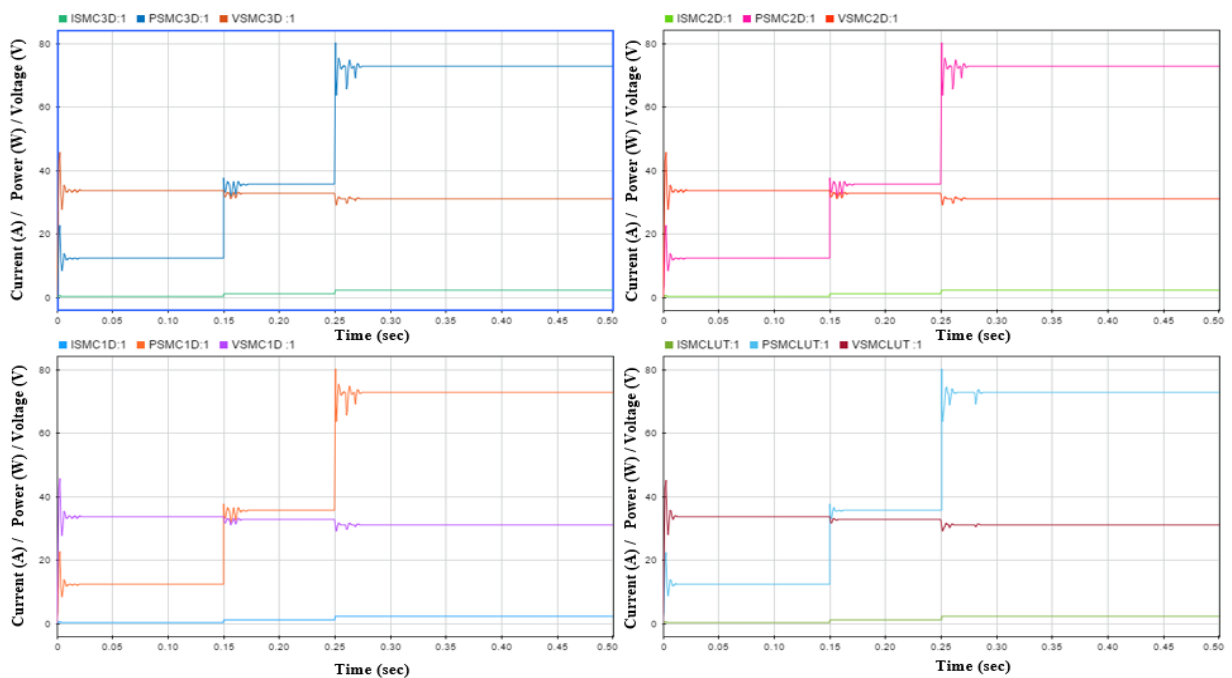
Figure 5.29: Dynamic response of SMC controlled PVE

The solution of the system simulated by the above-mentioned computed values indicates that the system is stable. As a result, the inferred control law can be used to achieve desired results in ambiguous environments. The values of amplifiers included in the model are shown in Table 5.2. The dynamic behaviour of the system is due to changing load conditions and irradiance due to partial shading of panel. Thus, it is proved that the main advantage of choosing SMC controller over the traditional controllers like P, PI and PID. is existence of stability and robustness performance in uncertain system, where these controllers fail specially in the case of uncertain environment.
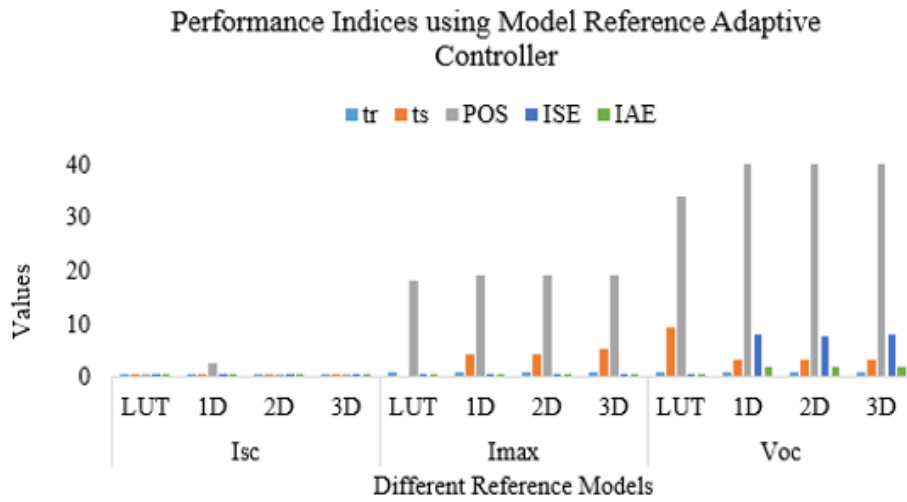
Figure 5.30: Performance analysis of MRAC for different reference model based PVE

Figure 5.30 concludes that MRAC has good responses in I_{sc} region with every diode model. MPP region has best results with LUT whereas diode models again show fine results near V_{oc}. Figure 5.31 concludes the results of transient response and the system shows good reference tracking for diode and LUT model during dynamic conditions.
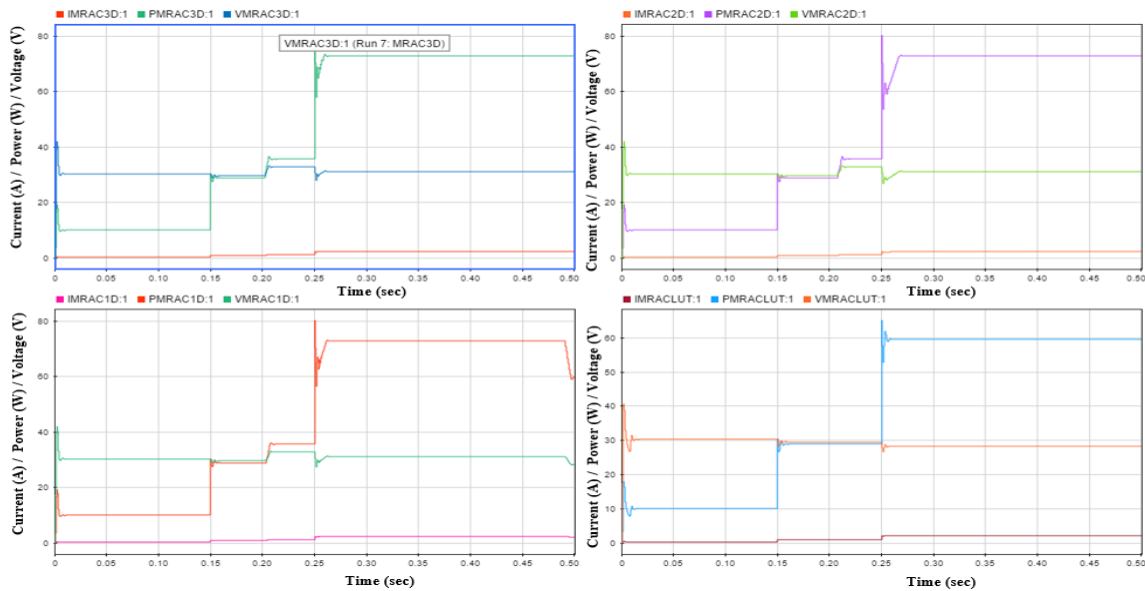
Figure 5.31: Dynamic response of MRAC controlled PVE
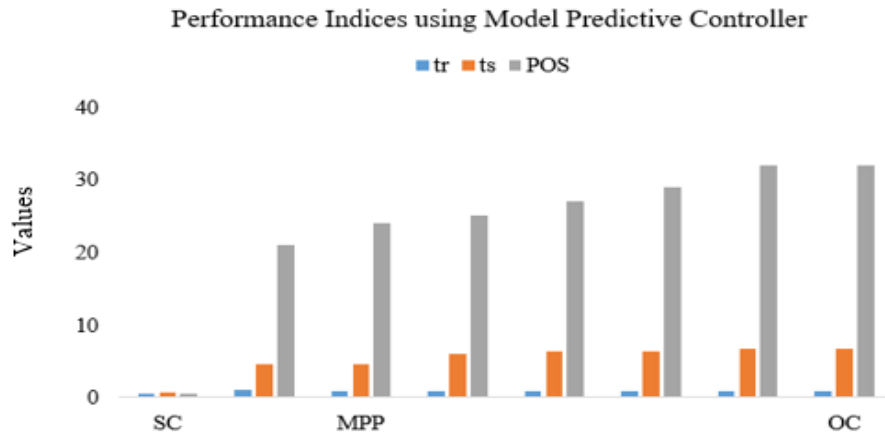
Figure 5.32: Performance analysis of MPC for different reference model based PVE

Figure 5.32 shows the performance indices of MPC based PVE. The model gives satisfactory results in SC region, but the system seems unable to reduce the POS in MPP and OC region of operation.
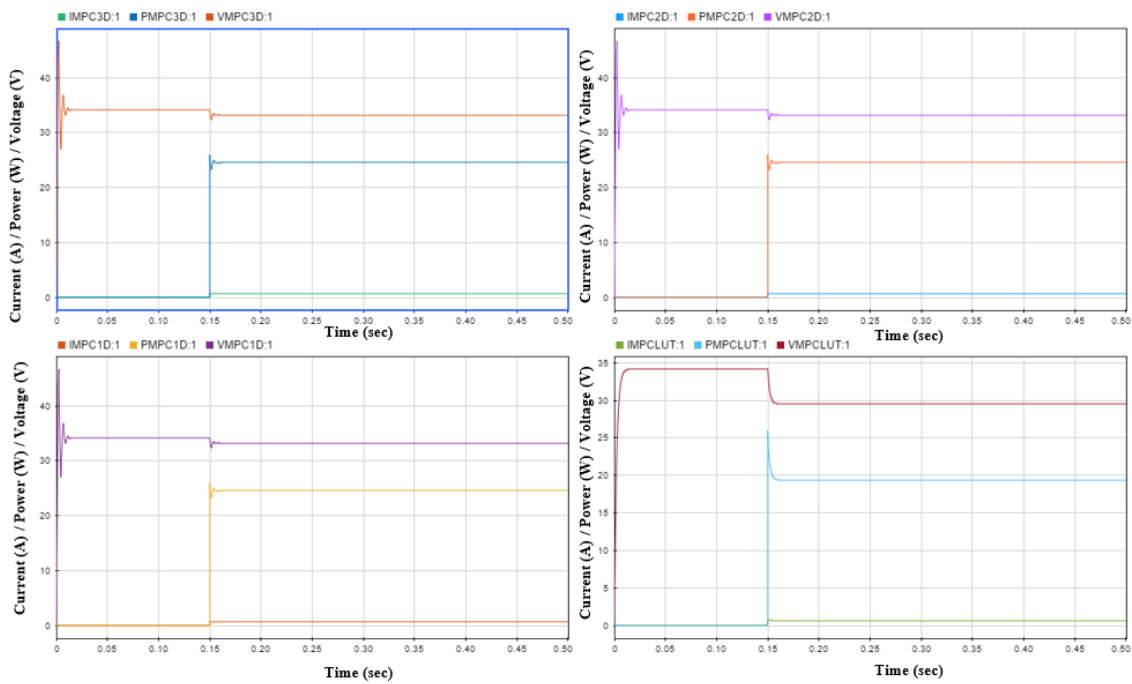
Figure 5.33: Dynamic response of MPC PVE

The dynamic response in Figure 5.33 shows that the MPC controlled PVE behaves satisfactorily for diode models and LUT. Transients are within acceptable limits and quick response is noticed during load dynamics.
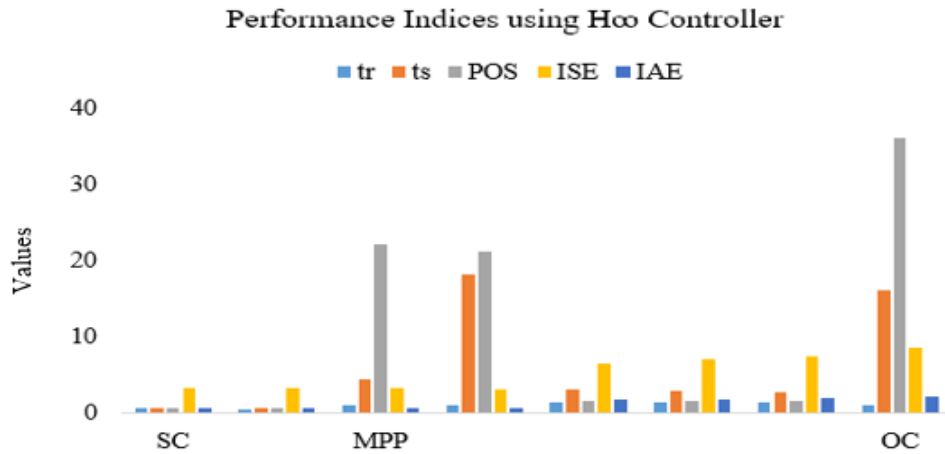
Figure 5.34: Performance analysis of Hω for different reference model based PVE

The robustness of the H_∞ controller over the entire operating range of the PVE is depicted in Figure 5.34. The values are higher at OC, but by implementing VMC according to the system's application, they can be reduced to a lower range. The response time is comparably faster than previously implemented controllers.

Table 5.8: Summarized rise time and settling time using MRAC, MPC and Hω controllers

Controller	Current Point	t_r (msec)	t_s (msec)
MRAC	SC	0.39	0.38
	MPP	0.9	4.1
	OC	0.8	3.2
MPC	SC	0.4	0.6
	MPP	0.9	4.5
	OC	0.9	6.9
Hω	SC	0.5	0.6
	MPP	0.9	4.3
	OC	0.9	16

Table 5.8 depicts comparison of robust controller performance based on rise time and settling time. Rise time at SC is 0.39 msec in MRAC and fastest settling time of 0.6 msec is attained by implementation of Hω controller. The fast response of robust controllers in dynamic conditions provide a good foundation for the PVE.
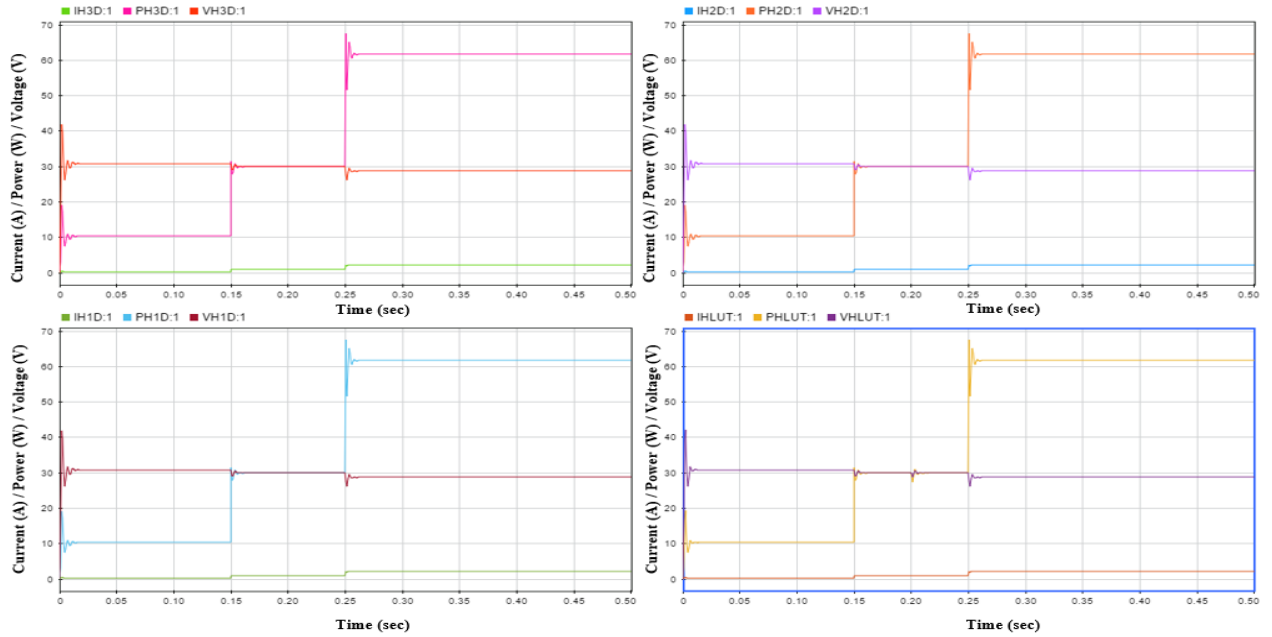
Figure 5.35: Dynamic response of H∞ based PVE

The dynamic response of the H_∞-PVE model is summarised in Figure 5.35. The system's robustness across the entire range of PV panel characteristics is significant and it provides a good foundation for selecting this controller for calculating overall system's reliability and availability in the following chapter.

In order to select best controller among robust controllers, the VI and PV characteristics of MRAC, H_∞ and MPC controllers are plotted against reference PV panel as shown in Figure 5.36 and 5.37 respectively.
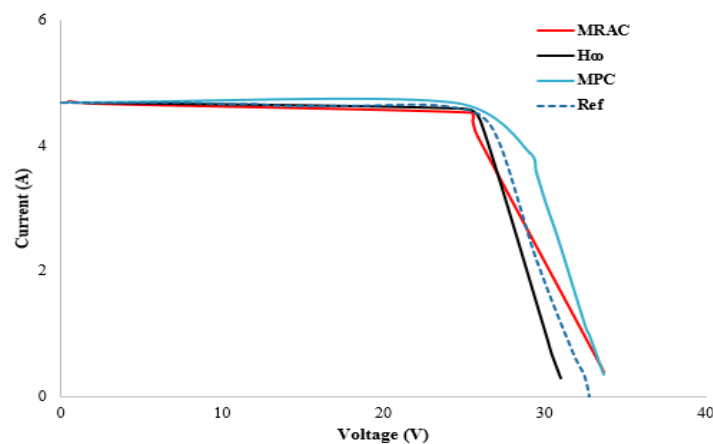
Figure 5.36: Comparative VI analysis of robust controllers
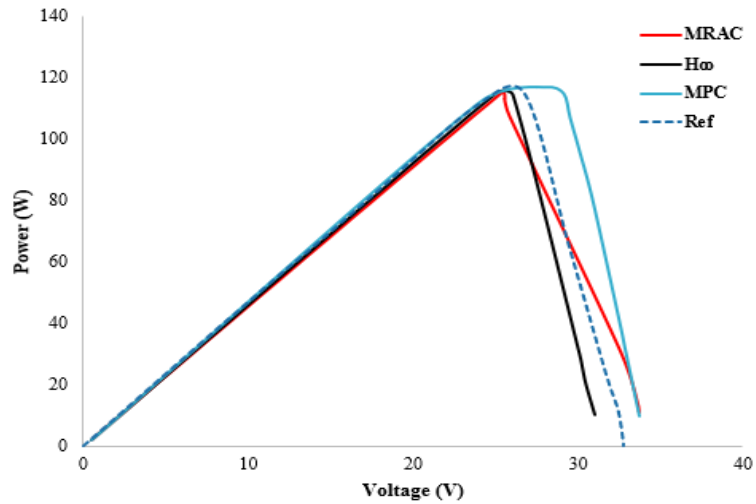
Figure 5.37: Comparative PV analysis of robust controllers

Figure 5.36 and 5.37 signify that H_∞ controller outperforms among robust controllers and the characteristics plot show close approximation to PV panel characteristics. These comparison plots help in selecting a controller for study of PVE on digital platform.

Following transient responses are obtained by considering non-ideal conditions with H_∞ controller and different reference model. The delay time, ESR of inductor and capacitor are primarily introduced in the model.
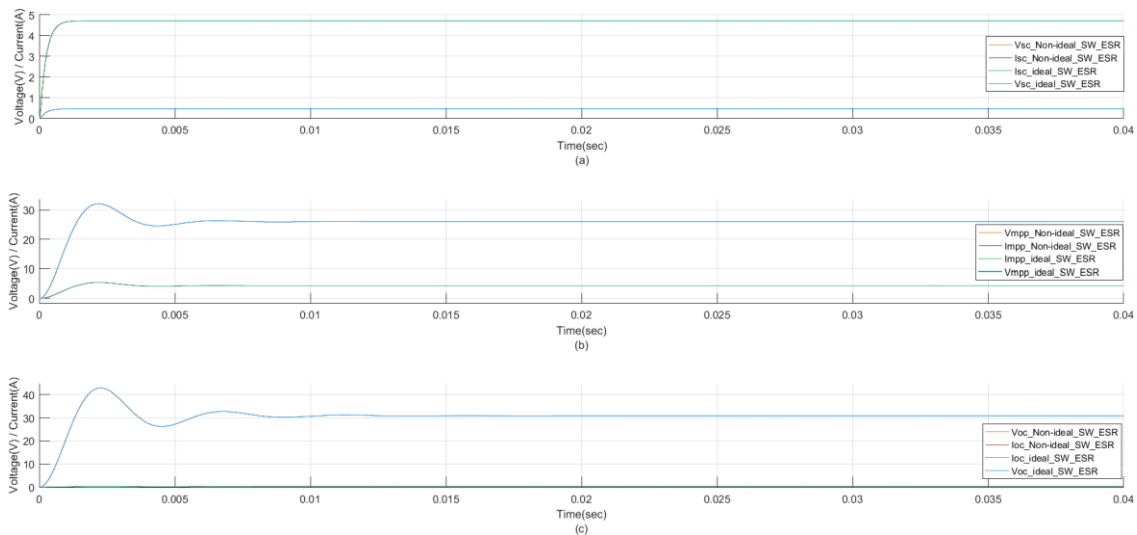
Figure 5.38: Voltage and current at (a) Short circuit(sc) (b) Maximum Power Point(mpp) (c) Open Circuit (oc) using H_∞ controller with LUT model as reference model.
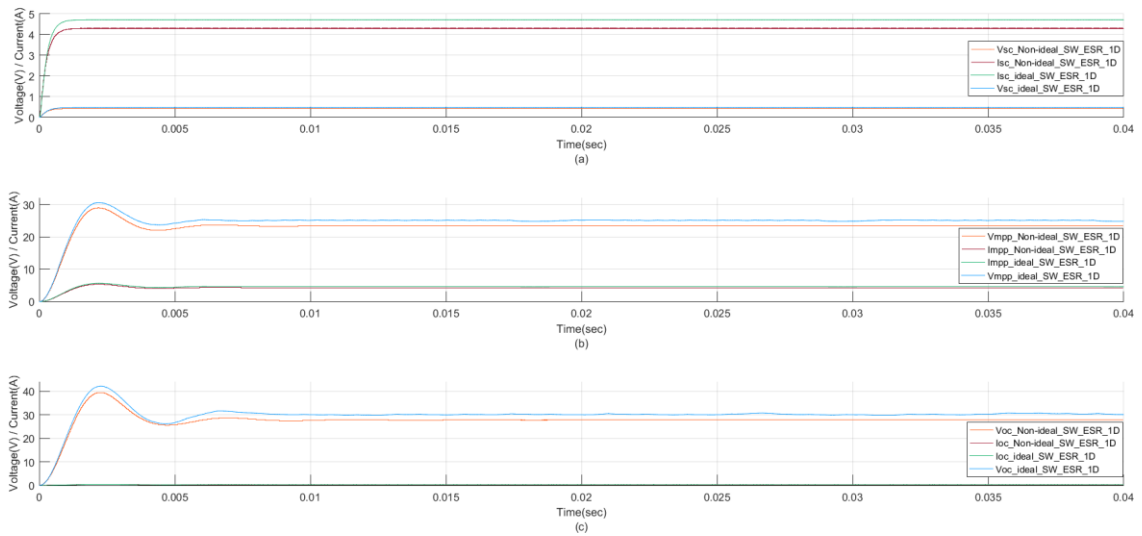
Figure 5.39: Voltage and current at (a) Short circuit(sc) (b) Maximum Power Point(mpp) (c) Open Circuit (oc) using H$_\omega$ controller with 1Diode model as reference model.
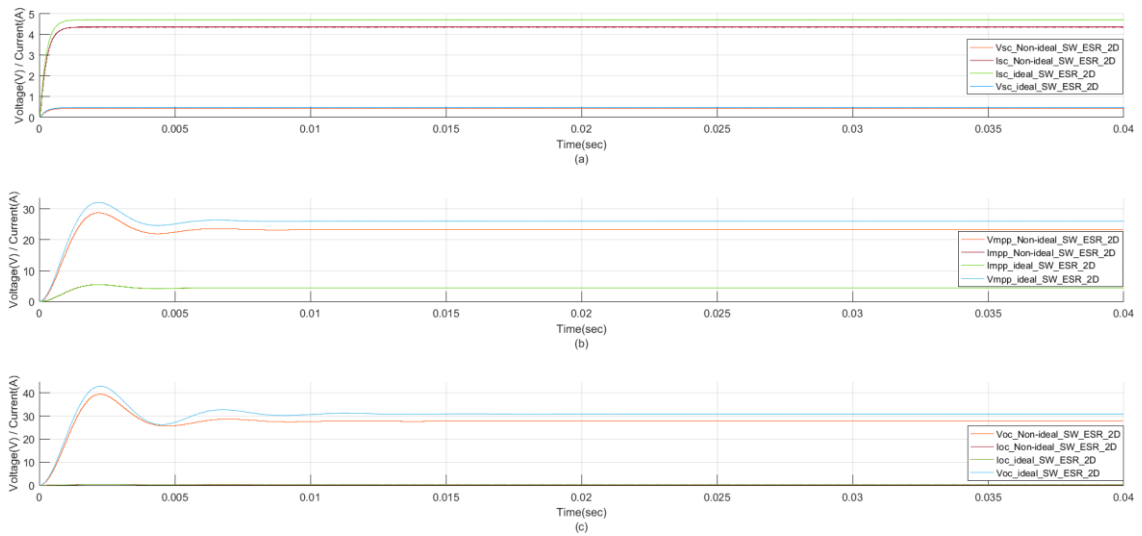
Figure 5.40: Voltage and current at (a) Short circuit (sc) (b) Maximum Power Point (mpp) (c) Open Circuit (oc) using H$_\omega$ controller with 2Diode model as reference model.
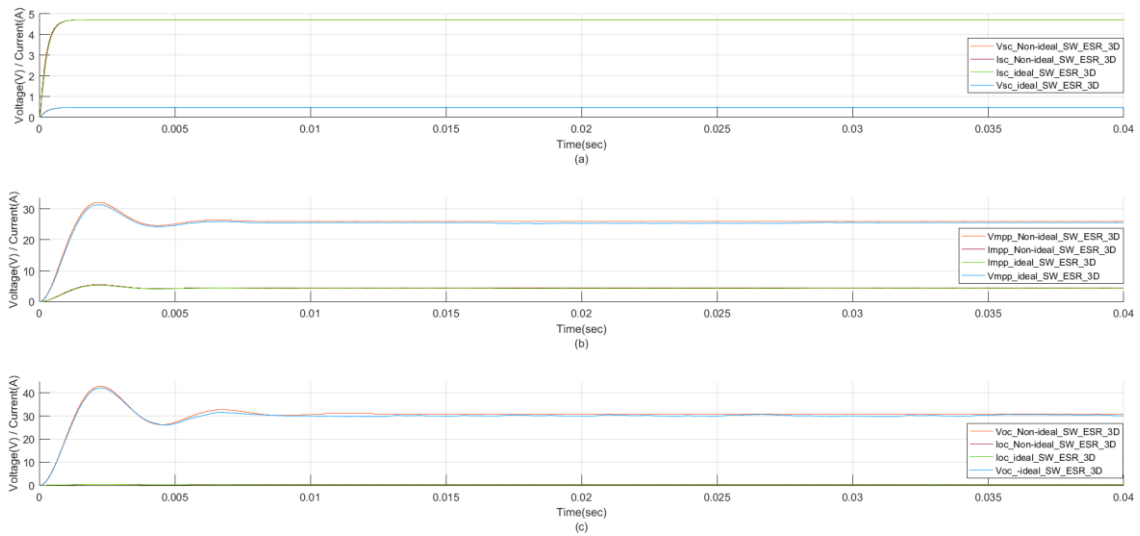
Figure 5.41: Voltage and current at (a) Short circuit (sc) (b) Maximum Power Point (mpp) (c) Open Circuit (oc) using H$_\omega$ controller with 3Diode model as reference model.

Figures 5.38, 5.40 and 5.41 show the transient response of digital control based PVE model. The transient is taken for short circuit, maximum power point and open circuit points of PVE. These are the main three points indicated in the datasheets of PV panels as they help in deciding the application of particular panel. These responses help in deciding the selection of panel. The responses of LUT and 3D model show the best results matching the reference values.

Results of Transfer Function approach to design PVE with converter without ESR
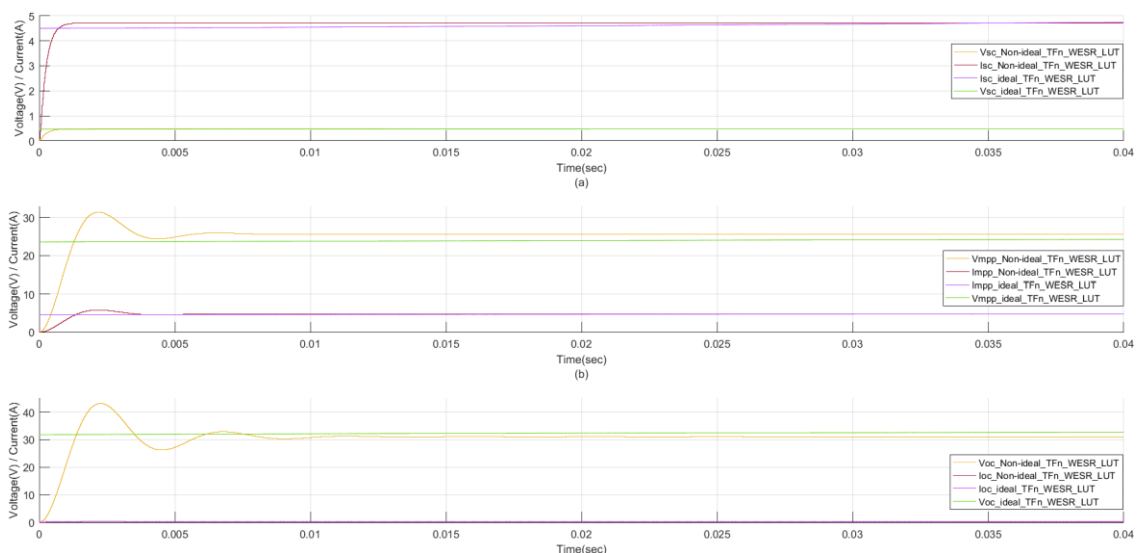
Figure 5.42: Voltage and current at (a) Short circuit (sc) (b) Maximum Power Point (mpp) (c) Open Circuit (oc) using converter without ESR, H$_\omega$ controller and LUT model as reference model.
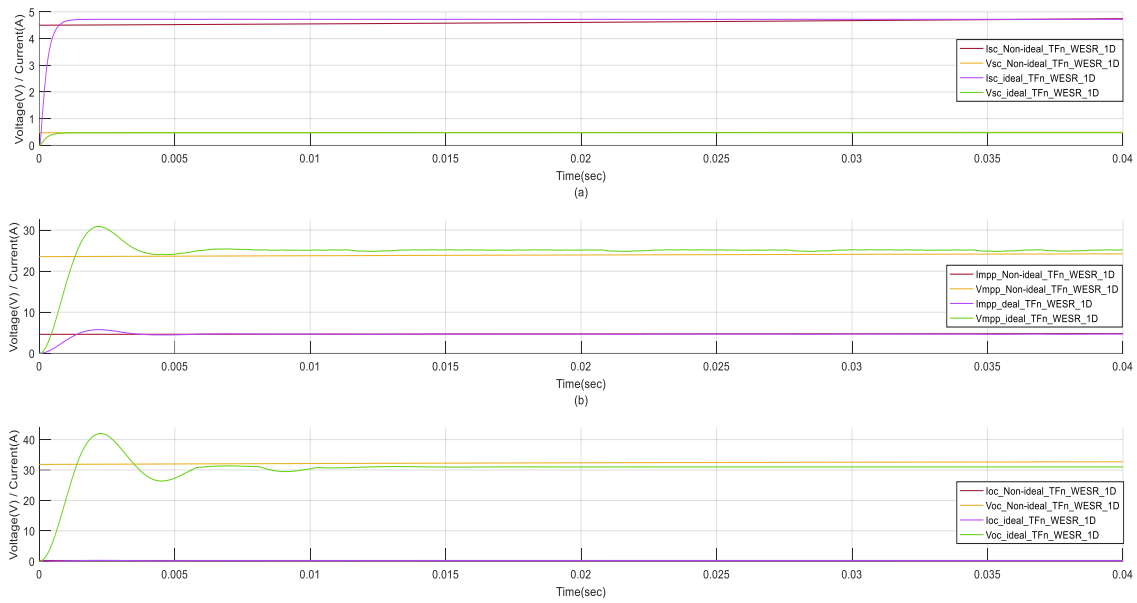
Figure 5.43: Voltage and current at (a) Short circuit (sc) (b) Maximum Power Point (mpp) (c) Open Circuit (oc) using converter without ESR, H$_\omega$ controller and 1Diode model as reference model.
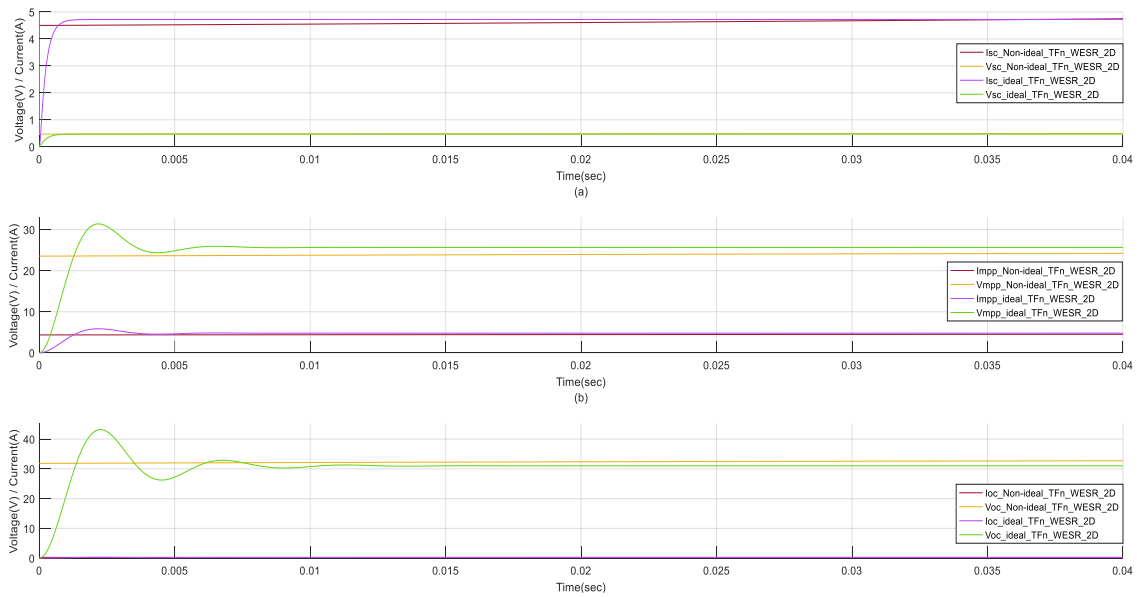
Figure 5.44: Voltage and current at (a) Short circuit (sc) (b) Maximum Power Point (mpp) (c) Open Circuit (oc) using converter without ESR, H$_\omega$ controller and 2Diode model as reference model.

91
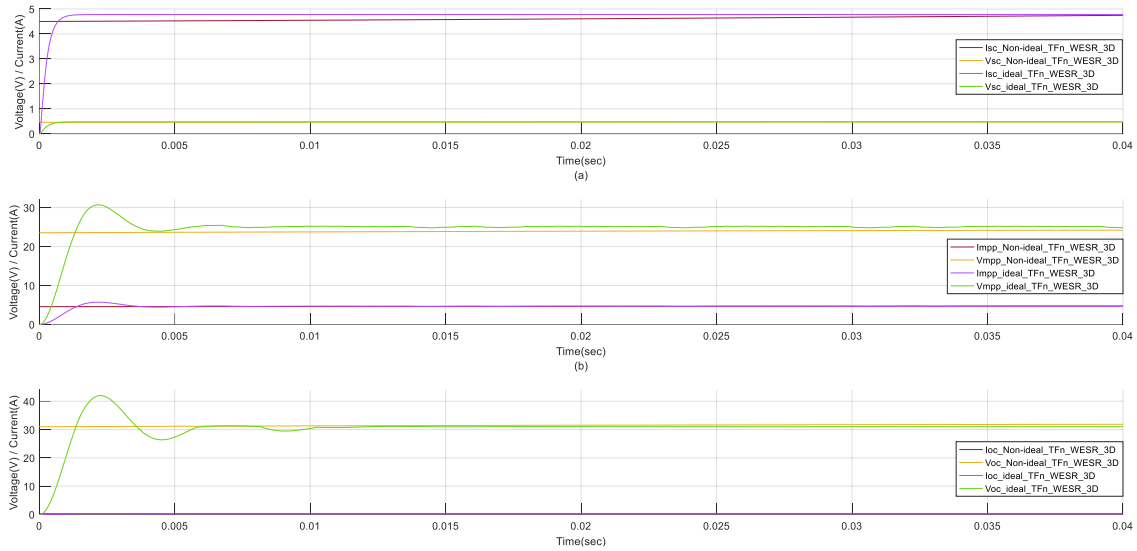
Figure 5.45: Voltage and current at (a) Short circuit (sc) (b) Maximum Power Point (mpp) (c) Open Circuit (oc) using converter without ESR, H$_\omega$ controller and 3Diode model as reference model.

Figures 5.42, 5.43, 5.44 and 5.45 compare the transient response characteristics for short circuit, maximum power point and open circuit points of PV characteristic curve. The plots show that sc and mpp results match with reference values in acceptable range and open circuit variations are close to reference values and can further be improvised by VMC application to PVE model.

5.9 CONCLUSION

Controllers are implemented in PVE to reduce the error and obtain characteristics similar to reference model. Various controllers are categorized according to their application and tuning methods and results provide following conclusions:

- In conventional methods, PID parameters are derived from manual tuning experience (such as the Z-N tuning rule). However, the objective must be expressed mathematically and the framework must be reliable. It is found that PID is not capable enough to effectively control PVE because of its non-linearity. They only function at a single required value and do not compensate when the constrained region changes.

- Advanced methods like AI based techniques require expert systems as in FLC and NN. These methods provide a rule base for online use.

- Optimization methods are regarded as a special type of optimal control, where PID parameters are obtained by optimization method for a single composite objective.

- Adaptive tuning methods are for automated tuning, using one or a combination of the previous methods based on real-time identification.

- The transient response analysis obtained by including delays, ESR values and the transfer function approach aided in the overall study of PVE by allowing time domain comparisons of all models. Many solutions have been reported in the literature, but an ideal solution depends on the cases involved and the primary goal of application.

- The 3D reference model with H_∞ control strategy outperforms all other controllers in terms of robustness, application time, response, and ease of use. As a result, these models are carried forward to the following chapter for detailed reliability and availability analysis of the entire PVE.

CHAPTER - 6

RELIABILITY AND AVAILABILITY ANALYSIS OF DESIGNED PVE

6.1 INTRODUCTION

Reliability analysis of the designed system is another important aspect of this work. If PVE accurately monitors the VI characteristics of the reference PV panel, it is considered efficiently modeled emulator. Reliability is accomplished by reducing premature failures and predicting maintenance time. It can be alluded to as the probability of performance to achieve the desired goal. PVE as a meaningful system requires mathematical reliability assessment. For designing a reliable PVE, providing a systematic framework for reliability assessment is extremely important. Literature review in chapter 2 summarized the studies and methodologies found in papers for assessing reliability of power electronic converters.

6.2 CLASSIFICATION OF RELIABILITY ANALYSIS

The classification of Reliability Analysis is based on the methodologies applied for analysing the reliability of the models. The three main categories are:

- **Part failure method**: It is one of the simplest assessment models and have capability of differentiating architectures for comparative analysis but offers limitation in reliability estimation of repairable systems.

- **Combination method**: The models of PVE in this case are based on reliability block diagrams or fault trees. They are used for analysing reliability of redundant systems but they lack specifying the details like repairs, state-dependent failure rates and system reconfiguration.

- **State space method**: State space modeling like Markov model is a popular method of reliability analysis. It is a graphical method of representing system states as from failure rate prospective. Markov model states are further presented as working or failed states.

The failure cost is another factor for reliability analysis, which reveals that one-fourth of failures resulted in more than 80% of failure cost/system cost. It means that whenever a PV system fails, a significant cost is imposed on it. As a result, researchers use reliability analysis to try to minimise the cost ratio. MOSFETs and capacitors constitute the most fragile components in PVE, while resistors and inductors play no role in failure occurrence [183]. Critical power electronic components are dependent on their applications.

6.3 TERMS DESCRIBING RELIABILITY

- **The mean time to failure (MTTF)**: It is used to determine the reliability of complete non-repairable systems. It denotes the time elapsed between the start and the first failure point. According to the bath tub curve, failure rates are classified into three categories: infant mortality, constant or working state and wear out. Out of these zones, reliability calculations in the constant zone can be undertaken using MTTF.

- **Failure in Time (FIT)**: It indicates the number of failures that can occur in one billion hours of operation. These units are generally used in semiconductor related reliability analysis.

The maximum failure rate occurs post manufacturing state and the debugging and aging of components lower these failure rates. In case of semiconductor devices, the consumer assembles, adjusts and calculates the aging of devices. Upon installation for a particular application, the stress level is reduced and failure rates are reported in a range of low FIT to several hundreds of FIT. An important factor to increase the reliability is the manner in which the components work with other components in the circuit.

- **Failure Analysis:** It is performed on fail devices at all stages of their life cycle i.e. from manufacturing to failure stage. The degree of reliability of semiconductor devices majorly depends upon its usage and environmental conditions. Thus, the basic failure rate λ is determined by dissipated power and operating temperature.

Reliability of a device under usage is calculated by multiplying factors defining the design and manufacturing parameters. In engineering notation failure rates are often low and are expressed as failures per million, especially for individual components.

There are three ways to obtain failure rate data:

- Historically available data.
- Government failure rate data
- Testing

6.4 SYSTEM CONSIDERATION FOR RELIABILITY ANALYSIS

A PV is estimated to operate for 25-30 years. During this tenure, however the components like MOSFET, diode, capacitor, inductor experience stress due to switching circuitry, temperature and irradiance factors. Reliability techniques evaluate reliability indices by mathematical modeling and simulation of real panel along with its random behaviour respectively [122-123, 125, 127]. Many research papers are available for calculation of components and PV system

reliability but very little research is done on entire PVE reliability. This work intends to calculate the reliability of overall systems using following methods:

- MIL-HDBK-217 (1995), FIDES (2009) RBD component failure rate determination method.
- State Transition Method (STM) – Markov's Method.
- Petri net Fuzzy Fork Method.

6.5 MIL-HDBK 217F

The reliability of every component of PVE (modeled in previous chapters) is primarily evaluated using MIL-HDBK 217F. Life time target is estimated by considering performance indices like power losses, efficiency, number of devices, initial cost and maintenance. Mathematical modeling of PVE consists of selection of MOSFET, diode, capacitor, inductor and load resistance, controller, reference model according to the required V-I characteristics of actual PV panel (chapter 3 and 4)

6.6 RELIABILITY ANALYSIS OF PVE COMPONENTS- PART FAILURE METHOD

To calculate part failure rate, MIL-HDBK-217 is taken as reference.

a) MOSFETs reliability analysis

Power losses in MOSFET are calculated by following equation:

$$P_{static} = I^2_{rms} * R_{ds(on)} \tag{6.1}$$

Switching Loss of MOSFET is calculated using following equation:

$$P_{sw\,(CCM)} = P_{(ton)} + P_{(toff)} = \frac{1}{2} V_{off} * I_{on} * (t_{on} + t_{off}) * f_s \tag{6.2}$$

$$P_{\,Total} = P_{static} + P_{sw(CCM)} \tag{6.3}$$

$$T_J = T_C + \theta_{JC} * P_{Total\,Loss} \tag{6.4}$$

$$T_J = 50 + (0.3) * (3.74) \tag{6.5}$$

$$\Pi_T = e^{-1925\left(\frac{1}{Tj+273} - \frac{1}{298}\right)} \tag{6.6}$$

Reduction of power loss results in decrease of Π_T, affecting failure rate too. So, a MOSFET switch having lower R_{on} is used to lower failure rate [184].

$$\lambda_p = \lambda_b * \Pi_T * \Pi_A * \Pi_Q * \Pi_E \text{ failure/ } 10^6 \text{ hours} \tag{6.7}$$

$$\lambda_b = 0.012; \quad \Pi_T = 1.6; \quad \Pi_A = 4; \quad \Pi_Q = 1; \quad \Pi_E = 1$$

$$\lambda_{MOSFET} = 0.0192 \text{ failure/ } 10^6 \text{ hours} \tag{6.8}$$

b) Diode Reliability Analysis

Static losses of diode are calculated using following equation:

$$P_{reverse} = V_r * I_r (1\text{-}D) \qquad (6.9)$$

Switching Diode loss is calculated using following equation:

$$P_f = V_f * I_f + I_f^2 * r_d \qquad (6.10)$$

Lower value of V_f, results in low power losses and thereby lesser failure rate.

$$P_{Total} = P_{reverse} + P_f \qquad (6.11)$$

Temperature factor, $\Pi_T = e^{-3091\left(\frac{1}{Tj+273}-\frac{1}{298}\right)} \qquad (6.12)$

$$\lambda_p = \lambda_b * \Pi_T * \Pi_S * \Pi_C * \Pi_Q * \Pi_E \qquad (6.13)$$

$\lambda_b = 0.0010;$ $\quad \Pi_T = 1.93;$ $\quad \Pi_S = 1;$ $\qquad \Pi_C = 1;$ $\qquad \Pi_Q = 1;$ $\qquad \Pi_E = 6$

$$\lambda_{Diode} = 0.01 \text{ failure/ } 10^6 \text{ hours} \qquad (6.14)$$

c) Capacitor Reliability Analysis

$$\lambda_p = \lambda_b * \Pi_T * \Pi_C * \Pi_V * \Pi_{SR} * \Pi_Q * \Pi_E \qquad (6.15)$$

$\lambda_b = 0.00012;$ $\Pi_T = 1;$ $\quad \Pi_{C1} = 3.79 \text{ μf};$ $\quad \Pi_v = (\frac{s}{0.6})^{0.5} + 1 = 10.4;$ $\quad \Pi_{SR} = 1$

$\Pi_Q = 1;$ $\qquad \Pi_E = 1$

$$\lambda_P = 0.0054 \text{ failure/ } 10^6 \text{ hours} \qquad (6.16)$$

d) Inductor Reliability Analysis

*Magnetic devices are most reliable electronic components.

Part failure rate, $\lambda_p = \lambda_b * \Pi_T * \Pi_Q * \Pi_E$ failure/ 10^6 hours $\qquad (6.17)$

$\lambda_b = 0.00003$

$$T_{HS} = T_A + \frac{1.1*11.5*P_{Loss}}{W_L^{0.6766}} \qquad (6.18)$$

For $T_{HS} = 70$, $\lambda_p = 1.59*10^{-4}$ failures/10^6 hours which shows affordable behaviour. $\qquad (6.19)$

Inductor failure rate is least among all other components and thus can be ignored.

e) Failure rate of controller

The microcontrollers like Arduino are reported to be highly reliable as:

- They have multiple power options including USB port, V_{cc} port.
- It has inbuilt voltage regulator avoiding spikes or dips and to bring down the excess voltage.
- They will certainly last a long time if supplied with a constant power supply.
- They have protection diodes for over currents.

But external circuitry protection is essential in case of use of a microcontroller. Considering above points the λ of microcontroller is taken as 0.01 failures/10^6 hours.

f) Gate Driver Reliability Analysis

To avoid driver failure, a resistor is installed from Gate to source and the circuitry is not stretched to a large area to avoid impedances in control circuits and reduce susceptibility to interference. So, the failure rate of resistor is calculated as 0.00034 failures/10^6 hours.

g) Diode Model Reliability Analysis

$$\lambda_p = \lambda_b * \Pi_T * \Pi_C * \Pi_S * \Pi_Q * \Pi_E \tag{6.20}$$

$\lambda_b = 0.0020$; $\Pi_T = 1.6$; $\Pi_C = 1$; $\Pi_S = 0.054$; $\Pi_Q = 1$; $\Pi_E = 1$

$$\lambda_p = 0.00017 \text{ failure}/10^6 \text{ hours} \tag{6.21}$$

h) Load Resistance failure rate is calculated as 0.00004 failure/10^6 hours $\tag{6.22}$

All components are connected in series so, the total λ_T = Sum of λ's of all series connected blocks.

$\lambda_T = \sum_{n=1}^{m} \lambda_m$ where m = no. of components connected in PVE

Therefore, $\lambda_T = 0.06$ failure/10^6 hours $\tag{6.23}$

$$\text{Reliability, } R(t) = e^{-\lambda t} = e^{-0.06t} \tag{6.24}$$

$$R(t) = 0.88 \text{ at } t = 2. \tag{6.25}$$

$$\text{MTBF} = \frac{1}{\lambda} = 16.6 * 10^6 \text{ hrs} \tag{6.26}$$

Figure 6.1 shows relation between reliability and failure w.r.t time. As time proceeds, the failure of components results in decrease of reliability.
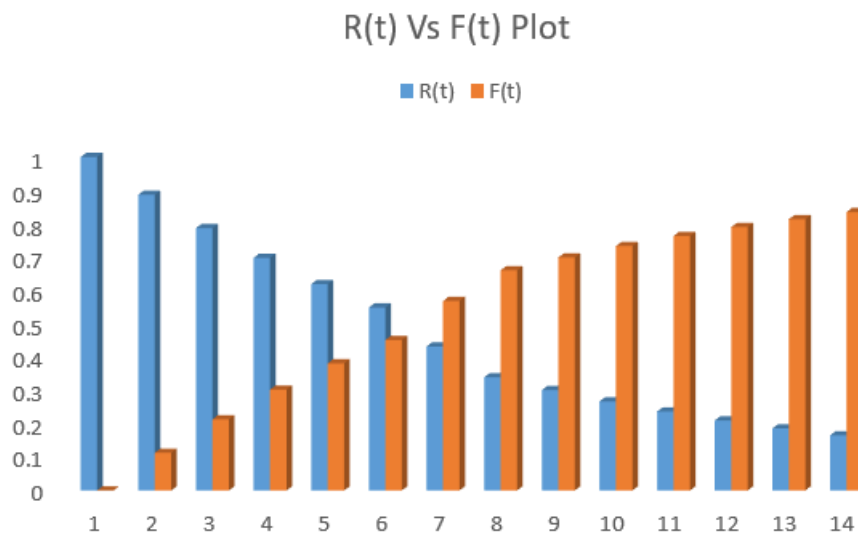
Figure 6.1: Basic Reliability R(t) vs Failure, F(t) plot
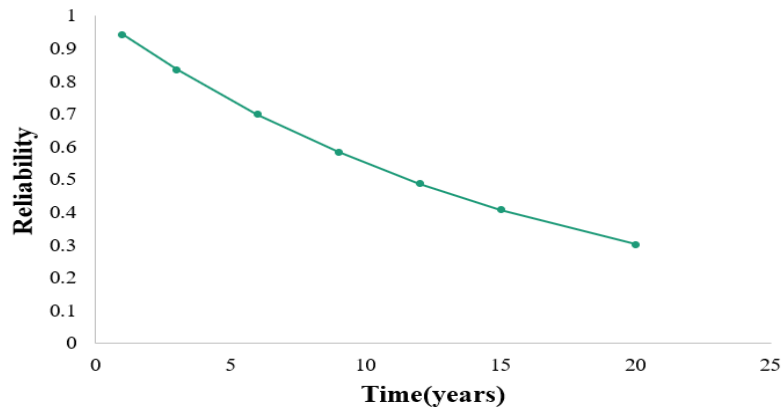
Figure 6.2: Reliability plot using MHBK 217F

Figure 6.2 shows the reliability plot obtained by using MHBK 217F for obtaining failure rates of components used in implementation of PVE model. The plot shows decrease in reliability over years due to factors like overheating, aging of components etc.

6.6.1 Limitations of MIL HDBK 217F RELIABILITY ANALYSIS

According to the MIL-HDBK-217 reliability evaluation, electrolytic capacitors and switches have a high failure rate., but by reducing component's stress reliability can be improved. Some accelerated tests are used by manufacturers to calculate their product's reliability and in each test, single or even more environmental variables are emphasized more than usual. Another option is the Markov method, which is an interactive and time-dependent reliability analysis technique. Total failure rate is the sum of all component failure rates in a series system and system reliability is the multiplication of component reliability [185].

6.7 STATE TRANSITIONS FOR MODELED PVE

Markov's Chain Method

Markov's chain method is prevalently used to anticipate the upcoming state of a variable based on its previous state. It uses a probabilistic approach to predict the next state. The chains are defined by directed graphs that define the current and prior states as well as the probability of shifting from one state to the next. The transition matrix is the matrix describing the Markov chain.
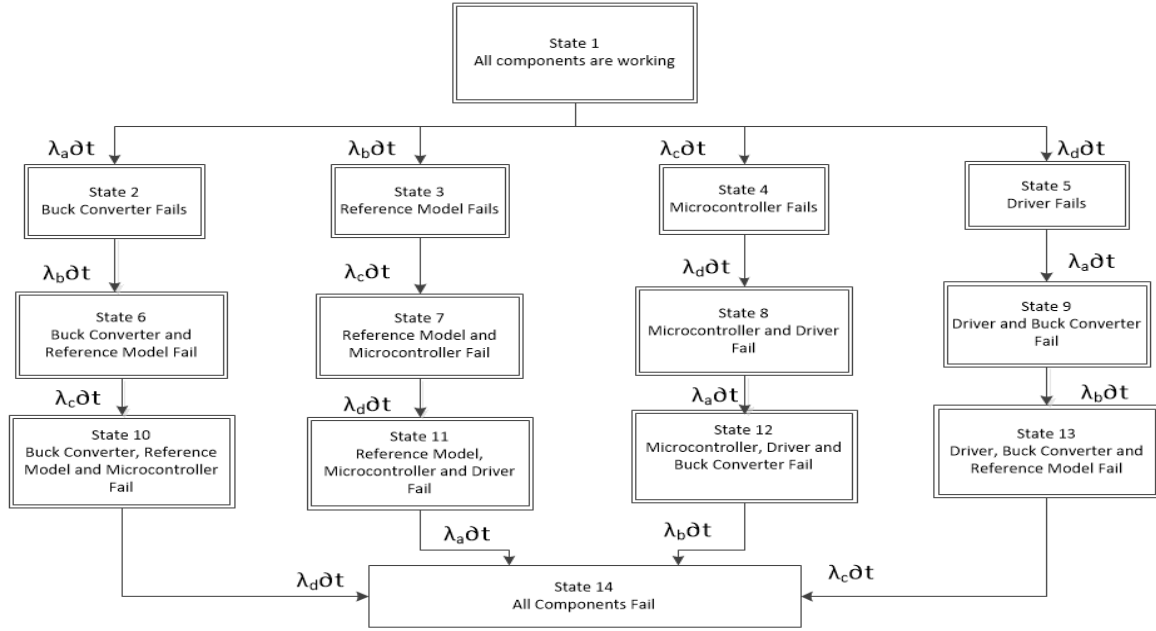
Figure 6.3: State Transition Model (STM) – Markov's Chain

Figure 6.3 shows the state transition of failure of components using Markov's Chain Model. These transition states are taken as base for differential equations defining the transition probabilities [124].

$$P_1(t_o) [1- (\lambda) \partial t] = P_1(t_o+\partial t) \qquad (6.27)$$

$$P_1(t_o) [1- (\lambda_{bcd}) \partial t] (\lambda_a \partial t) P_2(t_o) = P_2(t_o+\partial t) \qquad (6.28)$$

$$P_1(t_o) [1- (\lambda_{acd}) \partial t] (\lambda_b \partial t) P_3(t_o) = P_3(t_o +\partial t) \qquad (6.29)$$

$$P_1(t_o) [1- (\lambda_{abd}) \partial t] (\lambda_c \partial t) P_4(t_o) = P_4(t_o +\partial t) \qquad (6.30)$$

$$P_1(t_o) [1- (\lambda_{abc}) \partial t] (\lambda_d \partial t) P_5(t_o) = P_5(t_o +\partial t) \qquad (6.31)$$

Above equations are formed by considering that state 1 is connected to states 2,3,4 and 5 as shown in Figure 6.4.
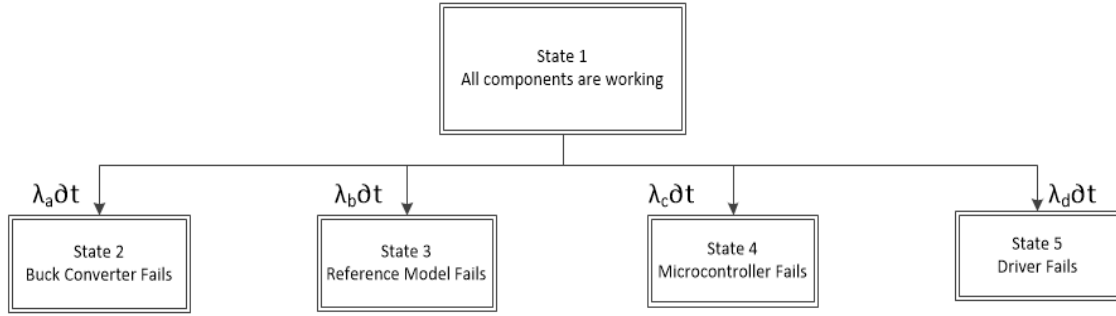
Figure 6.4: STM of states 2,3,4 and 5 from 1

From Figure 6.5, describes how State 2 is connected to state 6, state 3 is associated with state 7, state 4 is linked to state 8, state 5 is connected to state 9, so further probability transition equations become:
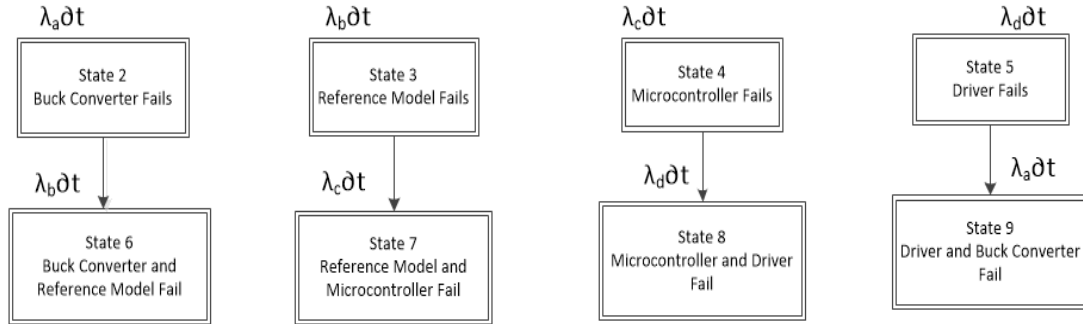
Figure 6.5: STM of states 6,7,8,9 from 2,3,4 and 5 respectively

$$P_2(t_o) [1- (\lambda_{cd}) \partial t] (\lambda_b \partial t) P_6(t_o) = P_6(t_o+\partial t) \tag{6.32}$$

$$P_3(t_o) [1- (\lambda_{ad}) \partial t] (\lambda_c \partial t) P_7(t_o) = P_7(t_o+\partial t) \tag{6.33}$$

$$P_4(t_o) [1- (\lambda_{ab}) \partial t] (\lambda_d \partial t) P_8(t_o) = P_8(t_o+\partial t) \tag{6.34}$$

$$P_5(t_o) [1- (\lambda_{bc}) \partial t] (\lambda_b \partial t) P_9(t_o) = P_9(t_o+\partial t) \tag{6.35}$$

State 6,7,8and 9 are connected to state 10,11,12 and 13 respectively as per state transition diagram shown in Figure 6.6 so, probability transition equations are represented as follows:
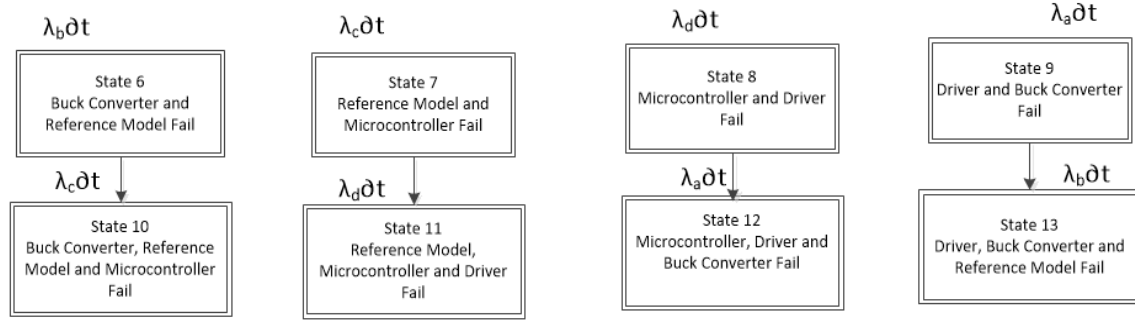
Figure 6.6: State transition of state 6,7,8,9 to 10,11 12 and 13 respectively

Following equations are obtained from state transitions shown in Figure 6.7.

$$P_6(to) [1- \lambda_d \partial t] (\lambda_c \partial t) P_{10}(t_o) = P_{10}(t_o+\partial t) \tag{6.36}$$

$$P_7(to) [1- \lambda_a \partial t] (\lambda_d \partial t) P_{11}(t_o) = P_{11}(t_o+\partial t) \tag{6.37}$$

$$P_8(to) [1- \lambda_b \partial t] (\lambda_a \partial t) P_{12}(t_o) = P_{12}(t_o+\partial t) \tag{6.38}$$

$$P_9(to) [1- \lambda_c \partial t] (\lambda_b \partial t) P_{13}(t_o) = P_{13}(t_o+\partial t) \tag{6.39}$$

$$P_{10}(t_o) (\lambda_d \partial t) + P_{11}(t_o) (\lambda_a \partial t) + P_{12}(t_o) (\lambda_b \partial t) + P_{13}(t_o) (\lambda_c \partial t) + P_{14}(t_o) = P_{14}(t_o+\partial t) \tag{6.40}$$
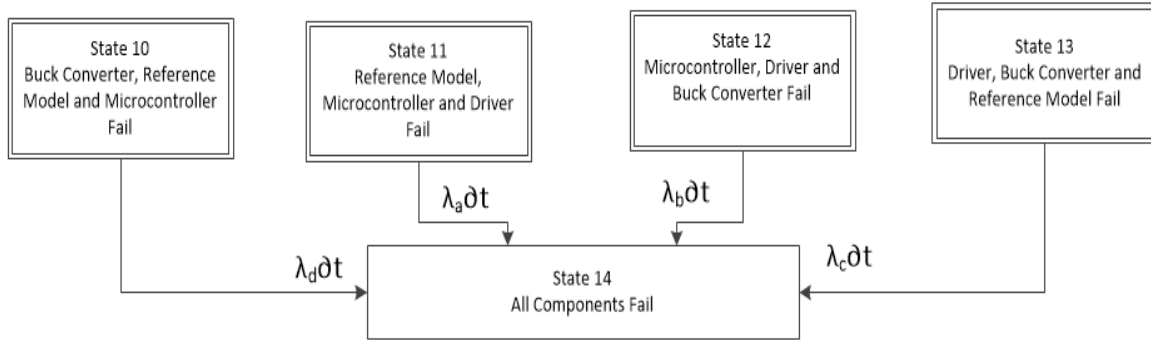
Figure 6.7: Final transitions from state 10,11,12 and 13 to fail state 14

$$P_6(t_o) (\lambda_c \partial t) [1- \lambda_d \partial t] P_{10}(to) = P_{10}(t_o+\partial t) \tag{6.41}$$

$$P_7(t_o) (\lambda_d \partial t) [1- \lambda_a \partial t] P_{11}(t_o)= P_{11}(t_o +\partial T) \tag{6.42}$$

$$P_8(t_o) (\lambda_a \partial t) [1- \lambda_b \partial t] P_{12}(t_o)= P_{12}(t_o +\partial t) \tag{6.43}$$

$$P_9(t_o) (\lambda_b \partial t) [1- \lambda_c \partial t] P_{13}(t_o) = P_{13}(t_o +\partial t) \tag{6.44}$$

$P_{10}(t_o)\ (\lambda_d\ \partial t) + P_{11}(t_o)\ (\lambda_a\ \partial t) + P_{12}(t_o)\ (\lambda_b\ \partial t) + P_{13}(t_o)\ (\lambda_c\ \partial t) + P_{14}(to) = P_{14}(t_o+\partial t)$ (6.45)

Substituting the initial value of P at t=0 as 1 in above equations:

$$P_1(t_o) = -e^{-(\lambda)t_o} \tag{6.46}$$

$$P_2(t_o) = -e^{-(\lambda)t_o} + e^{-(\lambda_{bcd})t_o} \tag{6.47}$$

$$P_3(t_o) = -e^{-(\lambda)t_o} + e^{-(\lambda_{acd})t_o} \tag{6.48}$$

$$P_4(t_o) = -e^{-(\lambda)t_o} + e^{-(\lambda_{abd})t_o} \tag{6.49}$$

$$P_5(t_o) = -e^{-(\lambda)t_o} + e^{-(\lambda_{abc})t_o} \tag{6.50}$$

For next transitions, the equations become:

$$P_6(t_o) = \frac{\lambda_b}{\lambda_{ab}}e^{-(\lambda)t_o} - e^{-(\lambda_{bcd})t_o} + \frac{\lambda_a}{\lambda_{ab}}e^{-(\lambda_{cd})t_o} \tag{6.51}$$

$$P_7(t_o) = \frac{\lambda_c}{\lambda_{bc}}e^{-(\lambda)t_o} - e^{-(\lambda_{acd})t_o} + \frac{\lambda_b}{\lambda_{bc}}e^{-(\lambda_{ad})t_o} \tag{6.52}$$

$$P_8(t_o) = \frac{\lambda_d}{\lambda_{cd}}e^{-(\lambda)t_o} - e^{-(\lambda_{acd})t_o} + \frac{\lambda_c}{\lambda_{cd}}e^{-(\lambda_{ab})t_o} \tag{6.53}$$

$$P_9(t_o) = \frac{\lambda_a}{\lambda_{ad}}e^{-(\lambda)t_o} - e^{-(\lambda_{abc})t_o} + \frac{\lambda_4}{\lambda_{ad}}e^{-(\lambda_{bc})t_o} \tag{6.54}$$

From state transition between 10,11,12 and 13 onwards, the transition equations become:

$$P_{10}(t_o) = \frac{(\lambda_b*\lambda_c)}{(\lambda_{ab}*\lambda_{abc})}e^{-(\lambda)t_o} + \frac{\lambda_c}{\lambda_{bc}}e^{-(\lambda_{bcd})t_o} - \{\frac{(\lambda_a*\lambda_d)}{(\lambda_d*\lambda_{bc})}e^{-(\lambda_{ad})t_o} + \frac{(\lambda_b*\lambda_c)}{(\lambda_{ab}*\lambda_{abc})} - \frac{\lambda_c}{\lambda_{bc}} +$$
$$\frac{(\lambda_a*\lambda_d)}{(\lambda_d*\lambda_{bc})}\}e^{-\lambda_d t_o} \tag{6.55}$$

$$P_{11}(t_o) = \frac{(\lambda_c*\lambda_d)}{(\lambda_{bc})*\lambda_{bcd}}e^{-(\lambda)t_o} + \frac{\lambda_d}{\lambda_{cd}}e^{-(\lambda_{acd})t_o} - \{\frac{(\lambda_b*\lambda_d)}{(\lambda_d*\lambda_{bc})}e^{-(\lambda_{ad})t_o} + \frac{(\lambda_c*\lambda_d)}{(\lambda_{bc}*\lambda_{bcd})} - \frac{\lambda_d}{\lambda_{cd}} +$$
$$\frac{(\lambda_b*\lambda_d)}{(\lambda_d*(\lambda_{bc})}\}e^{-\lambda_a t_o} \tag{6.56}$$

$$P_{12}(t_o) = \frac{(\lambda_a * \lambda_d)}{(\lambda_{cd} * \lambda_{acd})} e^{-(\lambda)t_o} + \frac{\lambda_a}{\lambda_{ad}} e^{-(\lambda_{abd})t_o} - \{\frac{(\lambda_a * \lambda_c)}{(\lambda_a * \lambda_{cd})} e^{-(\lambda_{ab})t_o} + \frac{(\lambda_a * \lambda_d)}{(\lambda_{cd} * \lambda_{acd})} - \frac{\lambda_a}{\lambda_{ad}} +$$

$$\frac{(\lambda_a * \lambda_c)}{(\lambda_a * \lambda_{cd})}\}e^{-\lambda_b t_o} \tag{6.57}$$

$$P_{13}(t_o) = \frac{(\lambda_a * \lambda_b)}{(\lambda_{ad} * \lambda_{abd})} e^{-(\lambda)t_o} + \frac{\lambda_b}{\lambda_{ab}} e^{-(\lambda_{abc})t_o} - \{\frac{(\lambda_b * \lambda_d)}{(\lambda_b * \lambda_{ad})} e^{-(\lambda_{bc})t_o} + \frac{(\lambda_a * \lambda_b)}{(\lambda_{ad} * \lambda_{abd})} - \frac{\lambda_b}{\lambda_a + \lambda_b}$$

$$+ \frac{(\lambda_b * \lambda_d)}{(\lambda_b * \lambda_{ad})}\}e^{-\lambda_b t_o} \tag{6.58}$$

$$P_{14}(t_o) = 1 - P_1(t_o) - P_2(t_o) - P_3(t_o) - P_4(t_o) - P_5(t_o) - P_6(t_o) - P_7(t_o) - P_8(t_o) - P_9(t_o)$$
$$- P_{10}(t_o) - P_{11}(t_o) - P_{12}(t_o) - P_{13}(t_o) \tag{6.59}$$

$$\sum_{i=1}^{13} P_i(t_o) \tag{6.60}$$

Failure rate $F(t_o)$ + Reliability $R(t_o)$ = 1

Figure 6.8: Reliability plot using STM

The reliability plot obtained by applying the STM approach to the PVE model is shown in Figure 6.8. The application takes a broader view of reliability, although it also includes mathematical modeling, which is a time-consuming process.

6.8 PETRINET METHOD FOR RELIABILITY ANALYSIS

Petri net is a model for description of distributed systems. It is a directed bipartie-graph that has nodes representing transitions and places. This analysis considers the physics of failure of components and the fuzzy fork net architecture is followed to obtain the final failure rate of considered system. The basic structure of PVE considered in this work is explained using Transformation Logic gates in Figure 6.9.
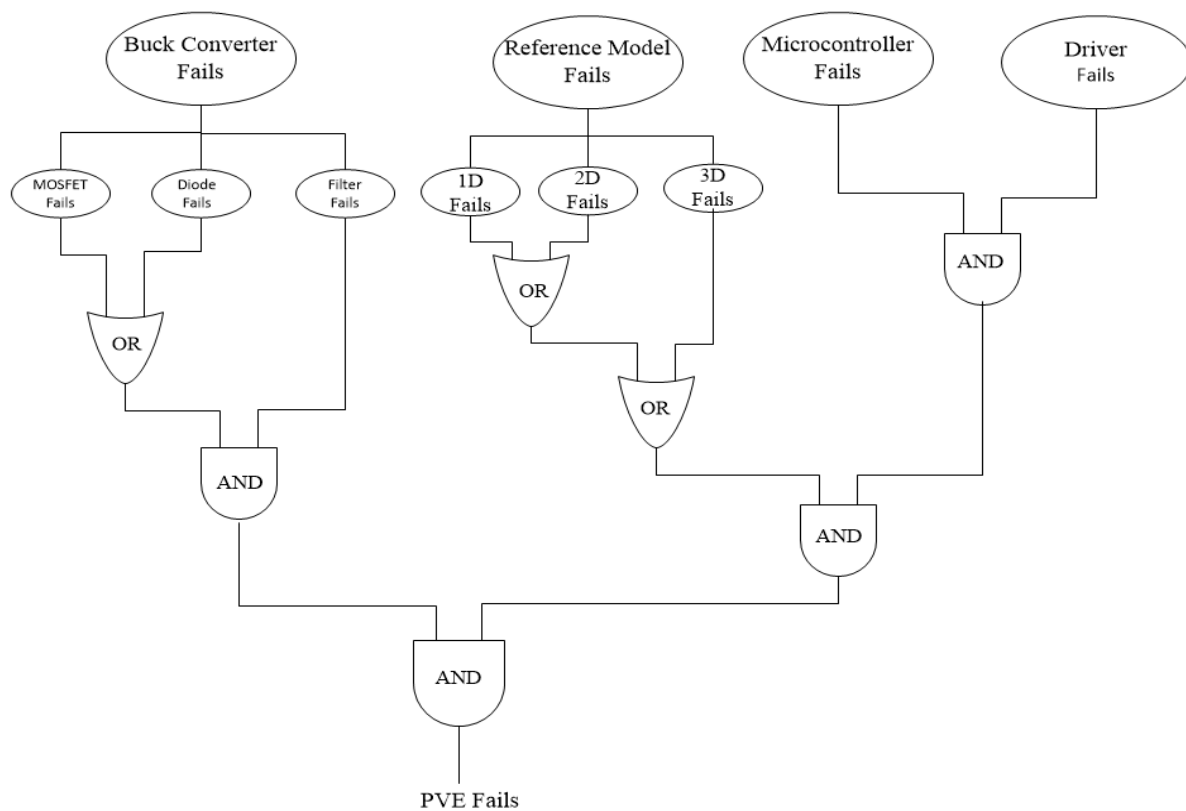
Figure 6.9: Logic Fault tree representation of PVE

Figure 6.9 is taken as basic diagram for obtaining Petri net diagram as shown in Figure 6.10. It shows the transition states by bars and various stages are interconnected through these bars. The statics include transitions, places, arrows and the tokens define the dynamics of the system. States are presented by circles, transitions by bars. This is called as fuzzy petri net as it involves fuzzy if-then rule base and the architecture resembles a fork shape so is called as Fuzzy fork petri net method.
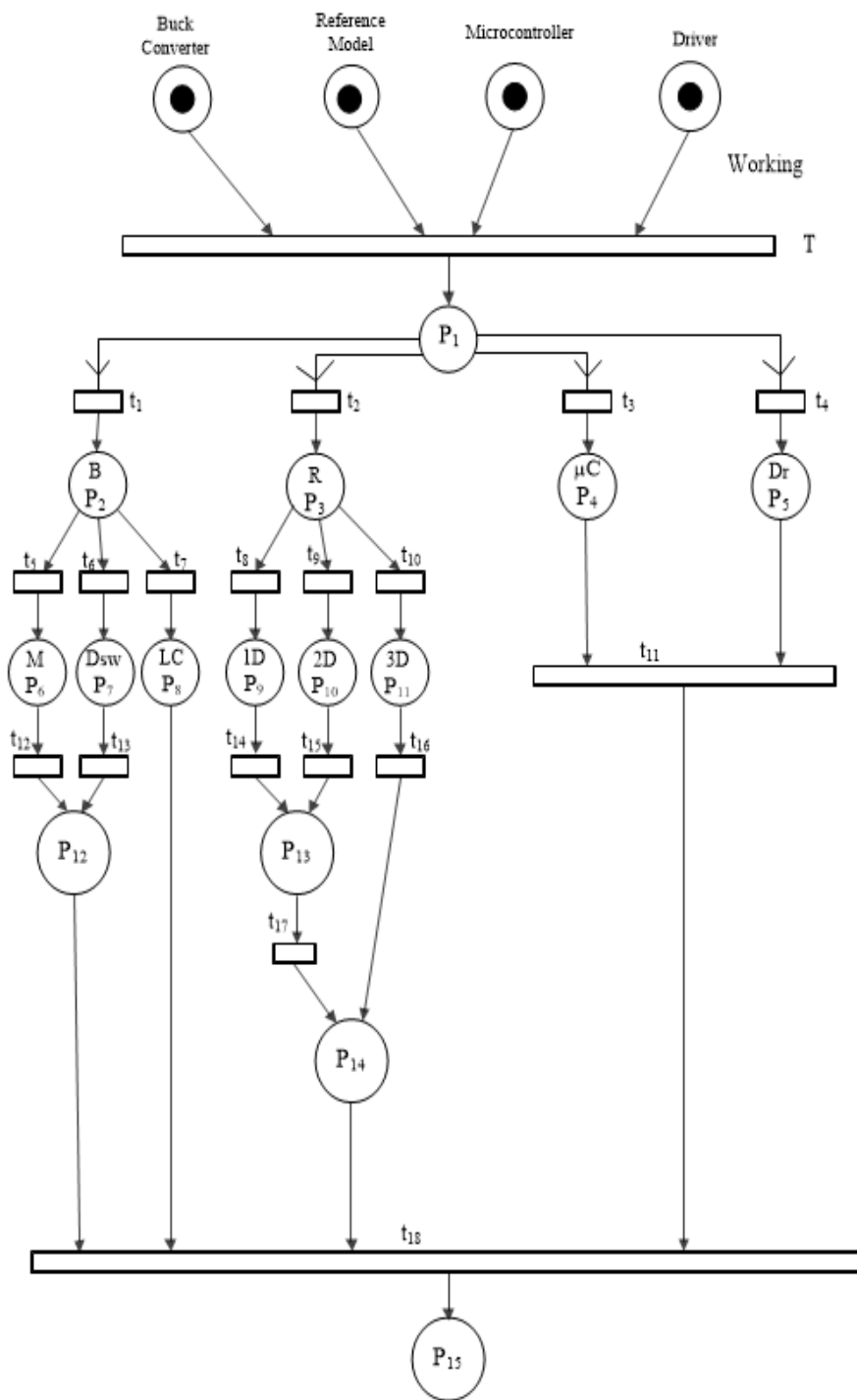
Figure 6.10: Petri net diagram of PVE
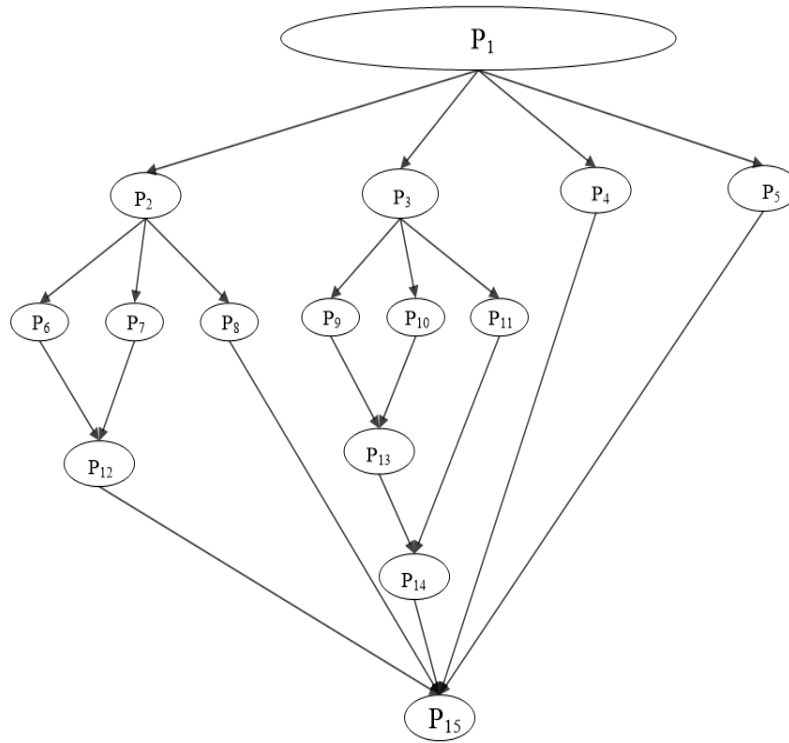
Figure 6.11: Petri net Failure node- Probability diagram

Figure 6.11 is failure node probability diagram which is simplified form of Figure 6.10. The failure rates of components are substituted and logic gate algebra is applied to calculate the overall reliability of PVE. Taking failure rates of individual components and applying logic gate mathematics, the reliability of PVE, R(t) is shown in figure 6.12.
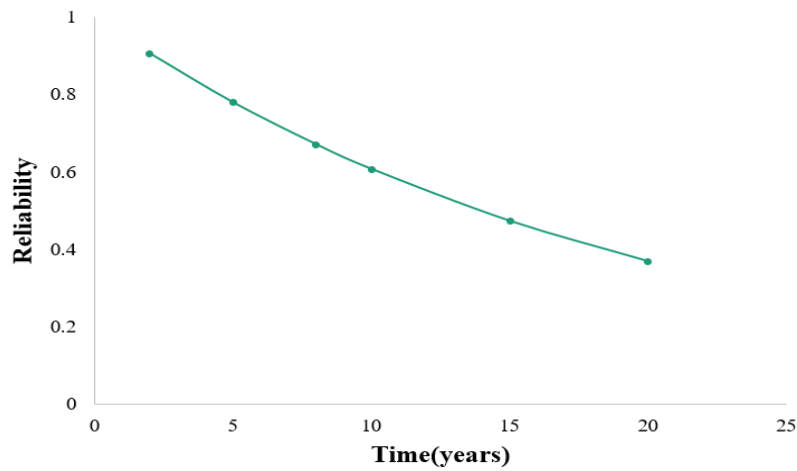
Figure 6.12: Reliability Plot using Petri net Method

6.9 AVAILABILITY ANALYSIS OF PVE

Design parameters are important when modeling PVE because they determine reliability and the availability determined by MTTF and μ(t), which is calculated using λ(t). In the mathematical modeling of availability, a probabilistic approach and difference differential calculations are used [186]. For steady-state conditions, these equations are solved. Basic block diagram to obtain these equations is shown in figure 6.13. Static and dynamic modeling is done using following equations obtained from analysis of following model [187].
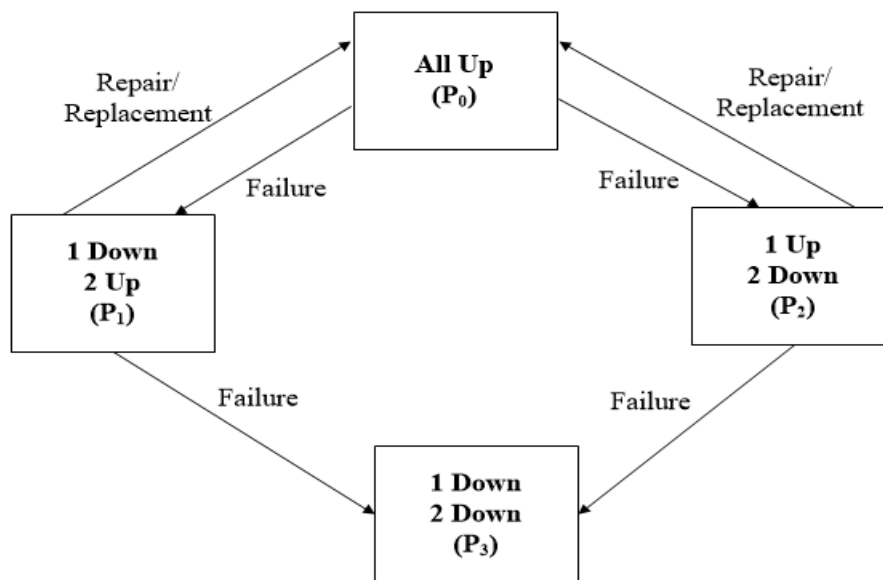
Figure 6.13: Block diagram of Availability model

$$
\begin{bmatrix} \dot{P}_0 \\ \dot{P}_1 \\ \dot{P}_2 \\ \dot{P}_3 \end{bmatrix} = \begin{bmatrix} \alpha_{00} & \mu_1 & \mu_2 & 0 \\ \lambda_1 & \alpha_{11} & 0 & 0 \\ \lambda_2 & 0 & \alpha_{22} & 0 \\ 0 & \lambda_2 & \lambda_1 & \alpha_{33} \end{bmatrix} \begin{bmatrix} P_0 \\ P_1 \\ P_2 \\ P_3 \end{bmatrix}
$$

While solving equations in MATLAB, term P_0 is taken as y(1), P_1 as y(2), P_2 as y(3) and P_3 as y(4) to represent dynamics of the system.

Here, initial states are taken as:

$$y(1)_{(t=0)} = 1; \tag{6.61}$$

$$y(2)_{(t=0)} = y(3)_{(t=0)} = y(4)_{(t=0)} = 0 \tag{6.62}$$

$$\dot{y}(1)\,(t) = - (\lambda_1 + \lambda_2)\, y(1)(t) + \mu_1 y(2)(t) + \mu_2 y(3)(t) \tag{6.63}$$

$$\dot{y}(2)(t) = (\lambda_1)\, y(1)(t) - (\mu_1 + \lambda_2) y(2)(t) \tag{6.64}$$

$$\dot{y}(3)(t) = (\lambda_2)\, y(1)(t) - (\mu_2 + \lambda_1) y(3)(t) \tag{6.65}$$

$$\dot{y}_4(t) = (\lambda_2)\, y(2)(t) + (\lambda_1) y(3)(t) \tag{6.66}$$

For static availability $\frac{dy}{dt}$ terms are taken as zero, values of failure rates calculated with the help of Military Hand book [115] are taken and the repair/replacement rate is taken constant. The availability of the designed system is evaluated using:

- Static modeling
- Dynamic modeling
- MHBK
- GA

While reliability analysis using GA, the setting of parameters of GA is important to obtain best results. Table 6.1 summarizes the GA settings for reliability model analysis in MATLAB toolbox.

Table 6.1 shows parameter settings of GA reliability model

S.No.	Parameters	Settings
1	Population (200)	Double vector
2	Creation	Uniform
3	Selection Type	Stochastic Uniform
4	Mutation	Adaptive Feasible
5	Crossover	Heuristic
6	Migration	Forward
7	Stopping Criterion	200 Generations

Table 6.2: Comparative analysis of failure and repair rates

Parameters	Bounds	Values obtained from MHBK	Values obtained by GA
λ_1	[0.1 0.5]	0.47	0.449
λ_2	[0.001 0.03]	0.02	0.001
μ_1	[0 0.03]	0.02	0.001
μ_2	[0 0.03]	0.02	0.027

Table 6.1 summarizes values of failure and repair rates obtained by using MHBK and GA. These values are further used to calculate availability of PVE model at static and dynamic conditions.

6.10 RESULTS AND DISCUSSION

Comparison of Reliability using applied methods
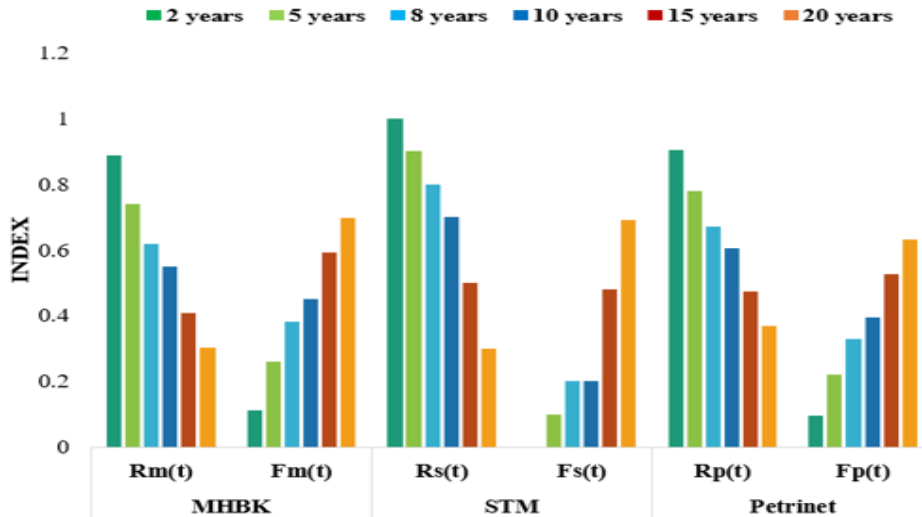
Figure 6.14: Reliability and Failure rate using different reliability methods

Figure 6.14 depicts a histogram comparing the failure and reliability rates of the PVE model using three different approaches, namely MHBK, STM and Petrinet. All plots are comparable for timeframes up to 20 years, but the MHBK and Petrinet approaches are indeed very close. The plot depicts the availability of PVE over time and the system appears to be reliable as well.
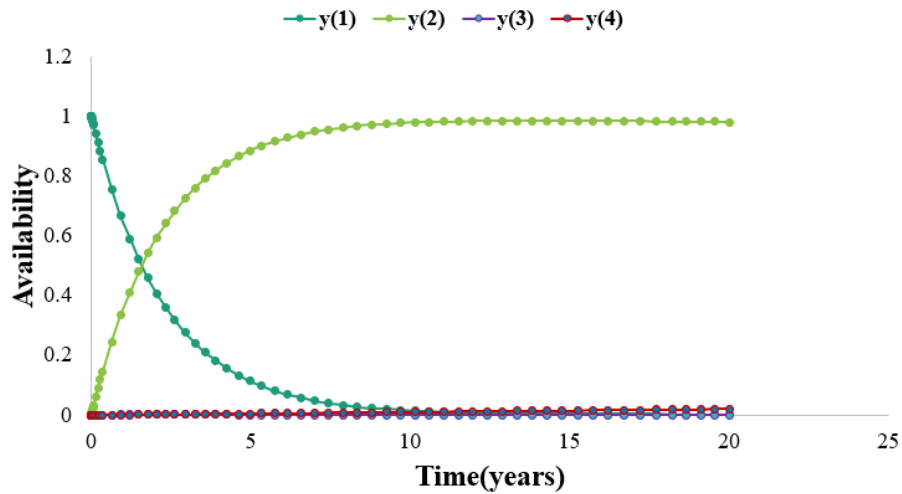
Figure 6.15: Individual Availability with repair/replacement rate with MHBK.
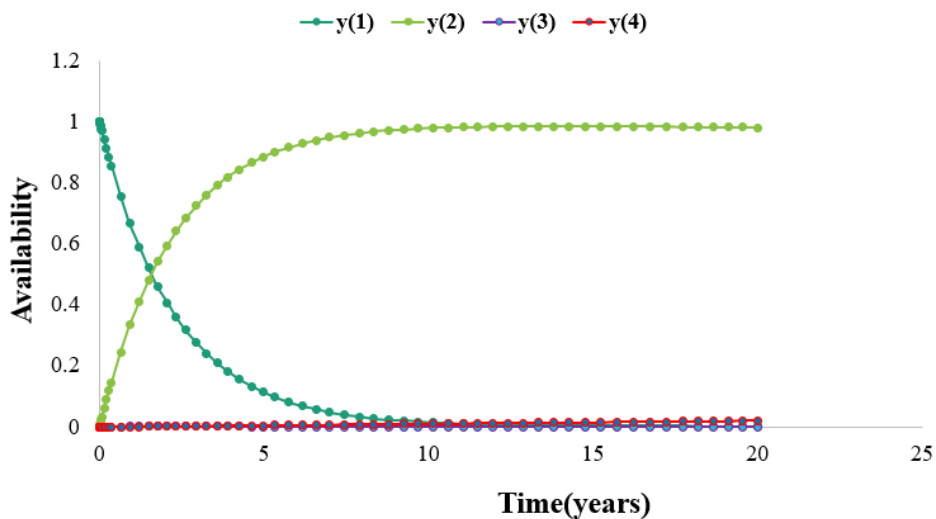
Figure 6.16: Individual Availability with repair/replacement rate with GA.

Figures 6.15 and 6.16 depict the availability of various PVE states in relation to time over years. Both methods produce close approximations, but GA produces better results in terms of complexity in large systems, time and ease of implementation.

The overall analysis using three different approaches show that the reliability analysis requires a good mathematical model of the system and methods like STM require differential equations. So, before calculating complete system reliability, it is mandatory to obtain its mathematical model and analysis of each part of the model as covered in Chapter 3 and 4 of this work.

6.11 CONCLUSION

The results obtained above conclude that:

- The reliability of each component is calculated from the failure rate λ. Derived equations show dependence of failure rates on loading and loses. So, military hand book MIL-HDBK217F is used where part count and part stress have been provided.

- The other two methods following physics of failure are then implemented to calculate the overall reliability of PVE. Petri net shows comparatively good results with lesser time consumption as compared to STM.

- Further the availability calculation for static and dynamic behaviour provides a complete analysis of PVE for its effectiveness over the years.

- Reliability and availability analysis of complete PVE is a novel work carried out in this work considering mathematical modeling and control of PVE explained in previous chapters.

CHAPTER 7

CONCLUSIONS AND SCOPE FOR FUTURE WORK

7.1 CONCLUSIONS

The chapters that follow, significantly improve the performance of PVE reported in the Ph.D. work;

Chapter 1: Introduction.

Chapter 2: Literature Review.

Chapter 3: Mathematical Modeling of PVE.

Chapter 4: Reference Model Topologies and their Implementation.

Chapter 5: PVE Control Strategies and their Implementation.

Chapter 6: Reliability and Availability Analysis of Designed PVE.

Chapter 7: Conclusions and Scope for Future Work.

Apart from chapters 1 and 2, which include an introduction to solar power and the conceptualization of a problem using literature survey, the key findings reported in chapters 3 and 4, 5 and 6 can be outlined in chapter 7 as follows;

Chapter 3 describes the mathematical modeling of PVE, which is the basic requirement before designing any system. The topologies and sub-systems of PVE are explained in detail with their individual significance and characteristics. Small signal analysis followed by transfer function calculation for ideal and non-ideal components of buck converter is calculated by KVL-KCL approach and novel SFG method.

Chapter 4 covers the feedback architecture of PVE is explained by taking reference model design considering following four different ways:

- 1D model
- 2D model
- 3D model
- LUT method
- PLA method

The results of implementation of these methods in MATLAB Simulink are illustrated using comparison plots that included PI, PID, PSO-PID, PSOFOPID, SMC, FLC, ANFIS, MRAC,

MPC and H_∞ control strategies to show the effectiveness of model in a broader way. All models show approximation to PV characteristics but the selection of best is based on performance indices as explained in chapter 5

Chapter 5 includes designing of various controllers for PVE. The comparative plots using different reference models for a particular controller are obtained using simulation for better understanding. The plots include indices like t_r, t_s and POS along with ISE and IAE at three main operating points of a PVE namely SC, MPP and OC points. Transient response is analyzed by implementing model with delay and introducing ESR in inductor and capacitor. H_∞ controller is applied to optimize the response of the system for different reference models. The results show the effectiveness of 3D and LUT w.r.t reference model.

Chapter 6 involves reliability and availability analysis of the designed PVE. Part stress and physics of failure are the basics of any reliability problem. So, both are covered by three different methods. MIL-HBK 217F is referred for part failure of every component. STM involving Markov's chain is used to derive the equations relating the reliability of PVE. Finally, a novel Petri net method is applied to find the reliability of complete PVE The last method is simpler and found to be effective when compared to other two existing methods. The availability of PVE is calculated for static and dynamic behavior of PVE using MHBK and GA. The modeled system is found to be available up to 20 years.

7.2 SCOPE FOR FUTURE WORK

The Ph.D. work may be expanded for future research in the following areas:

- Few researchers have reported metaheuristic approach towards PVE. This area can be explored to speed up the designing part.
- Reference models can be designed by advanced algorithms.
- Partial shading, dust, overheating can be included in reference model design.
- More non-linearities and breakdowns can be considered in mathematical modeling, reliability and availability analysis.
- More performance indices can be included for comparison of different reference models and controllers applied to same PVE.

REFERENCES:

[1] https://www.sullivansolarpower.com/about/blog/famous-solar-powered-buildings.

[2] https://mnre.gov.in/solar/current-status/.

[3] Ministry of New and Renewable Energy (12 February 2019). "Installed Capacity of Various Renewable Modes of Energy". pib.gov.in, retrieved 26 June 2021.

[4] https://www.pib.gov.in/PressReleseDetailm.aspx?PRID=1685046.

[5] Annual Report 2016-17 Ministry of New and Renewable Energy, Government of India. pp 58, retrieved on 28 June 2021, archived on 21 April 2021.

[6] Annual Report 2017-2018. Ministry of New and Renewable Energy, Government of India. pp 34, retrieved on 28 June 2021, archived on 21 April 2021.

[7] Annual Report 2019-2020. Ministry of New and Renewable Energy, Government of India. pp 19, retrieved on 28 June 2021, archived on 21 April 2021.

[8] State-wise installed capacity of Grid Interactive Renewable Power as on 31.03.2021, mnre.gov.in, archived on 13 May 2021, retrieved 31 March 2021.

[9] Solar Energy Overview, Ministry of New and Renewable Energy, Government of India. retrieved on 28 June 2021, archived on 4 June 2021.

[10] https://mnre.gov.in/solar/solar-offgrid, Jan 2022.

[11] https://mnre.gov.in/solar/solar-ongrid, Jan 2022.

[12] Available: http://apps1.eere.energy.gov/state_energy_program/Green Energy DC program (District of Columbia, Washington DC, USA), [Online]Available: http://www.green.dc.gov.

[13] The California Solar Initiative program (California, USA), [Online] Available: http:// www.gosolar california.ca.gov/csi/index.html.

[14] IEEE Standards Association, "IEEE 1547 Standard for Interconnecting Distributed Resources with Electric Power Systems", 2014. [Online]. Available: grouper.ieee.org/groups /scc21/1547/1547_ index. html.

[15] https://www.nsenergybusiness.com/features/largest-solar-power-plants.

[16] https://energsustainsoc.biomedcentral.com/articles/10.1186/s13705-019-0232-1

[17] Cazzaniga, R., Clot, M., Clot, P., Giuseppe, T., "Floating tracking cooling concentrator (FTCC) systems", 38th IEEE Photovoltaic Specialists conf., pp. 000514-000519, 2012.

[18] Han, Y., Feng, Y., Yang, P., Xu, L., Xu, Y., and Blaabjerg, F., "Cause, Classification of Voltage Sag and Voltage Sag Emulators and Applications: A Comprehensive Overview', IEEE Access, vol. 8, pp. 1922-1934, 2020.

[19] https://www.nrel.gov/research/re-photovoltaics.html.

[20] Matos, F., Camacho, J., "A Model for Semiconductor Photovoltaic (PV) Solar Cells: The Physics of the Energy Conversion from the Solar Spectrum to DC Electric Power", IEEE Int. conf. Clean Electri. Power (ICCEP), pp. 352-359, May 2007.

[21] Agrawal, J., Aware, M., "Photovoltaic System Emulator", IEEE Int. conf. Power Electronics, Drives Energy Sys. (PEDES), pp. 1-6, Dec. 2012.

[22] Ajaamoum, M., Kourchi, M., Bouachrine, B., Ihlal, A., Bouhouch, L., "Modeling an Emulator of Photovoltaic Panels", Int. J. Enhanced Research Sci. Tech.& Engg., vol. 3(10), pp. 163-171, Oct. 2014.

[23] Pelin, D., Antolovic, J., Rapcan, V., "PV Emulator", Int. J. Electri. and Computer Engg. Syst., vol. 5(1), pp. 21-26, 2014.

[24] Medina, R., Patrao, I., Garcera, G., Figueres, E., "A Low-Cost Photovoltaic Emulator for Static and Dynamic Evaluation of Photovoltaic Power Converters and Facilities", J. Prog Photovolt: Res. Appl., vol. 22, pp. 227-241, April 2012.

[25] Shah, R., Rana, A., "Voltage Controlled Buck Convertor based PV Emulator", IEEE Int. conf. Electri., Electro., Signals, Comm. Opti. (EESCO), pp. 1-4, Jan. 2015.

[26] Shinde, U., Kadwana, S., Gawande, S., Keshri, R., "Solar PV Emulator for Realizing PV Characteristics under Rapidly Varying Environmental Conditions", IEEE Int. conf. Power Electro., Drives Energy Sys. (PEDES), pp.1-4, 2016.

[27] Xenophontos, A., Rarey, J., Trombetta, A., Bazzi, A., "A Flexible Low-Cost Photovoltaic Solar Panel Emulation Platform", IEEE Power Energy conf., pp. 1-6, Feb. 2014.

[28] Iqbal, M., Tariq, M., "Analytical Study of Different DC-DC Converter Topologies for Photovoltaic Emulator", J. Automation Sys. Engg. (JASE), pp. 245-254, 2015.

[29] Savita, N., Nema, R. and Agnihotri, G., "MATLAB/Simulink based Study of Photovoltaic Cells/Modules/Array and their Experimental Verification," Int. J. Energy Environ, vol. 3, pp. 487–500, 2010.

[30] Gowda, A., Samosir, N., "Modeling and Evaluation of Solar Photovoltaic Emulator based on Simulink Model", ARPN J. Engg. and Applied Sci., vol. 10(22), pp. 10288-10295, Dec. 2015.

[31] Elyaqouti, M., Bouhouch, L., Ihlal, A., "Modeling and Simulation of an Emulator of Photovoltaic Generator", J. Comm. Applied Electro. (CAE), vol. 5(8), Aug. 2016.

[32] Thale, S., Wandhare, R., Aggarwal, V., "A Novel Low-Cost Portable Integrated Solar PV, Fuel cell and Battery Emulator with Fast Tracking Algorithm", IEEE conf. Photovoltaic Specialist, pp. 3138-3143, 2014.

[33] Hua, C., Lin, J., Shen, C., "Implementation of a DSP-Controlled Photovoltaic System with Peak Power Tracking", IEEE Trans. Indust. Electro., vol. 45(1), Feb. 1998.

[34] Enrique, J., Duran, E., Cardona, M., Andujar, J., "Theoretical Assessment of the Maximum Power Point Tracking Efficiency of Photovoltaic Facilities with Different Converter Topologies", Sci. Direct Solar Energy, vol. 81, pp. 31-38, 2007.

[35] Shiau, J., Li, M., Wei, Y., Chen, B., "Circuit Simulation for Solar Power Maximum Power Point Tracking with Different Buck Boost Converter Topologies", IEEE 1st Int. e-conf. Energies, pp. 1-17, March 2014.

[36] Moussa, I., Khedher, A., Bouallegue, A., "Design of a Low-Cost PV Emulator Applied for PVECS", MDPI J. Electro., vol. 8(2), pp. 1-15, Feb. 2019.

[37] Rana, A., Patel, H., "Current Controlled Buck Converter based PV Emulator," J. Industrial Intelligent Info., vol. 1(2), June 2013.

[38] Ishaque, K., Salam, Z., Taheri, H., "Accurate MATLAB Simulink PV System Simulator based on a Two Diode Model", J. Power Electo., vol. 11(2), March 2011.

[39] Gowda, M., Kiran, Y., Parthasarthy, S., "Modeling of Buck DC-DC Converter using Simulink", Int. J. Innovative Research Sci., Engg. Tech. (IJIRSET), vol. 3(7), pp. 14965-14975, July 2014.

[40] Solaiam, H., Hasan, M., Adnan, M., Kawsar, S., Hasan, A., "Performance Analysis of DC to DC Boost Convertor using Different Control Methods", IEEE Int. conf. Electri. Computer Comm. Tech. (ICECCT), pp. 1-3, 2015.

[41] Haripriya, T., Parimi, A., Rao, U., "Modelling of DC-DC Boost Converter using Fuzzy Logic Controller for Solar Energy System Applications", IEEE Asia Pacific conf. Postgraduate Research Microelectro. Electro., pp. 147-152, Dec. 2013.

[42] Lu, D., Nguyen, Q., "A Photovoltaic Panel Emulator using a Buck-Boost DC/DC Converter and a Low-Cost Microcontroller", J. Solar Energy, Sci. Verse, vol. 86, pp. 1477-1484, March 2012.

[43] Choudhary, P., Mahendra, S., "Feedback Control and Simulation of DC-DC Cuk Converter for Solar Photovoltaic Array", IEEE Int. conf. Electri., comp. Electro. Engg. (UPCON), pp. 591-596, Dec 2016.

[44] Babaei E., Mahmoodieh M., "Systematical Method of Designing the Elements of the Cuk Converter," Int. J. Electri. Power Energy Sys., vol. 55, pp. 351–361, 2014.

[45] Zhuo, Z., Zhang, J., Sun, H., Wang, G., Hu, X., Zhao, S., "Research on Photovoltaic Array Emulator System based on a Novel Zero-Voltage Zero Current Switching Converter,'' Proc. Asia–Pacific Power Energy Engg. conf., pp. 1-4, 2010.

[46] Dolan, D., Durago, J., Taufik, ''Development of a Photovoltaic Panel Emulator using Labview,'' Proc. 37th IEEE Photovoltaic Spec. conf., pp. 1795-1800, June 2011.

[47] Can, H., "Model of a Photovoltaic Panel Emulator in MATLAB-Simulink", Turk J. Elec. Comp. Sci., vol. 21, pp. 301-306, 2013.

[48] Ayop, R., Tan, C., Norazizul, S., Nasir, S., Lau, K., Toh, C., "Buck Converter Design for Photovoltaic Emulator Application", IEEE Inter. conf. Power Energy, PECON, pp. 293-298, May, 2021.

[49] Pradhan, A., Panda, B., "A Simplified Design and Modeling of Boost Converter for Photovoltaic System", Int. J. Electrical Computer Engg. (IJECE), vol. 8(1), pp. 141-149, Feb. 2018.

[50] Shi, J., Zhang, D., Ling, L., Xue, F., Li, Y., Qin, Z., Yang, T., "Dual-Algorithm Maximum Power Point Tracking Control Method for Photovoltaic Systems based on Grey Wolf Optimization and Golden-Section Optimization", J. Power Electro., vol. 18(3), pp. 841-852, May 2018.

[51] Jenkal, S., Kourchi, M., Rachdy, A., Oussalem, O., "Modeling a Photovoltaic Emulator using Four Methods and Buck-Boost Converter", Engg., Letters, EL-29-2-10, vol. 29(2), June 2021

[52] Suganthi, K., Sundararaman. K., Venkatakrishna, V., "A Low-Cost PV Emulator using Labview and Arduino", Int. J. Engg. Advanced Techno. (IJEAT), vol. 9(2), pp. 523-528, Dec. 2019.

[53] Suryoatmojo, H., Arsya, N., Putra, H., Nandiwardhana, A., Anam, S., Mardiyanto, R., Ashari, M., "Comparison of Cuk, Sepic and Zeta Converter Performance for Harmonics Mitigation and PFC in BLDC Speed Control", IEEE Int. seminar Intelligent Techno. Application, pp. 681-686, 2016.

[54] Parthsarathy, H., Udaya, L., Balasubramanian, G., "Modeling and Simulation of PV Module and Zeta Converter", Int. Conf. Circuit, Power Computing Techno. [ICCPCT], pp. 1-5, 2016.

[55] Mallal, Y., Bahir, L., Hassboun, T., "High-Performance Emulator for Fixed Photovoltaic Panels", Int. J. Photoenergy, vol. 2019, pp. 1-11, 2019.

[56] Alaoui, M., Maker, H., Mouhsen, A., Hihi, H., "Real Time Emulation of Photovoltaic Energy using Adaptive State Feedback Control", SN Applied Sci., vol. 492(2), pp. 1-8, Feb. 2020.

[57] Azharuddin, S., Vysakh, M., Thakur, H., Nishant, B., Babu, T., Muralidhar, K., Paul, D., Jacob, B., Balasubramanian, K., Rajasekar, N., "A Near Accurate Solar PV Emulator using dSPACE Controller for Real-Time Control", Sci. Direct, Energy Procedia, vol. 61, pp. 2640-2648, 2014.

[58] Shahabuddin, M., Asim, M., Sarwar, A., Riyaz, A., Shadab, M., Anees, A., "Performance based Analysis of Solar PVEs: A Review", Int. conf. Computational Characterization Techni. Engg. & Sci. (CCTES) Integral Uni., pp. 94-99, Sep. 2018.

[59] Andrew, X., Anand, M., Sivakumar, P., "Modelling and Analysis of Emulator for Distributed Generation Sourced Smart Grid using Digital Signal Controller (TMS320F28335)," ISGT, pp. 160-166, 2011.

[60] Gutierrez, A., Bressan, M., Jimenez, J., Alonso, C., "Development of Real-Time Supervision HIL Emulator of Shaded PV Systems", IEEE Int. Conf. Renewable Energy Research Applications (ICRERA), Nov. 2017.

[61] Rezkallah, M., Hamadi, A., Chandra, A., Singh, B., "Real-Time HIL Implementation of Sliding Mode Control for Standalone System based on PV Array without using Dump Load," IEEE Trans. Sustainable Energy, vol. 6(4), pp. 1389-1398, Oct. 2015.

[62] Ullah, N., Nisar, F., Alahmad, A., "Closed Loop Control of Photo Voltaic Emulator using Fractional Calculus", IEEE Access, vol. 8, pp. 28880-28887, Feb. 2020.

[63] Gour, R., "Small Signal Modeling of a Buck Converter using State Space Averaging for Magnet Load", Int. J. Recent Research Electri. Electro. Engg. (IJRREEE), vol. 3(3), pp. 11-17, Sept. 2016.

[64] Kazimierczuk, M., Sathappan, N., Czarkowski, D., "Voltage-Mode-Controlled PWM Buck DC-DC Converter with a Proportional Controller", IEEE conf. NAECON, pp. 413-419, 1993.

[65] https://techweb.rohm.com/knowledge/dcdc/s-dcdc/02-s-dcdc/97, accessed 2022.

[66] Reatu, A., Kazimierczuk, M., "Current Controlled Current Source Model for a PWM DC-DC Converters Operated in Discontinuous Current Mode", IEEE Int. Symposium Circuits Sys., ISCAS, vol. 3, pp.239-242, May 2000.

[67] Solaiam, H., Hasan, M., Adnan M., Kawsar, S., Hasan, A., "Performance analysis of DC-DC Boost Convertor using Different Control Methods", IEEE Int. conf. Electri., Computer Comm. Techno. (ICECCT), pp. 1-3, 2015.

[68] Jindal, V., Joshi, D., "A Comparative Analysis of Classical Tuning Methods of PI Controllers on Non-ideal Buck Converter", 2nd Int. conf. Power Elect. & IoT Applications Renewable Energy Control (PARC), pp. 1-5, 2022.

[69] Balakishan, C., Sandeep N., "Development of a Microcontroller based PV Emulator with Current Controlled DC-DC Buck Converter", Int. J. Renewable Energy Research, vol. 4(4), pp. 1-7, 2014.

[70] Prusty, S., Padhee, S., Pati U., Mahapatra, K., "Comparative Performance Analysis of Various Tuning Methods in the Design of PID Controller", Michael Faraday IET Int. Summit MFIIS, pp. 43-48, Sept. 2015.

[71] Cech, M., Schlegel, M., "Generalized Robust Stability Regions for Fractional PID Controllers", IEEE Int. Conf., Industrial Techno. (ICIT), pp. 1-6, Feb. 2013.

[72] Sahin, E., Ayas, M., Altas, I., "A PSO Optimized Fractional-Order PID Controller for a PV System with DC-DC Boost Converter", 16th Int. Power Electro. Motion Control Conf. Exposition, pp. 1-5, Sept. 2014.

[73] Haroon, Y., Khattak, A., "Design and Analysis of Fractional Order Control System (FOCS) For Buck Converter PV Emulator", J. Global Scientific, vol. 8(2), pp. 4759-4777, Feb. 2020.

[74] Bagyaveereswaran, V., Petchinathan, G., Anitha, R., "Particle Swarm Optimization based PID Controller for MPPT", Int. J. Mechanical Engg. Techno. (IJMET), vol. 9(12), pp. 1057-1065, Dec. 2018.

[75] Gupta, R., Lamba, R., "PSO based Optimal Design of Fractional Order Controller for Industrial Application", World Academy Sci., Engg. Techno. Int. J. Electri. Computer Engg., vol. 9(6), pp. 665-672, 2015.

[76] Sowjanya, K., Srinivas, L., "Tuning of PID Controllers using Particle Swarm Optimization", Int. J. Industrial Electro. Electri. Engg., vol. 3(2), pp. 17-22, Feb. 2015.

[77] LI, Z., "The Optimization Design of PID Controller Parameters based on Particle Swarm Optimization", 5th Int. conf. Advanced Materials Computer Sci. (ICAMCS), pp. 460-464, 2016.

[78] Muftah, M., Faudzi, A., Sahlan, S., Shouran, M., "Modeling and Fuzzy FOPID Controller Tuned by PSO for Pneumatic Positioning System", J. Energies, vol. 15, pp. 1-21, May 2022.

[79] Bhise, K., Pragallapati, N., Thale, S., Agarwal V., "Labview based Emulation of Photovoltaic Array to Study Maximum Power Point Tracking Algorithms", Proc. 38th IEEE Photovoltaic specialists Conf. (PVSC), pp. 2961–2966, 2012.

[80] Durago, G., "Photovoltaic Emulator Adaptable to Irradiance, Temperature and Panel-specific I–V Curves", Master Sci. Electr. Engg. California Polytechnic State University, San Luis Obispo, 2011.

[81] Savita, N., Nema, R., Agnihotri, G., "MATLAB/Simulink based Study of Photovoltaic Cells/Modules/Array and their Experimental Verification," Int. J. Energy Environment, vol. 3, pp. 487–500, 2010.

[82] Adbulkadir, M., Samosir, A., Yatim, A., "Modeling and Simulation based Approach of Photovoltaic System in Simulink Model", ARPN J. Engg. Applied Sci., pp. 616-623, vol. 7(5), 2012.

[83] Mattavelli, P., Rossetto, L., Spiazzi, G., "Small Signal Analysis of DC-DC Converters with Sliding Mode Control", IEEE Trans. Power Electro., vol. 12(1), pp. 96-102, 1997.

[84] Guldemir, H., "Study of Sliding Mode Control of DC-DC Buck Converter", Energy Power Engg., vol. 3, pp. 401-406, 2011.

[85] He, Y., Luo, F., "Study of Sliding-Mode Control for DC-DC Converters", Int. Conf. Power Sys. Tech. (POWERCON), pp. 1969-1974, 2004.

[86] Das, S., Qureshi, M., Swarnkar, P., "Design of Integral Sliding Mode Control for DC-DC Converters", J. Sci. Direct Proc. Materials Today, vol. 5, pp. 4290–4298, 2018.

[87] Tan, S., Lai, Y., Tse, C., "A Unified Approach to the Design of PWM-based Sliding-Mode Voltage Controllers for basic DC-DC Converters in Continuous Conduction Mode", IEEE Trans. Circuits Sys., vol. 53, pp. 1816-1827, 2006.

[88] Gambhir, S., Kishore, D., Londhe, P., Pawar, S., "Review of Sliding Mode-based Control Techniques for Control System Applications", Int. J. Dynamics Control Springer-Verlag Germany, pp. 1-16, 2020.

[89] Raja, R., Udhaya L., Kumar, S., "Fuzzy Logic Controller for Photovoltaic Array Simulator", Int. J. Engg. Techno. (IJET), vol. 5(2), pp.1625-1630, May 2013.

[90] Chen, L., Xu, Y., Liu, Y., Jin, R., "Small-Signal Analysis and Simulation of Fuzzy Controlled Buck Converter", IEEE 4th Int. Conf. Industrial Electro. Applications (ICIEA), pp. 816-820, 2009.

[91] Shaoa, W., Menga, Z., Zhoub, H., Zhang, K., "A Photovoltaic Array Simulator based on Current Feedback Fuzzy PID Control", J. Intelligent Fuzzy Sys., vol. 29, pp. 2555–2564, 2015.

[92] Iqbal, M., Tariq, M., Khan, S., "Fuzzy Logic Control of Buck Converter for Photo Voltaic Emulator", IEEE 4th Int. Conf. Development Renewable Energy Techno. (ICDRET), pp. 1-6, 2016.

[93] Ayop, R., Tan, C., Ayob, S., Muhamad, N., Jamia, J., Noorden, Z., "Photovoltaic Emulator using Error Adjustment Fuzzy Logic Proportional-Integral Controller", Int. J. Power Electro. Drive Sys. (IJPEDS), vol. 13(2), pp. 1111-1118, June 2022.

[94] Atig, A., Lefebvre, F., Abderrahim K., Abdennour, R., "On Lyapunov Stability of Non-Linear Adaptive Control based on Neural Networks Emulator and Controller", IEEE 20th Mediterranean Conf. Control Automation (MED), pp. 272-277, July 2012.

[95] Miloudi, L., Acheli, D., "Prediction Global Solar Radiation and Modeling Photovoltaic Module based on Artificial Neural Networks", IEEE 3rd Int. Conf. Control, Engg. Info. Techno. (CEIT), pp. 1-6, May 2015.

[96] Saraswathi, K., Arumugam, P., Swaminathan, G., Periasamy, S., "An Artificial Neural Network-based Comprehensive Solar Photovoltaic Emulator", Int. J. Photoenergy, vol. 20, pp. 1-14, May 2022.

[97] Ayop, R., Tan, C., "An Adaptive Controller for Photovoltaic Emulator using Artificial Neural Network", Indonesian J. Electri. Engg. Computer Sci., pp. 556-563, March 2017.

[98] Swarnkar, P., Jain, S., Nema, R., "Effect of Adaptation Gain in Model Reference Adaptive Control Scheme to Second Order System using MIT Rule", Int. conf. Electri. Power Energy Sys. (ICEPES), pp. 1-5, 2010.

[99] Swarnkar, P., Jain, S., Nema, R., "Effect of Adaptation Gain in Model Reference Adaptive Controller Second Order System", ETASR Engg., Techno. Applied Sci. Research, vol. 1(3), pp. 70-75, 2011.

[100] Jain, P., Nigam, M., "Design of a Model Reference Adaptive Controller using Modified MIT Rule for a Second Order System", J. Advance Electro. Electric Engg., vol. 3(4), pp. 477-484, 2013.

[101] Sowparnika, G., Sivalingam, A., Thirumarimurugan, M., "Modeling and Control of Renewable Source Converter using Model Predictive Controller", Int. J. Computer Application, vol. 5(7), pp. 43-51, Dec. 2015.

[102] Sultana, W., Sahoo, S., Sukchaib, S., Yamuna, S., Venkatesha, D., "A Review on State of Art Development of Model Predictive Control for Renewable Energy Applications", J. Renewable Sustainable Energy Reviews, vol. 76, pp. 391-406, 2017.

[103] Dehghanzadeh, A., Farahani, G., Vahedi, H., Haddad, K., "Model Predictive Control Design for DC-DC Converters Applied to a Photovoltaic System", J. Electri. Power Energy Sys., vol. 103, pp. 537-544, 2018.

[104] Samani, L., Mirzaei, R., "Model Predictive Control Method to Achieve Maximum Power Point Tracking without Additional Sensors in Standalone Renewable", Optik Optics J., vol. 185, pp. 1189-1204, Feb. 2019.

[105] Pradhan, R., Panda, A., "Modeling and Simulation of a MPC based Grid-Tied PVDG System", Int. J. Renewable Energy Research, vol. 12(1), March 2022.

[106] Lanzon, A., "Weight optimization in H-infinity loop-shaping", J. Automatics, vol. 41, pp. 1201-1208, 2005.

[107] Phurahong, N., Kaitwanidvilai, S., Ngaopitakkul, "A Fixed Structure Robust 2DOF H-infinity Loop Shaping Control for ACMC Buck Converter using Genetic Algorithm", Proc. Int. Multiconference Engineers Computer Scientist, pp.1-6, March 2012.

[108] Sampaio, L., Silva, S., "Robust Control Applied to a Photovoltaic Array Emulator using Buck Converter", Int. conf. Renewable Energies Power Quality (ICREPQ'15), vol. 13, pp. 665-670, April 2015.

[109] Malik, M., Sehgal, N., "A Comparative Study of Classical and Modern Controllers", Int. J. Engg. Research Techno., vol. 5(3), pp. 1-4, 2017.

[110] Azar, A., Serrano, F., Kamal, N., "Robust H_∞ Loop Shaping Controller Synthesis for SISO Systems by Complex Modular Functions", J. Mathematical Computational Appl., vol. 26, pp. 1-16, 2021.

[111] Holme, P., Manning, C., "Characterization of a Digital Current Mode Controlled Current-Fed Converter," Proc. 5th Int. Conf. Power Electro. Variable-Speed Drives, pp. 229 – 235, 26-28 Oct 1994.

[112] Boudreaux, R., Nelms, R., Hung, J., "Simulation and Modeling of a DC-DC Converter Controlled by an 8-bit Microcontroller", IEEE proc. Applied Power Electro. conf. (APEC), pp. 963-969, Feb 1997.

[113] Sustersic, J., Zeller, J., Gao, Z., Button, R., "Design and Implementation of a Digital Controller for DC-DC Power Converters", Society Automotive Engg., pp. 1-7, 2000.

[114] Alsumady, M., Alturk, Y., Dagamseh, A., Tantawi, M., "Controlling of DC-DC Buck Converters using Microcontrollers", Int. J. Circuits Sys. Signal Pro., vol. 15, pp. 197-202, 2021.

[115] Military handbook, "Reliability Prediction of Electronic Equipment", Department of Defence, USA, 1995.

[116] Billinton, R., Bagen, "Reliability Considerations in the Utilization of Wind Energy, Solar Energy and Energy Storage in Electric Power Systems", IEEE 9th Int. conf. Probabilistic Methods Applied Power Sys., pp. 1-6, June 2006.

[117] Fara, L., Craciunescu, D., "Reliability Analysis of Photovoltaic Systems for Specific Applications", Intech J. Reliability Ecological Aspects Photovoltaic Module, pp. 1-14, 2020.

[118] Sykes, J., Madani, V., Burger, J., Adamiak, M., Premerlani, W., "Reliabilty of Protection Systems", IEEE 63rd Annual Conf. Protective Relay Engineers, pp. 1-16, March 2010.

[119] Yao, B., Chen, H., He, X., Xiao, Q., Kuang, X., "Reliability and Failure Analysis of DC-DC Converter and Case Study", IEEE Int. Conf. Quality, Reliability, Risk Maintenance Safety Engg. (QR2MSE), pp. 1133-1135, Oct. 2013.

[120] Javadian, V., Kaboli, S., "Reliability Assessment of some High Side MOSFET Drivers for Buck Converter", Int. Conf. Electric Power Energy Conversion Sys., pp. 2-4, 2013.

[121] Zhang, P., Li, W., Li, S., Wang, Y., Xiao, W., "Reliability Assessment of Photovoltaic Power Systems: Review of Current status and Future Perspectives", Applied Energy, vol. 104, pp. 822-833, 2013.

[122] Chavan, S., "Reliability Analysis of Transformer Less DC-DC Converter in a Photovoltaic System", J. Mediamira Sci., vol. 57(5), pp. 579-582, 2016.

[123] Gharehkoushan, A., Abapour, M., Farakhor, A., "Design optimization of a Cuk DC-DC Converter based on Reliability Constraints", Turkish J. Electri. Engg. Computer Sci., vol. 25, pp. 1932-1945, 2017.

[124] Kalaiarasi, S., Merceline, A., Geethanjali, R., "Analysis of System Reliability using Markov Technique", Global J. Pure Applied Mathematics, vol. 13(9), pp. 5265-5273, 2017.

[125] Gupta, N., Garg, R., "Design, Development and Reliability Assessment of Dual Output Converters for SPV based DC Nanogrid", J. Renewable Sustainable Energy, vol. 10(2), pp. 1-17, March 2018.

[126] Navamani, J., Vijaykumar, K., Jegatheesan, R., Raj, A., "Reliability Analysis and SFG Modeling of a New Modified Quadratic Boost DC-DC Converter", J. Microelectronics, Electro. Components Materials, vol. 48(1), pp. 3-18, 2018.

[127] Mohammadi, H., Goldani, A., Amlashi, A., Moradpour, R., "Reliability Evaluation of a Buck Converter based on Thermal Analysis", Specialty J. Electro. and Computer Sci. ", vol. 4(3), pp. 1-11, 2018.

[128] Airoboman, A., Ogujor,E., Kokakwu, I., " Reliability Analysis of Power System Network: A Case Study of Transmission Company of Nigeria, Benin City", IEEE PES- IAS Power Africa, pp. 99-104, Sept. 2019.

[129] Kumar, N., Tewari, P., Sachdeva, A., "Reliability Assessment Tools for Multi-Component Complex Systems: An Overview", Int. J. Advance Research Sci. Engg. (IJARSE), vol. 4 (1), Feb. 2015.

[130] Juneja, P., Garg, R., Kumar, P., "Uncertain Data Processing of PMU Modules using Fuzzy Petri Net", J. Intelligent Fuzzy Sys., vol. 41, pp. 1855-1867, 2021.

[131] Kishor, Y., Patel, R., "Thermal Modelling and Reliability Analysis of Recently Introduced High Gain Converters for PV Application", J. Cleaner Energy Sys., vol. 3, pp. 1-13, 2022.

[132] Sayed, A., Shimy, M., Metwally, M., Elshahed, M., "Reliability, Availability and Maintainability Analysis for Grid-connected Solar Photovoltaic Systems", J. Energies, vol. 12(7), pp. 1-18, 2019.

[133] Yadav, G., Joshi, D., Gopinath, L., Soni, M., "Reliability and Availability Optimization of Smart Microgrid using Specific Configuration of Renewable Resources and Considering Subcomponent Faults", J. Energies, vol. 15(16), pp. 1-16, 2022.

[134] Li, Z., Cheng, K., Hu, J., "Modeling of Basic DC-DC Converters", 7th Int. Conf. Power Electro. Sys. Applications Smart Mobility, Power Transfer and Security (PESA), pp. 1-8, 12-14 Dec. 2017.

[135] Vorperian, V., "Simplified Analysis of PWM Converters using Model of PWM Switch Continuous Conduction Mode", IEEE Trans. Aerospace Electro. Sys., vol. 26, pp. 490-496, 1990.

[136] Yanarates, C., Zhou, Z., "Fast- Converging Robust PR-P Controller Designed by using Symmetrical Pole Placement Method for Current Control of Interleaved Buck Converter-based Emulator", J. Energy Sci. Engg., pp. 155- 176, Nov. 2021.

[137] Hekimoglu, B., Ekinci, S., "Optimally designed PID controller for a DC-DC Buck Converter via a hybrid Whale Optimization Algorithm with Simulated Annealing", Research Article Electrica, vol. 20(1), pp. 27, 2020.

[138] Rashid, M., "Power Electronics: Circuits, Devices and Applications", IIIrd Edition, 2003.

[139] Gopal M., "Modern Control Systems Theory", Wiley New York.

[140] Hekimoglu, B., Ekinci, S., "Non-Linear Modeling and simulation of DC-DC Buck Converter using Flow Graph Method", DUMF J. Engg. vol. 9(1), pp. 51-60, 2018.

[141] Erkaya, Y., Moses P., Flory I., Marsillac S., Ieee, "Development of a Solar Photovoltaic Module Emulator", Proc. 42nd Photovoltaic Specialist Conf., New York, 2015.

[142] Ickilli, D., Can H., Parlak S., "Development of a FPGA-based Photovoltaic Panel Emulator based on a DC-DC Converter", 38th IEEE Photovoltaic Specialists Conf. (PVSC), pp. 1417–1421, 2012.

[143] Patel, B., Rana A., "A Pole-Placement Approach for Buck Converter-based PV Array Emulator", Proc. IEEE 1st Int. Conf. Power Electronics, Intelligent Control Energy Systems (ICPEICES), pp. 1-5, 2016.

[144] Vijayakumari, A., Devarajan, T., Devarajan N., "Design and development of a Model-based Hardware Simulator for Photovoltaic Array", Int. J. Electr. Power Energy Sys. vol. 43, pp.40-46, 2012.

[145] Jensen, M., Louie, R., Etezadi, M., Fadali, M., "Model and Simulation of 75kW PV Solar Array", IEEE Trans. Distribution Conf. Expo., USA, April,2010.

[146] Gow, J., Manning, C., "Development of a Photovoltaic Array Model for use in Power Electronics Simulation Studies", IEEE Proc. Electric Power Applications", vol. 146(2), pp. 193-200, March,1999.

[147] Bhuvaneswari, G., Annamalai, R., "Development of a Solar Cell Model in MATLAB for PV based Generation System", Annual IEEE India Conf., Dec, 2011.

[148] Basha, C., Rani, C., Brisilla, M., Odofin, "Mathematical Design and Analysis of Photovoltaic Cell using MATLAB/Simulink", Soft Computing for Problems solving Springer Singapore, pp.711-726, 2020.

[149] Rana, K., "Mathematical Analysis of Three-Diode Model with P&O MPPT using MATLAB/ Simulink", Int. J. Engg. Research Techno. (IJERT), vol. 9(6), pp.1364-1367, June 2020.

[150] Ukoima, N., Ekwe, A., "Three Diode Model and Simulation of Photovoltaic (PV) Cells, Umudike J. Engg. Techno. (UJET), pp. 108-116, June 2019.

[151] Iqbal, T., Tariq M., Khan U., "Fuzzy Logic Control of Buck Converter for Photo Voltaic Emulator", Proc. 4th Int. Conf. Development in the Renewable Energy Technology (ICDRET), pp. 1-6, 2016.

[152] Kim, Y., Lee, W., Pedram M., Chang N., "Dual-Mode Power Regulator for Photovoltaic Module Emulation", J. Appl. Energy, vol. 101, pp.730-739, 2013.

[153] Medina, G., Raul, P., Ivan, G., Gabriel, F., Emilio, "A Low-Cost Photovoltaic Emulator for Static and Dynamic Evaluation of Photovoltaic Power Converters and Facilities", Prog. Photovolt Appl. vol. 22, pp. 227–41, 2012.

[154] Rajguru, V., Gadge, K., Karyakarte, S., Kawathekar, S., Menon, V., "Design and Implementation of a Prototype DC Photovoltaic Power System Simulator with Maximum Power Point Tracking System", IEEE Proc. 1st Int. Conf. Power Electro., Intelligent Control Energy Sys. (ICPEICES), pp. 1-5, 2016.

[155] Ziming, Z., Jianwen, Z., Haimeng, S., Gang, W., Xiwen, H., Shi, Z., "Research on Photovolta Array Emulator System based on a Novel Zero-Voltage Zero-Current Switching Converter", Power Energy Engg. Conf. (APPEEC), Asia-Pacific, pp.1-4, 2010.

[156] Abidi, H., Ben, A., Montesinos, D., "MPPT Algorithm and Photovoltaic Array Emulator using DC-DC Converters", 16th IEEE Mediterranean Electrotechnical Conf. (MELECON), pp. 567–572, 2012.

[157] DDC L., Nguyen, N., "A Photovoltaic Panel Emulator using a Buck-Boost DC-DC Converter and a Low-Cost Microcontroller", J. Sol Energy, vol. 86, pp.1477–1484, 2012.

[158] Astrom, K., Hagglund, T., Hang, C., Ho, W., "Automatic Tuning and Adaptation for PID Controllers- A Survey," Control Engg. Pract., vol. 1(4), pp. 699–714, 1993.

[159] Ziegler, J., Nichols, N., "Optimum Settings for Automatic Controllers," Trans. ASME, vol. 64, pp. 759–768, 1942 copyright J. Dynamic Sys., Measurement Control, vol. 114,1993.

[160] Bansal, S., Saini, L., Joshi, D., "Design of PI and Fuzzy Controller for High Efficiency and Tightly Regulated Full Bridge DC-DC Converter", Int. J. Electri., Computer, Energetic, Electro. comm. Engg., vol. 7, pp.446-452, 2013.

[161] Necaibia, A., Ladaci, S., Charef, A., Loiseau, J., "Fractional Order Extremum Seeking Approach for Maximum Power Point Tracking of Photovoltaic Panels", J. Frontiers Energy, vol. 9(1), pp.43-53, 2015.

[162] Podlubny, I., "Fractional-Order Systems and $PI_\lambda D_\mu$ Controllers", IEEE Trans. Automatic Control, vol. 44(1), pp. 208–214, 1999.

[163] Agrawal, P., "A General Formulation and Solution Scheme for Fractional Optimal Control Problems", J. Nonlinear Dynamics, vol. 38(1), pp. 323–337, 2004.

[164] Gaing, L., "A Particle Swarm Optimization Approach for Optimum Design of PID Controller in AVR System", IEEE Trans. Energy Conversion, vol. 19(2), pp. 384-391, Nov. 6, 2002.

[165] Kennedy, J., Eberhart, R., "Particle Swarm Optimization," Proc. IEEE Int. Conf. Neural Networks, vol. 4, pp. 1942–1948, 1995.

[166] Shi, Y., Eberhart, R., "A Modified Particle Swarm Optimizer," Proc. IEEE Int. Conf. Evol. Comput., Anchorage, AK, pp. 69-73, May 1998.

[167] Shi Y., Eberhart, R., "Empirical Study of Particle Swarm Optimization," Proc. IEEE Int. Conf. Evol. Comput., pp. 1945–1950, July 1999.

[168] Yuan, L., Taewon, L., Peng, Z., Dichen, L., "A Hybrid Control Strategy for Photovoltaic Simulator", Applied Power Electro. Conf. Exposition, APEC, pp. 899–903, 2009.

[169] Solihin, M., Tack, L., Kean, M., "Tuning of PID Controller using Particle Swarm Optimization (PSO)", Pro. Int. Conf. Advanced Sci., Engg. Info. Techno., Malaysia, pp. 458-461, 2011.

[170] Rajesh, R., "Optimal tuning of FOPID Controller based on PSO Algorithm with Reference Model for a Single Conical Tank System", Springer Nature Applied Sci., pp. 1-14, March 2019.

[171] Castaneda, G., Tornez, M., Flores, M., Arellano, O., Moreno, A., Ieee, "Photovoltaic Panel Emulator in FPGA Technology using ANFIS Approach", Proc. 11th Int. Conf. Electri. Engg., Computing Sci. Automatic Control (CCE), pp. 1-6, 2014.

[172] Kulaksiz, A., "ANFIS-based Estimation of PV Module Equivalent Parameters: Application to a Stand-Alone PV System with MPPT Controller", Turkish J. Electr. Engg. Computer Sci. TUBITAK, pp. 2127-2139, 2013.

[173] Jang, J., "ANFIS Adaptive Network based Fuzzy Inference System", IEEE Trans. Syst. Maint. Cybernetics, vol. 23(3), pp. 665–685, 1993.

[174] Ahtiwash, O., Abdulmuin, M., Alexandrov, V., "An Adaptive Neuro-Fuzzy Approach for Modeling and Control of Nonlinear Systems", ICC, LNCS 2074, pp. 198–207, 2001.

[175] Ahmed, M., Kuisma, M., Tolsa, K., Silventoinen, P., "Implementing Sliding Mode Control for Buck Converter", IEEE Annual Conf. Power Electro. Specialist, PESC, pp. 634-637, June 2003.

[176] Emadi, J., Toliyat, H., "Application of State Space Averaging Method to Sliding Mode Control of PWM DC-DC Converters", IEEE Industry Applications Society Annual Meeting, pp. 820-827, Oct. 1997.

[177] Wester, G., Middlebrook, R., "Modeling and Analysis Methods for DC--DC Switching Converters", IEEE Trans. Aeros Electro. Sys., pp. 376-385, 1973.

[178] Gupta, A., Joshi, D., "Comparative Analysis of Non-Linear SMC Controller with Linear PID Controller for Flyback Converter", Springer ESIEE book series, pp. 71-87, Sept. 2021.

[179] Shekhar, A., Sharma, A., "Review of Model Reference Adaptive Control", Int. conf. Info., Communication, Engg. Techno. (ICICET), pp. 1-5, Aug 2018.

[180] Mandal, S., Mishra, D., "Robust Control of Buck Converter using H-infinity Control Algorithm", Pro. IEEE Applied Signal Processing Conf. (ASPCON), pp. 163-167, 2018.

[181] Chilali, M., Gahinet, P., "H_∞ Design with Pole Placement Constraints LMI Approach," IEEE Int. Trans. Automat. Control, vol. 41(3), pp. 358-367, 1996.

[182] Glover, K., Doyle, J., "State-Space Formulae for all Stabilizing Controllers that Satisfy an H_∞ norm Bound and Relations to Risk Sensitivity," Sys. Control Letters, vol. 11(8), pp. 167–172, 1988.

[183] Wang, H., Ma, K., Blabjerg, F., "Design for Reliability of Power Electronic Systems," 38th Annual Conf. IEEE Industrial Electro. Society, pp. 33-44, 2012.

[184] Calleja, H., Chan, F., Uribe, I., "Reliability-Oriented Assessment of a DC-DC Converter for Photo Voltaic Applications", Power Electro. Specialists Conf. PESC, pp. 1522-1527, 2007.

[185] Chen, G., Burgos, R., Liang, Z., Lacaux, F., Wang, J., Wyk, V., Odendaal, W., Boroyevich, D., "Reliability-Oriented Design Considerations for High-Power Converter Modules," IEEE 35th Annual Power Electro. Specialists Conf. PESC., pp. 419-425, 2004.

[186] Singh, A., Patil A., Tripathi V., Sharma R., Jarial, R., "Reliability Modelling and Simulation for Assessment of Electric Arc Furnace Transformers", Proc. 2020 IEEE Int. Conf. Computing, Power Communication Techno. (GUCON), pp. 239–244, Oct. 2021.

[187] Gupta, S., "Stochastic Modelling and Availability Analysis of a Critical Engineering System", Int. J. Qual. Reliability. Management, vol. 36(5), pp. 782-796, April 2019.

APPENDIX I

Datasheet of S115 panel

S.No.	Parameter	Value
1	STC power rating	115W
2	Open Circuit Voltage, V_{oc}	32.8V
3	Short Circuit Current, I_{sc}	4.7A
4	Voltage at maximum power point, V_{mpp}	26.8V
5	Current at maximum power point, I_{mpp}	4.29A
6	Material	Polycrystalline

PUBLICATIONS from Ph.D. RESEARCH WORK

Following are publications in Journals, Conferences and Magazines out of this research work.

Journals

[1] Sharma, S., Joshi, D., "Modeling and Control of PV Emulator with Different Controllers and Transient Load Conditions", Indian J. Engg. & Material Sci. (IJEMS) **SCI Journal**, vol. 30, pp. 73-79, Feb. 2023.

[2] Sharma, S., Joshi, D., "Analysis of Designed PV Emulator using FOPID Controller and Fuzzy Logic Controller by Load Variation", J. Information and Optimization Sci., Taylor & Francis, **ESCI Journal**, ISSN: 0252-2667 (Print) 2169-0103 (Online), vol. 41(1), pp. 283-292, Feb. 2020.

Conferences

[1] Sharma, S., Joshi, D., "Reference Model Design, Control and Reliability Analysis of PV Emulator", Springer 2nd Int. conf. Renewable Techno. Engg. (ICRTE), ISBN: 978-981-19-8963-6, e-book chapter in Springer "Renewable Energy Optimization, Planning and Control", pp. 151-163, March 2023.

[2] Sharma, S., Joshi, D., "Modeling and Control of Photo Voltaic Emulator by Robust Controller", 4th Int. conf. Computing Informatics & Networks (ICCIN-2022), Dec. 2022, ISSN: 2454-8421, pp. 1-6, proc. in process "Bodh Journal", vol. 8(2).

[3] Sharma, S., Joshi, D., "PV Emulator Model Design using AI based Controllers", Springer Nature Singapore, Proc. 3rd Int. conf. Computing Informatics & Networks (ICCIN), Lecture notes in "Networks and Systems", ISBN: 978-981-15-9712-1, vol. 167, pp. 439-448, March 2021.

[4] Sharma, S., Joshi, D., "PV Emulator Modeling and Design using Buck Converter", Springer Int. conf. Manufacturing, Advance Computing, Renewable Energy and Communication (MARC), Springer Singapore e-book chapter in "Applications of Computing, Automation and Wireless Systems in Electrical Engineering", Online ISBN: 978-981-13-6772-4, vol. 553, pp. 639-648, June 2019.

[5] Sharma, S., Joshi, D., "Design and Control Aspects of PV Emulator", IEEE 4th Int. conf. Computing for Sustainable Global Development, INDIA Com, ISBN: 978-93-80544-24-3, conf. ID: 40353, pp. 1-4, March 2017.